COASTAL SEDIMENT TRANSPORT SIMULATION BY SMOOTHED PARTICLE HYDRODYNAMICS

by

Shan Zou

A dissertation submitted to The Johns Hopkins University in conformity with the requirements for the degree of Doctor of Philosophy.

Baltimore, Maryland

January, 2007

Abstract

The coastal sediment transport is very important for the planning and design for shore protection and coastal structures. And it is a challenge for coastal engineers and scientists due to its complicated features including the wave breaking, turbulence and mixing, fluid-sediment interaction and flow-topography coupling.

This study is to present a nearshore hydrodynamics, sediment transport and morphological model by Smoothed Particle Hydrodynamics (SPH) Method, especially in the surf zone. The hydrodynamics model provides the necessary information and driving force for the sediment transport and morphological model. The SPH hydrodynamics model solves the Navier-Stokes equations including the sub-particle scheme for the Large-Eddy Simulation. The sediment transport is modeled as concentration equation by solving convection-diffusion equation. The morphological model is based on the sand mass conservation.

The SPH hydrodynamics is validated by the wave flume experiments about the breaking waves on plane beach. The results show satisfactory agreement with the experiment data and its capability to simulate the complicated physics pretty well due to its Lagrangian method which includes the nonlinear convective term without efforts.

An upwind SPH numerical scheme is proposed to solve the settling term in convection-diffusion equation in the sediment suspension model. And the numerical experiment shows the standard SPH scheme has the numerical diffusion and dispersion problem. The sediment suspension model is tested by the experiments for oscillatory flow above the ripples, which the convective motion dominates the process

and play an important mechanism for the sediment suspension and distribution. The comparisons indicate the model can predict sediment concentration under the wave condition fairly well.

The morphological model is applied in the flat bed case and verified by mass conservation. It needs further research for practical application. Finally the three SPH models is used to study the wave breaking, sediment transport and the resulting beach evolution under the different wave conditions.

Expensive computation is the disadvantage of SPH method. The parallel algorithm in the SPH model is also discussed in the last. The parallel algorithm has very good efficiency by using buffer communication and load balancing techniques.

Advisor:

Prof. Robert A. Dalrymple

Readers:

Prof. Lian Shen

Prof. Takeru Igusa

Acknowledgements

I would like to gratefully and sincerely thank Professor Robert A. Dalrymple for his guidance, understanding, patience and friendship during my studies. His excellence in academics and personality will inspire me for my future. He encouraged me not only grow as a coastal engineer and researcher but also as an independent thinker. For everything you've done for me, Dr. Dalrymple, I thank you.

I would also like to thank all of the members of the Dalrymple group, Muthu Narayanaswamy, Blair Johnson, Varjola Nelko, and Benedict Rogers. They provide not only help in academics but also needed humor and entertainment in the lab. I especially thank Blair Johnson and Muthu Narayanaswamy for their help for my dissertation during Christmas holiday.

I would like to thank Professor Lian Shen for his assistance and guidance during my graduate career, and also for his careful and thorough classroom instruction and insightful comments for our research projects.

I would like to thank the members of my doctoral committee, Takeru Igusa, Charles Meneveau, and Peter Wilcock, for their input, valuable discussion and accessibility.

I acknowledge the financial support to this research by the Office of Naval Research.

Finally, and most importantly, I would like to thank my wife, Yu Sun, my son, Alexander Zou and my parents-in-law. The time and effort necessary to complete this research would not have been possible without their encouragement, dedication and love.

Contents

List of Tables

List of Figures

Chapter 1

Introduction

The coastal area is highly populated and there are many kinds of properties subjected to erosion. The understanding of nearshore hydrodynamics and the resulting sediment transport is very important to take effective engineering steps to protect the shoreline. There are two methods to protect the beach and properties: one is a soft engineering project, such as beach nourishment, as the beach provides the natural protection from the damage of water wave forces; the other is a hard engineering project, in which coastal structures are built to protect the properties. Both of these methods require the understanding of the interaction between waves, currents and sediment.

The analysis and modeling of coastal sediment transport have become essential tools for coastal engineers, who aim to optimize and evaluate coastal engineering design with the availability of high speed computers. The scientific community has put much effort into creating different models in order to obtain a better understanding and accurate prediction of coastal sediment transport. The purpose of this study is for the feasibility to use the Smoothed Particle Hydrodynamics for coastal sediment transport simulation and beach evolution prediction, which is a pure Lagrangian and grid-free method.

1.1 Breaking Waves and Nearshore Sediment Transport

Surf zone refers to the region on a gently sloping beach in the region from the initiation of wave breaking to the shore line. Most of the wave energy is dissipated in this region: the breaking process turns the wave energy into turbulence, heat, sound; generates the strong currents; and suspends the sediments. This area is the most active region for sediment transport process, which is responsible for the coastal morphological change.

The hydrodynamics in the surf zone are very complicated due to the wave breaking, irregular bathymetry and their interaction. It is a formidable challenge for scientists and engineers to study the hydrodynamics and sediment transport in this region because their interactions are poorly understood. Due to the existence of wave breaking, the surf zone is characterized by the irreversible and virtually complete transformation of the organized motion of the incident waves into motions of different types and scales, including small-scale turbulence, larger-scale coherent vortices motions, low-frequency waves, and steady flows [5]. There are many challenging hydrodynamics problems in surf zone: wave set-up; cross-shore, longshore currents and their stability; turbulence and mixing; edge waves; shear waves, and rip currents.

Wave breaking is a very complicated hydrodynamic process; yet it is crucial in nearshore processes: increasing the rate of transfer of energy, momentum, heat, mass between air and water; generating significant loading on coastal engineering structures; dissipating wave energy; and other disturbances.

Wave breaking is caused by excessive energy input or the instability caused by the shoaling effects. Wave breaking generates different scales of motion of water including small-scale turbulence, large-scale coherent eddies, low-frequency waves and steady flows.

There are several criteria for the initiation of breaking:

1. the front of surface becomes locally vertical.

2. the maximum downslope acceleration equals to the downslope component of

the gravitational acceleration.

3. the water particle velocity at the crest is larger than the phase velocity of the wave form.

Battjes [5] describes the wave breaking process based on the following observation: the overturning wave front curls forward, forming a jet that then plunges into the trough ahead of it; a plunging breaker forms a cavity and transforms into a turbulent bore; the cavity rapidly collapses while the air entrapped in it mixes with the water, which result in large-scale vortices and high concentration of bubbles.

Breaker types are determined by deep water wave characteristics and beach slope. There are four types of breakers based on the motion and geometry during the breaking events: spilling, plunging, collapsing and surging breaker. Each has the different characteristics[83]:

In *spilling* breakers, the crest becomes unstable and flows down the front part of the wave, resulting in frothy water reminiscent of a bore. In the surf zone, spilling occurs when steep waves advance up a gentle beach and continue over a number of wavelengths.

Plunging is the most dramatic form of breaking, during which the crest curls over and crashes into the water near the toe of wave front, creating a large splash which advances like a bore. Plunging occurs on slightly steeper beaches, often within a single wavelength.

Surging occurs on the steepest beaches: the crest does not break, but the base of the front face of wave advances rapidly up the beach with mild breaking and significant reflection.

Collapsing is the most recent classification of breaker, between plunging and surging. The crest itself does not break but the lower part of the front face steepens and falls, creating a foamy surface that slides up the beach.

Spilling and plunging breakers are more important to beach evolution than surging and collapsing breaker because of their fluid dynamics. The first two begin offshore and end at the shoreline, whereas the latter two occur only at the shoreline. There are many studies on the sand bar and trough system formation related to spilling and

plunging breakers[96].

Both spilling and plunging breakers have the jet overturning starting at the crest. In spilling breakers, the jet overturns and falls near the crest. The difference occurs in plunging breakers, which are characterized when the jet touches the undisturbed water surface near the toe of the wave. The place and the instance of time where the falling jet touches the undisturbed water surface is called the plunging point. An air pocket is maintained during most of this time period. After the plunging point the jet evolves into the splash and a chaotic motion of water. The splashes may be higher than the original wave[73].

Wave breaking can also produce steady motions within the surf zone[5]. Wave-induced streaming is one of steady motions that occurs in the boundary layer by the perturbation of nonuniform phase or amplitude of external oscillatory flow. Another horizontal flow system is wave-induced nearshore circulation, that can be found by time-averaging the equations of conservation of mass and momentum, driven by gradient of the wave radiation stress.

The radiation stress is the flux of momentum due to waves only[87]. The total flux of momentum through a vertical plane for a progressive wave is shown in the figure 1.1:

$$F(t) = \int_{-h_0}^{\zeta} (\rho u^2 + p) dz \tag{1.1}$$

The time average of $F(t)$ over a wave period is:

$$F = \overline{\int_{-h_0}^{\zeta} (\rho u^2 + p) dz} \tag{1.2}$$

where $\overline{?} = \int_t^{t+T} (?) dt$ means the time average over the wave period T, ζ is the surface elevation above mean water surface (MWS), h_0 is the depth below x-axis, local mean water depth is defined as $h(x) = h_0(x) + \overline{\zeta}(x)$.

The definition of wave radiation stress S_{xx} is the mean momentum flux or mean force caused by wave motion only, which is obtained by subtracting the hydrostatic part from the time-averaged total flux of momentum F.

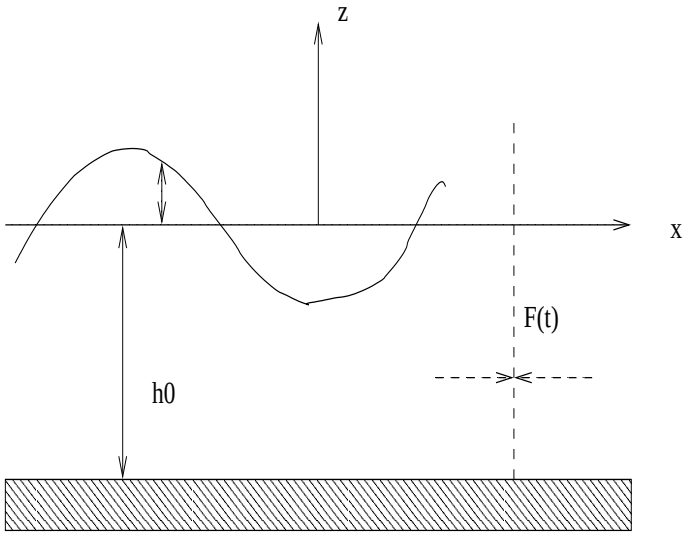

Figure 1.1: Flux of momentum F(t) action on the two sides of a vertical section.

$$
\begin{aligned}
S_{xx} &= \overline{\int_{-h_0}^{\zeta} (\rho u^2 + p) dz} - \overline{\int_{-h_0}^{\bar{\zeta}} (\rho u^2 + p) dz} \\
S_{xy} &= \overline{\int_{-h_0}^{\zeta} (\rho uv + p) dz} - \overline{\int_{-h_0}^{\bar{\zeta}} (\rho uv + p) dz} \\
S_{yy} &= \overline{\int_{-h_0}^{\zeta} (\rho v^2 + p) dz} - \overline{\int_{-h_0}^{\bar{\zeta}} (\rho v^2 + p) dz}
\end{aligned}
\tag{1.3}
$$

where u is the velocity along the wave direction and v is the velocity transverse the wave direction. The wave radiation stress is the main driving force for the wave-induced steady motion.

Most modeling of horizontal nearshore circulation is based on the depth-integrated equations, which do not show the vertical structure of flow that is relevant to sediment transport and beach evolution. Vertical circulation in the nearshore region is caused by an imbalance of mass and momentum fluxes due to the topography or change of wave conditions. Breaking waves transfer the momentum to generate the onshore mean flow in the range of wave crest and trough. At the same, a strong offshore flow occurs below the trough level due to mass balance, which is called undertow.

Surf zone dynamics, especially in vertical plane, is important for nearshore sediment transport, as well as the formation and migration of sand bar systems[43]. In storm seasons, large waves propagate to the shoreline, shoal, and finally break on the sand bar. The excess of mass and momentum flux drives the strong offshore undertow, carrying sediment seaward, resulting in offshore sandbar migration. Otherwise, when non-breaking waves pass the sandbar, the peaky wave crest has greater onshore orbital velocity than the offshore velocity of a broad trough and results in net sediment transport and sand bar migration shoreward.

1.2 Review of Modeling Breaking Waves

Many scientists and engineers have researched breaking waves through experimentation and numerical modeling. Turbulent flow is one of the most difficult topics in fluid mechanics.

Nadaoka [68] measured particle velocities in the bore region of a periodic wave breaking on a slope and separated the constant-phase averaged velocity field into an irrotational part and a rotational part. The results clearly show the existence and extent of a region of forward-directed rotational velocity in and downstream of the breaking-wave crest, called the wake. The wake acts as an area of diffused momentum left behind by the breaking wave front, which acts as a source of forward momentum moving forward (in this reference frame with the phase speed of the wave).

Ting and Kirby [93] [94] conducted a series of experiments on spilling and plunging breakers. They made the following conclusions for plunging and spilling breakers: plunging breaker turbulence intensity is highest under the wave front and decreases rapidly after the wave crest passes, causing turbulence to diminish between breakers; plunging turbulence created by the surface roller immediately saturates the entire flow depth and the area behind the wave front; plunging breaker turbulence production and energy dissipation are not in local equilibrium but are of the same order of magnitude; spilling breakers differ from plunging breakers primarily in the way in which energy is supplied to the turbulence, and the effects of the mean flow on the large-scale turbulence; the fact that the rate of change of turbulent kinetic energy

and turbulence production are poorly correlated suggests that production is roughly balanced by energy dissipation, since it is this difference that contributes to the rate of change of turbulent energy.

Chang and Liu [11] used PIV technique to capture the wave breaking process. The experiments were conducted in a wave tank which is 30 m long, 0.6 m wide and 0.9 m deep. The water depth was kept at 20 cm. Monochromatic waves with wave height of 14.5 cm and wave length of 121 cm were generated by wavemaker periodically in time. The measurements showed that the measured fluid particle velocity at the tip of the overturning jet reached 1.68 times the phase velocity calculated from the linear wave theory and the overturning jet enters the horizontal water surface with an acceleration of 1.1g at an angle of 88 degrees downward. The PIV technique was also used to measure the instantaneous vertical vortices generated by breaking waves and showed that the number and locations of the vortices on the horizontal plane appear to be random.

There are a variety of numerical models to analyze breaking waves, here some of them are reviewed:

The *roller model* [88] is bore propagation model based on the nonlinear shallow-water equations. A bore is represented as a discontinuity that conserves mass and momentum. The bore connects two regions of uniform flow, with different depths, h1 and h2 respectively ($h2 > h1$), which implies that energy is dissipated at a rate

$$D' = \frac{1}{4}\rho g^{3/2}(\frac{h_1 + h_2}{2h_1h_2})^{1/2}(h_2 - h_1)^3$$

It has been used in the *depth-integrated model* in horizontal or vertical momentum equations. One of the methods is the Boussinesq-type equation for the breaking waves in which the breaker is modeled as a surface roller. The dissipation caused by the roller is expressed as either an excess momentum term caused by the nonuniform velocity distribution or as an additional pressure term in the momentum equation (e.g. surface roller concept for spilling breakers, its effect on the wave motion is taken into account by additional convective terms in the momentum equation)[82][60]. By calibrating the parameters in the model, the simulation results show reasonable agreement with experimental data for free-surface profile[48][77]. But the velocity field obtained from

these models has not established, because the depth-integrated equation is not able to produce accurate velocity field, especially in the roller region. So these methods lack in its capability to accurately predict velocities in the bore and the spatial distribution of the turbulence kinetic energy (TKE).

Another method for simulate the breaking wave is the *Reynolds Averaged Navier-Stokes* (RANS)[53] model, which consists of RANS equations coupled with a second-order $k-\epsilon$ turbulence closure model. The mean flow is given by the Reynolds equations, including viscous stress and Reynolds (turbulent) stress. The closure assumption of Reynolds stress is solved by the transport equation for the turbulent kinetic energy k and the turbulence dissipation rate ϵ. The Reynolds equations are solved by the finite difference method, and the volume of fluid (VOF) is used to track the free surface locations. This method has the ability to describe two-dimensional spilling and plunging breaking waves in surf zones. With the appropriate boundary conditions, this method has successfully predicted many complex turbulent flows [80]. The model results compare very well with experimental data, especially in the inner surf zone. Compared with large-eddy simulation (LES), the LES approach requires much finer grid resolution than the RANS approach.

The large-eddy simulation (LES) is a recent method to simulate the turbulence in breaking waves. The turbulence is taken into account in the Navier-Stokes (N-S) equations by coupling with a turbulence model for the sub-grid scales (SGS) of the flow. Watanabe *et al.*[98] used a fully three dimensional LES model to investigate the large scale vortex structures under spilling and plunging breakers. The sub-grid stress term is obtained by spatially filtering the N-S equations, which is described by SGS viscosity form. In their modeling, the N-S equations with LES simulation are solved by predictor-corrector method, pressure is calculated by Poisson equation, and higher-order VOF method is used to represent the complex surfaces. The model results show the formation and evolution of large-scale three dimensional vortex structures. Obliquely descending eddies are identified in plunging breakers. Lubin *et al.* [58] investigated the plunging breaker by solving N-S equation, coupling with a dynamics sub-grid scale turbulence model (LES), with Direct Numerical Simulation (DNS) of two-phase flows on Eulerian grids. Traditional DNS method can resolve the all scales

of turbulence by choosing a grid and time step fine enough to capture the Kolmogorov length scale of turbulence. Instead, to avoid the expensive cost of computation, they considered the large scale turbulence through the sub-grid scale model (LES), with the philosophy of LES that is to represent the dissipative effect of the small turbulent structures with a turbulent viscosity. The sub-scale model used the mixing scale model, instead of the commonly used Smagorinsky model, with a selective function to turn it on or off, depending on the local velocity field. The free surface is tracked by solving the phase function directly, instead of the VOF method. The model can not only accurately reproduce the complicated dynamics under the plunging breaker in terms of free surface and velocity field, but also illustrate the air entrainment phenomenon in the energy dissipation process due to its features of the two-phase flow model.

All the above breaking models are Eulerian methods, which suffer numerical diffusion problems for the nonlinear convection term. So recently the emergence of *Smoothed Particle Hydrodynamics method* (SPH) provided a new numerical method to study the breaking waves, which is a pure Lagrangian particle method developed in the astrophysics community in the late 1970's[59][32]. It has been applied in coastal engineering since late 1990's.

Monaghan and Kos initiate the study the water motion by using SPH method and showed the promising results for wave problems[66].

Dalrymple and Knio[19] set up a numerical wave tank (NWT) system, including wavemaker, which is able to study the wave generation, propagation, and breaking on the plane beach by the SPH model. The NWT system can be used for many coastal engineering studies[101]. Rodgers and Dalrymple [81] used the two and three dimensional SPH method to study the weakly plunging breakers by solving the N-S equation, coupling with sub-particle scheme (LES). The sub-particle scale of turbulence is expressed by Smagorinsky model. By using incompressible fluid approximation, which will be discussed in Chapter 3, the pressure is given by the equation of the state. The convection term is included without no effort and the free surface is automatically tracked because it is Lagrangian and meshfree method. The model results show the details of jet-splash, mixing during the breaking process. The obliquely descending

eddies can be identified even in the low resolution.

Colagrossi and Landrini [16] used the SPH two-phase model to deal with two dimensional interface flow with low density ratios, such as air-water flow problems. They proposed a first-oder accurate interpolation scheme on irregularly scattered points to re-initialize the density field with the moving-least-square kernel, which gives more regular pressure distribution and better conserved total energy. The Shepard filter can obtain the similar benefit. With the modified equation of the state, including the a cohesion force, the interface can be better modeled. The model results show the improved SPH model can treat a variety of air-water flows with interface breaking and air-entrapment. The density re-initialization procedure filters out small scale pressure oscillations and improves energy conservation when artificial viscosity is used.

Both of the above SPH models used the incompressible fluid approximation, in which the pressure is solved by the equation of state.

Koshizuka *et al.*[49] used moving particle semi-implicit (MPS) method to conduct the simulation of the wave breaking on a uniform slope, in which the pressure is obtained by solving the Poisson equation of pressure. It has been applied to many kinds of wave breaking and other problems[37][36][38]. MPS method is a extension of SPH method. The difference between SPH and MPS is that the incompressibility of fluid in MPS is satisfied by keeping the number density of fluid particle constant, because the density of fluid is proportional to the number density of fluid particles. The number density of fluid is the number of fluid particles per unit area, instead of explicit equation of the state. In MPS, the Poisson equation of pressure is the function of the number density. The kernel function used in the model has lower order accuracy, compared with standard SPH method.

$$W(r) = \begin{cases} \frac{r_e}{r} - 1 & \text{for } r \leq r_e \\ 0 & \text{for } r > r_e \end{cases} \tag{1.4}$$

where r is the distance between particles, r_e is the kernel size.

1.3 Review of Modeling of Coastal Sediment Transport

Coastal sediment transport not only involves the complicated nearshore hydrodynamics but also covers a wide range of spatial and time scales. Horikawa [44] classified coastal processes into three scales: macroscale, mesoscale and microscale. These correspond to space and time scales as kilometer/year, meter/day(hour), and millimeter/second, respectively. Macroscale and mesoscale are more important for practical engineering purpose than the microscale; but the microscale is important to understand the others.

The difficulties in modeling coastal sediment transport are due to many factors: coastal sediment transport is an interacting system including wave, current and bottom topography. Sediment particles of millimeter size are transported by the momentum of the water, the bottom topography is modified by sediment transport, the new topography profile then affects the hydrodynamics. Wave, current and bottom topography interact until they reach equilibrium state if the wave conditions are constant. Further turbulent flow dominates in nearshore region, especially after waves break. Turbulent flow itself is one of the most difficult topics in fluid mechanics. In addition, the detailed mechanism of interaction between fluid and sediment particles is not yet clarified.

For simplicity, coastal sediment transport is separated into cross-shore and long-shore sediment transport. The cross-shore sediment transport is more related to beach profile evolution than long-shore sediment transport. The following will focus on cross-shore sediment transport, which is the main topic of this thesis.

For the cross-shore sediment transport, occurring from the critical depth (where sediment particles first feel influence of wave motion) to the shoreline, the nonlinearity of the wave motion dominates the dynamics and sand ripples are an essential factor to sediment transport. In this region, the net sediment transport is onshore directed when bed-load is dominant; the net sediment transport is offshore directed when the suspended-load is dominant[45]. At the breaking point, the breaker type determines the amount of sediment suspended due to the turbulence and coherent

vortex structures.

Schoonees and Theron [84] evaluated ten well-known cross-shore sediment transport and morphological models. All of the ten models can be classified into three approaches: empirical, energetic and deterministic models.

Empirical models are reliable and simple because the predictions are based on observation of actual data, and the evolution of other beaches under similar conditions. The result is qualitative and does not involve precise physics. The Swart Model (transport rate related to difference between equilibrium profile and existing profile)[89], the Kriebel and Dean model (refined equilibrium profile with energy dissipation)[50], the Nishimura and Sunamura Model (transport rate is formulated as a function of Ursell number U_γ and Hallermeier parameter θ)[70], are classified as empirical models here. These two dimensionless parameters are:

$$U_\gamma = \frac{HL^2}{d^3}$$

$$\theta = \frac{(a_0\omega)^2}{sgd}$$

where H is the wave height, L is the wave length, d is the water depth including wave set-up, a_0 the near-bed orbital diameter, ω is the wave angular frequency of waves, d is the grain size of sediment, $s = 2.65$ is the relative density of sediment (ratio of density of sediment to density of water).

The *energetic models* are based on the relation of sediment transport rate and the energy dissipation of the flow. This method is more accurate than the empirical methods because the transport rate is related to the dynamics and the sediment properties. The Bailard Model is a typical and popular energetics method[1]. There are some assumptions limiting its application: it is valid only there is a planar beach with constant slope (means no ripples and variable slope); no sediment incipient motion criterion; there is no wave-induced turbulence and phase information considered.

The *deterministic models* include the wave propagation, wave-induced current and suspended sediment transport models. The sediment transport rate is calculated based on the net flux of sediment. The Dally and Dean Model is based on net time-average flux of sediment, using linear wave theory and steam function wave theory

for hydrodynamics and a concentration profile of the sediment over the depth given by the solution of one dimensional diffusion equation[18]. The Shibayama Model obtains the wave transformation and velocity field from a wave model, then the sediment transport rate formula depends on the types of transport classified by Shields parameter and ratio of maximum fluid velocity and sediment fall velocity[85]. The Watanabe Model has four sub-modules. The difference is that the sediment transport rate is calculated by bottom shear stress instead of the net sediment flux. Watanabe *et al.*[97] stated that the undertow and wave breaking turbulence are important for transport in the surf zone. The Steezel Model is similar with the Dally and Dean Model but with a refined wave-averaged diffusion equation for suspended sediment. The Larson and Kraus Model (SBEACH) relates the equilibrium profile to the equilibrium wave energy dissipation equation[51]. The Danish Hydraulic Institute Model (LITCROSS) includes a hydrodynamics model to describe propagation, shoaling and breaking, and a sediment transport model to calculate bed load and suspend load by solving vertical sediment diffusion equation. They also consider the streaming effects, nonlinearity of waves and production of turbulence in the surf zone.

In general, the deterministic models include: a wave module, a hydrodynamics module, a sediment transport module, and a bathymetry updating module. Rakha *et al.*[77] proposed a phase-resolving cross-shore sediment transport model for beach profile evolution. The wave module simulates the wave conditions across the beach by a phase-resolving model based on Boussinesq equations. The hydrodynamics module has two parts: an oscillatory boundary layer model to calculate the time variation of bed shear stress; an undertow model to calculate the mean undertow due to the wave breaking. The sediment transport module calculate the instantaneous sediment transport rate driven by the bed shear stress and currents, from the hydrodynamics module. The morphological change is calculated by solving the mass conservation of sediment based on the time-averaged sediment transport rate. Karamba and Koutitas's model has the similar system.

In this research, we propose a deterministic model of cross-shore sediment transport and morphological models, including phase-resolving breaking wave model, sediment suspension and morphological model. All these models are solved by SPH

method.

1.4 Outline of Present Work

The aim of this study is to develop a SPH model system including SPH hydrodynamics, SPH sediment transport and morphological model, and to apply the model to coastal sediment transport in the surf zone.

Chapter 2 gives an overview of SPH methodology including a brief history, numerical techniques, and some applications.

Chapter 3 describes the approaches for surf zone hydrodynamics, including the governing equations, boundary conditions, and numerical solutions for SPH hydrodynamics model. The closure of Large Eddy Simulation is included. Finally, the SPH model is applied as a numerical wave tank to validate the fluid dynamics predictions. The SPH results are compared with experimental data for breaking and non-breaking waves.

Chapter 4 reviews the SPH sediment transport model. We develop a SPH concentration model for suspended sediment and propose a new numerical scheme for convection in particle form. The numerical scheme will be investigated by some numerical experiments. A morphological model is presented based on the sediment flux between fluid and mobile bed. The sediment flux at the interface are calculated by pick-up function. Finally the models are applied into the sediment suspension simulation over different bed forms under the oscillatory flow: one is the sediment suspension on wave-generated ripples, and another is on flat bottom. They have different transport mechanisms.

In Chapter 5 the full SPH models, including hydrodynamics model (wave propagation, shoaling, breaking and mean flow), sediment transport model, and morphological model (bed level change based on sand mass conservation), are used to predict the cross-shore sediment transport and beach evolution under the different wave conditions.

The final chapter summarizes the work, draws the conclusions, and propose the future work in this research.

The appendix presents the parallel computing algorithm and its performance.

Chapter 2

Overview of the SPH Method

Classic numerical methods such as finite difference method (FDM) and finite element method (FEM) have traditionally been applied to solve differential equations. Both of methods need structured grids to discretize the numerical problem so that the ordinary differential equation (ODE) or partial differential equation (PDE) can be approximated by algebraic equations. These two numerical methods are widely used in computational fluid dynamics (CFD) and computational solid mechanics (CSM) for engineering and science problems.

Smoothed Particle Hydrodynamics (SPH) is a pure Lagrangian, meshfree method. This chapter discusses the brief history of SPH and introduces the fundamentals of the method.

The first section reviews some fundamentals of SPH method. The second section presents a procedure to discretize ODE's and PDE's using SPH, and some associated spatial and temporal numerical techniques. The last section shows some applications in different areas.

2.1 Fundamentals of SPH Method

SPH method was developed by Lucy [59] and Gingold & Monaghan [32] to solve problems in astrophysical fluid dynamics. In the conventional grid or mesh-based methods, FDM or FEM, a spatially fixed Eulerian grid/mesh is used. Each grid

point or node contains information about material properties at that point and is also used to express the derivatives in space. In contrast, SPH regards the material itself as a set of particles that can move with its material as mass points. Each particle carries its physical properties. As will be shown, the derivative in space can directly be approximated analytically by kernel estimation using a set of neighboring particles and thus eliminates the need for a fixed grid or mesh.

Monaghan [65] listed some of the attractive features of SPH method:

1. In SPH, pure convection is treated exactly. Compared with fixed grid methods, most numerical schemes have numerical dissipation, diffusion, and dispersion problems. For a large convection velocity, the finite difference solution can be easily corrupted.

2. Multiple materials can be easily modeled by assigning different material properties to individual particles so that SPH express the continuum and fragmentation problem in a natural way. This enables the interface problem trivial for SPH method.

3. The particles can be placed along any irregular shape of boundary and material interfaces. They can be tracked automatically without any efforts.

4. The resolution can be made to depend on the position and time with variable smoothing length.

5. SPH has the computational advantage, particularly in problems involving fragments, drops or stars, that the computation is only where the matter is, which can save storage and calculation.

6. SPH is similar with molecular dynamics so that it is possible to include complex physics.

Besides these advantages, SPH method is easier in coding than other grid-based numerical method.

Since the invention of SPH method, it has undergoing continuous development and improvement. Many numerical techniques have been developed to improve the accuracy and stability of SPH model so that it can eventually be an acceptable numerical method for practical engineering applications. It has also been used for the film special effects, such as Lord of the Rings, Ice Age 2[65] (www.nextlimit.com/realflow/).

The following sections present some fundamentals and numerical techniques used in SPH method such as kernel function and derivative expression in particle form.

Kernel Approximation

According to the fundamental property of the Dirac delta function δ, an arbitrary function $f(r)$ can be exactly expressed as [39]:

$$f(r) = \int_{-\infty}^{\infty} f(r')\delta(r - r')dr' \tag{2.1}$$

where the integral is over the entire space, otherwise there are boundary terms that appear or the kernel should be normalized or corrected. The δ function can be approximated by an analytic function $W(r - r')$, called a kernel function:

$$< f(r) >_k = \int_{-\infty}^{\infty} f(r')W(r - r', h)dr' \tag{2.2}$$

where $<>_k$ represents the kernel approximation, which is also called as 'integral approximation', h is the smoothing length or width of the kernel function. The kernel function $W(r-r', h)$ should satisfy the following conditions: the normalization condition, delta function condition, and compactness condition:

$$\begin{aligned} \int_{\Omega} W(r - r', h)dr' &= 1 \\ \lim_{h\to 0} W(r - r', h) &= \delta(r - r') \\ W(r - r', h) &= 0 \text{ when } |r - r'| > h \end{aligned} \tag{2.3}$$

The normalization condition and delta function condition relate to the approximation of delta function. The compactness condition means the kernel function has compact support so that the contribution of particles out of kernel can be neglected. It saves considerable computation time for neighboring search.

Particle Approximation

The difference between SPH method and other traditional numerical methods is that a function is approximated by a set of disordered particles instead of grid or mesh points. Then, the integral interplant 2.2 can be expressed in terms of discrete particles as:

$$< f(r) >_p = \sum_j f(r_j^{'}) W(r - r_j^{'}, h) \frac{m_j}{\rho_j} \tag{2.4}$$

where $<>_p$ is the particle approximation of $f(r)$, j is the particle label for the neighboring particles, and $\frac{m_j}{\rho_j}$ is the volume associated with the particle. It is assumed that only the neighboring particles in a certain range contribute to the interaction significantly and others are negligible so that the number of particles included in the sum is limited. Another important assumption is that the boundaries are far away, further away than $2h$, so the boundary term appearing from integration by parts can be neglected.

Derivatives

The distinguishing feature of this method is that if you choose a differentiable kernel function, the derivative operator can be expressed as ordinary differentiation of the kernel function as:

$$\frac{\partial f(r_i)}{\partial x_i} = \sum_j f(r_j) \frac{\partial W(r_i - r_j, h)}{\partial x_i} \frac{m_j}{\rho_j} \tag{2.5}$$

because $f'(r_i)$ is a scalar value of f associated with the particle at r_j. For this reason there is no need of grids or meshes that are essential in mesh methods to express the spatial derivative.

In conservative form ($f_i^{'} = -f_j^{'}$), the first derivative in SPH particle form is[65]:

$$\frac{\partial f_i}{\partial x_i} = \sum_j \frac{m_j}{\rho_j} (f_j - f_i) \frac{\partial W_{ij}}{\partial x_i} \tag{2.6}$$

or

$$\frac{\partial f_i}{\partial x_i} = \frac{1}{\rho_i} \sum_j m_j (f_j - f_i) \frac{\partial W_{ij}}{\partial x_i} \tag{2.7}$$

Second derivative is not as simple as the first derivative because of several disadvantages, as discussed by Monagahan[65]:

$$\left(\frac{\partial^2 f}{\partial x^2}\right)_i = \sum_j f(r_j^{'}) \frac{\partial^2 W_{ij}}{\partial x_i^2} \frac{m_j}{\rho_j} \tag{2.8}$$

A much better approach is an integral approximation, which is proposed by Brookshaw [9].

$$\begin{aligned} I &= \nabla \cdot (\kappa \nabla f) + O(h^2) \\ &= \sum_j \left(\frac{m_j}{\rho_j}\right)(\kappa_i + \kappa_j)(f_i - f_j) \frac{\vec{r_i} - \vec{r_j}}{|\vec{r_i} - \vec{r_j}|^2 + \eta^2} \cdot \nabla_i W_{ij} \end{aligned} \tag{2.9}$$

where f is a scalar variable such as temperature, κ is a scalar, $\eta = 0.01h^2$ is the clipping constant η to prevent the singularities, h is the smoothing length.

Cleary and Monaghan [15] applied this particle scheme for heat conduction problems successfully.

Kernel Function

Kernel function are functions that satisfy the following conditions mentioned above: normalization condition, delta function condition and compactness condition.

A numerical method should always be checked with consistency conditions, which tell how good the numerical scheme represents the differential equations. A numerical scheme is consistent if it can exactly represent the differential equations as the grid or mesh size approaches zero.

The consistency conditions for SPH method can be derived two ways: one is a Taylor expansion the same way as finite difference method; another is to express the kernel function in the form of polynomial function and imposed the consistency condition, which is shown as follows[55].

For a constant function $f(x) = c_0$ to be exactly represented as:

$$f(x) = \int_\Omega c_0 W(r - r', h) dr' = c_0 \tag{2.10}$$

So the zero-th order consistency condition, which is actually the normal condition, is

$$M_0 = \int_\Omega W(r - r', h) dr' = 1 \tag{2.11}$$

For a linear function $f(x) = c_0 + c_1 r$ to be exactly represented, it requires:

$$f(x) = \int_\Omega (c_0 + c_1 r')W(r - r', h)dr' = c_0 + c_1 r \tag{2.12}$$

So the first order consistency condition is

$$\int_\Omega r' W(r - r', h)dr' = r \tag{2.13}$$

which is also can be written as

$$M_1 = \int_\Omega (r - r')W(r - r', h)dr' = 0 \tag{2.14}$$

So the consistency condition of the k-th order accuracy for kernel function is:

$$\begin{aligned} M_0 &= \int_\Omega W(r - r', h)dr' = 1 \\ M_1 &= \int_\Omega (r - r')W(r - r', h)dr' = 0 \\ M_2 &= \int_\Omega (r - r')^2 W(r - r', h)dr' = 0 \\ &\cdots \\ M_k &= \int_\Omega (r - r')^k W(r - r', h)dr' = 0 \end{aligned} \tag{2.15}$$

The most widely used kernel functions are in polynomial form.

$$W(r - r', h) = W(q) = a_0 + a_1 q + a_2 q^2 + \cdots + a_n q^n \tag{2.16}$$

where $q = \frac{r - r'}{h}$ is the relative distance between particles, h is the smoothing length or radius of compact support of kernel function.

The consistency conditions are used to construct the kernel function and determine the coefficients $a_0, a_1, ..., a_n$.

If the quadratic kernel function is in the form of

$$W(q) = c_0 + c_2 q^2 = c_0 + c_2 (\frac{r}{h})^2 \tag{2.17}$$

For compact support property $W(1) = 0$ and normal condition for two dimension, leads to:

$$\begin{aligned} c_0 + c_2 &= 0 \\ 1 &= \int_0^h (c_0 + c_2 (\frac{r}{h})^2)(2\pi r)dr \\ &= 2\pi h^2 (\frac{c_0}{2} + \frac{c_2}{4}) \end{aligned} \tag{2.18}$$

Solving it and get:

$$\begin{aligned} c_0 &= \frac{2}{\pi h^2} \\ c_2 &= -\frac{2}{\pi h^2} \end{aligned} \tag{2.19}$$

So the quadratic kernel function is

$$W(q) = \frac{2}{\pi h^2}(1 - q^2)$$

There are other forms of quadratic kernel function, which is used in this study:

$$W(r,h) = \begin{cases} \frac{3}{2\pi h^2}(0.25q^2 - q + 1.0 & \text{if } 0 \le q \le 1 \\ 0 & \text{otherwise} \end{cases} \tag{2.20}$$

Fulk and Quinn [31] analyzed many SPH kernels for the one-dimensional case and concluded that no kernel functions are significantly better than the bell-shaped kernels.

SPH method differs from other conventional numerical methods not only in approximation of derivatives but also in other aspects such as boundary condition, expression of viscosity, etc.

2.2 SPH Numerical Techniques

In SPH method, coupled differential equations are solved for every particles at each time step as will be discussed in Chapter 3 and 4. If each particle interacts with all others, the computational load scales as N^2, which is too expensive for large number of particles N. In practice, only the interactions of particles in a certain range are necessary and those further away can be neglected. This idea can be implemented by designing kernel function with compact support, also called the short-range model, which reduces the computation work dramatically.

2.2.1 Link List

To calculate a smoothed value of a property of particle i in SPH form, we need the information from its neighboring particles j. However we need to know which of

the N particles are neighboring particles. It takes considerable computational time to calculate the distance between the particle i and the other particles, to determine neighboring particles in the range of kernel function, $2h$. There are two techniques to minimize the number of particles that must be checked for neighbors[75].

The first technique is called a neighbor list, proposed by Verlet[95]. For each particle, an array is used to store the position of the particles within the range of particle i so that all the other particles need not be checked.

The second technique is the link-cell method. At every time step all the particles are binned into cells of side length equal to the radius of kernel function, so that all neighboring particles are binned in the surrounding cells. When searching the neighboring particles, only the surrounding cells are needed to be checked and it saves computation time.

Plimpton[75] states that the fastest algorithms on serial and vector machines use a combination of neighbor lists and link-cell method. Optimal performance can be achieved if extended cutoff distance is used instead of exact kernel width, because the neighbor lists would need to be updated once a few time steps, not every time step.

In present study the domain is divided into cells with side length of radius of kernel function $2h$, storing the information of cells that the number of particles and the list of particles in that cell. For particle i, first determine which cell it is located, then neighbor searching is limited in its neighboring cells.

2.2.2 XSPH

In numerical simulations, spatial filtering techniques are often used to reduce the numerical noise (error) to help with convergence and stability. The XSPH correction is a similar technique in the SPH method. It is especially important for high speed flow simulation. The numerical noise in velocity can even cause the particle penetration problem to make the simulation fail. For example, there are closely spaced particles. Every particle's velocity is similar but not exactly the same. The particle with higher velocity will pass over the others and it should not happen for continuum material, which is the particle penetration problem. The goal of the XSPH technique is to

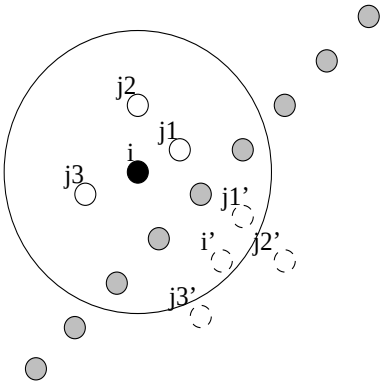

Figure 2.1: SPH boundary conditions: mirror-particle boundary, fluid particle on the northwest side of boundary particles, gray particles are boundary particles, dash particles are mirror particles of fluid particle, circle is the smoothing area of particle i.

use a corrected velocity which relates a particle's velocity with the velocity of its neighboring particle to move the particle smoothly.

$$\frac{dv_i}{dt} = v_i + \epsilon \Delta v_i \tag{2.21}$$

where

$$\Delta v_i = \sum_j \frac{m_j}{\rho_j}(v_j - v_i)W(r_i - r_j, h)$$

is the difference in velocity between the particle a and neighboring particles b. ϵ is a constant coefficient ranging from 0 to 1.

2.2.3 Boundary Condition

There are three categories boundary condition in SPH namely: mirror or ghost particle, real particle, and repulsive force methods. The figures 2.1 to 2.3 shows the three kinds of boundary conditions.

Mirror-particle boundary

Takeda *et al.*[92] and Libersky *et al.*[52] used imaginary particles (ghost particles) outside of boundary symmetric to the inside fluid particles to reduce the boundary effect on density and velocity. But this method will be difficult to use for irregular

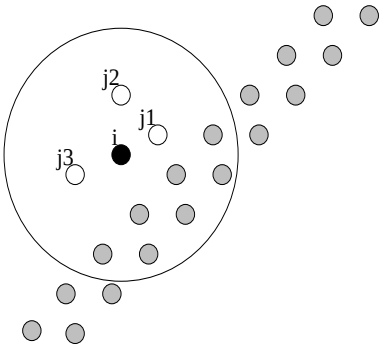

Figure 2.2: SPH boundary conditions: real particle boundary with staggered rows

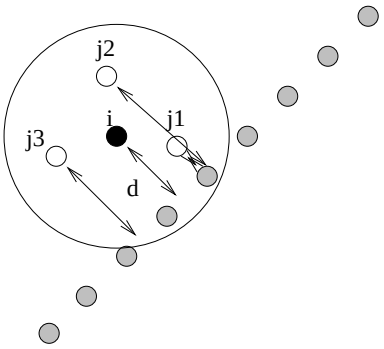

Figure 2.3: Three kinds of SPH boundary conditions: repulsive force boundary, d is the distance between fluid particles and boundary position

boundary shape or two phase flow problems. In the figure 2.1, the circle is the range of smoothing length of particle i. Particles $j1, j2, j3$ are the neighboring particles and $j1', j2', j3'$ are their mirror particles. When the smoothed or field value of particle i is calculated, the integration includes all neighboring particles, mirror particles and boundary particles.

Real particle boundary

Monaghan (1994) [63] used a pure repulsive force in the following Leonard-Jones form as the boundary force to mimic the known force between molecules:

$$f(\vec{r}) = \begin{cases} D[(\frac{r_0}{r})^{p_1} - (\frac{r_0}{r})^{p_2}]\frac{\vec{r}}{r^2}, & \text{if } r < r_0 \\ 0, & \text{otherwise} \end{cases} \tag{2.22}$$

where $f(\vec{r})$ is the force per unit mass acting on fluid particles by boundary, r is the distance between fluid and boundary particles, r_0 is the initial spacing of particles, p_1, p_2 are constants, D is a coefficient with dimension of v^2.

But another real particle condition is more stable and natural proposed by Dalrymple and Knio [19], which is shown in the figure 2.2. The smoothed or field value calculation of particle i includes neighboring particles and boundary particles. The double layers make sure that there is no truncation of integral if the smoothing length is selected carefully, for example, $h = 1.3\Delta x$. The advantage of this method is that the boundary particles are treated the same as all other particles, but just not allowed to move.

Repulsive force boundary

Monaghan[66] proposed another form based on interpolation to produce a uniform force normal to the boundary, which is good for particles more in a straight line at the boundary:

$$\vec{f}(x, y) = \vec{n}P(x)R(y) \tag{2.23}$$

where $\vec{n}$ is local unit normal vector from the boundary, x, y are the components of separation between fluid and boundary particle in horizontal and vertical direction, respectively.

$$P(x) = \begin{cases} \frac{1}{2}(1 + \cos\frac{\pi x}{\Delta p}), & \text{if } x < \Delta p \\ 0, & \text{otherwise} \end{cases}$$

$$R(y) = \begin{cases} A\frac{1}{\sqrt{q}}(1-q), & \text{if } q < 1 \\ 0, & \text{otherwise} \end{cases}$$

where $q = \frac{y}{\Delta p}$, Δp is initial particle spacing, $A = \frac{1}{h}(0.01h^2 + \beta c\vec{v_{ab}} \cdot \vec{n_b})$, and β is 1 as the particles are approaching, otherwise it is zero.

For particles near the boundary, the calculation of particle i only includes the neighboring water particles instead of boundary particles. The boundary particles only indicate the boundary position, not involving the calculation. The water particles in the force range feel a repulsive force from boundary, in which the magnitude of force depends on the perpendicular distance d between water particle and boundary, shown in the figure 2.3.

The implementation of real particle boundary condition in our SPH model is described as follows:

For a fixed boundary, we put particles along the boundary that have the same properties as the water particles and we calculate the density and pressure the same way as the water particles, but fix the particles location. In order to reduce the edge effects and prevent water particles from penetrating through the boundary on impact, we adopt the ragged double layer boundary. Because the velocity of boundary particle is zero, it is equivalent to a no-slip boundary condition.

For moving boundaries, we calculate the particles' density and pressure as if they are water particles but their motion is controlled by a given trajectory instead of by their neighbors. Each time step the moving boundary particle is put into a given position.

2.2.4 Kernel Correction (Normalization)

Another important aspect of SPH is kernel correction that is used for reducing the error caused by the truncation of kernel approximation integral for particles near the boundary. This is also called 'Corrected Smoothed Particle Hydrodynamics' (CSPH). The discrepancy can be eliminated by introducing an adjusting factor in the kernel function [8].

$$\widehat{W_b(x)} = W_b(x)\alpha(x)[1 + \beta(x)(r - r_b)] \tag{2.24}$$

where $\widehat{W_b(x)}$ is the kernel with first degree correction, α, β are the adjusting factors.

By imposing the consistency conditions, and solving the factor linearly, the corrected kernel is:

$$\widehat{W_b(x)} = \frac{W_b(x)}{\sum_{b=1}^{N} V_b W_b(x)} \tag{2.25}$$

where $V_b = m_b/\rho_b$.

2.3 SPH Applications

Since SPH method was invented in 1977 by the astrophysical community, it has been applied in many other fields, including engineering, to simulate dynamic response with material strength as well as fluid flow problem with large deformation. [54]

The SPH applications has been extended to both solid and fluid mechanics, including subjects as (fluid mechanics) multiphase flow [64], free surface flow [66], heat transfer and mass flow [15], flow through porous media and others; (solid mechanics) fracture of brittle materials [6], high velocity impact problem [74], etc.

Coastal engineering applications of SPH started in late 1990's [63][66].

The Dalrymple research group has developed and extended the SPH model to many coastal applications. Dalrymple and Knio [19] simulated the solitary wave propagation, breaking on plane beach using SPH numerical wave tank for the purpose of coastal engineering studies[19]. Gomez-Gesteira and Dalrymple[34] used the three dimensional SPH method to study the problem of the dam breaking and its impact on a tall structure. The model predict the velocity field, loading on the structure and the complicated free surface, compared with experimental data. They found that the dry bed and wet bed dam breaking have significant different consequences[20]. Zou and Dalrymple[101][72] used the two-phase flow SPH method to reproduce the landslide and wave generation, which happened in Lituya Bay, Alaska, the wave height and interaction between rock and water agree with scaled experiment fairly well. Rogers and Dalrymple[81] applied the two and three dimensional SPH model to study the wave breaking process and obliquely descending eddies (ODE) by solving N-S equation, coupling with LES. The model is able to show the details of wave propagation,

jet formation, breaking, forward and back splash, and vortices after breaking. With low resolution, the three dimensional model can capture the features of ODE, which is very important for sediment transport. Zou and Dalrymple[102][103][104] extend the SPH method to sediment transport simulation under the breaking waves. The wave breaking is modeled by SPH hydrodynamics model with LES. The sediment suspension is modeled by SPH sediment transport model by solving the convection-diffusion equation, including the sediment settling and sediment suspension by pick-up function and turbulent diffusion.

Colagrossi and Landrini[16] presented an original SPH implementation to deal with two dimensional interface flows with low density ratio, in which they used periodic re-initialization of density fields based on a moving-least-square interpolation. Cumo used two-phase SPH model to study the interaction of air and water phase.

Koshizuka *et al.*[49] proposed the moving particle semi-implicit method and has been applied for wave breaking[37], two-phase model for sediment settling[36], turbulence model[38].

Chapter 3

SPH Hydrodynamics Model

3.1 The Governing Equations and Boundary Condition

The SPH hydrodynamics model used in this study solves the momentum equation, conservation of mass, and equation of state for nearly compressible fluid.

Momentum Equation

The momentum equation describes the acceleration of fluid particles as determined by pressure gradient forces, body forces such as gravity, and viscous forces.

$$\frac{d\vec{v}}{dt} = -\frac{1}{\rho}\nabla P + \nu\nabla^2\vec{v} + \vec{f} + \frac{1}{\rho}\nabla\cdot\overline{\tau} \tag{3.1}$$

where $\frac{d}{dt}$ is total derivative, $\vec{v}$ is the velocity of the particle, $-\frac{1}{\rho}\nabla P$ is the pressure gradient force, $\nu\nabla^2\vec{v}$ is the viscous force, $\vec{f}$ is the body force, $\frac{1}{\rho}\nabla\cdot\overline{\tau}$ is the large eddy simulation term, accounting for the turbulent motion on scales smaller than the computational resolution, which will be explained in the next section. $\overline{\tau}$ is SPS stress tensor.

Conservation of Mass

This describes the mass conservation of water particles. Due to the compressibility, the change of density of particles, ρ, is determined by the divergence of particles.

$$\frac{1}{\rho}\frac{d\rho}{dt} + \nabla\cdot\vec{v} = 0 \tag{3.2}$$

Equation of State

For constant density or incompressible flow, there is no connection between pressure and density. Its continuity equation is expressed by solenoidal or divergence-free velocity field:

$$\nabla \cdot \overrightarrow{U} = 0 \tag{3.3}$$

Take the divergence of N-S equation and get:

$$(\frac{D}{Dt} - \nu\nabla^2)(\nabla \cdot \overrightarrow{U}) = -\frac{1}{\rho}\nabla^2 p - \frac{\partial U_i}{\partial x_j}\frac{\partial U_j}{\partial x_i} = 0 \tag{3.4}$$

So the Poisson equation is a necessary and sufficient conditions for a solenoidal velocity field to remain solenoidal.

$$\nabla^2 p = -\rho\frac{\partial U_i}{\partial x_j}\frac{\partial U_j}{\partial x_i} = \frac{\omega_{ij}^2}{2} - S_{ij}^2 \tag{3.5}$$

$$S_{ij} = \frac{1}{2}(\frac{\partial U_i}{\partial x_j} + \frac{\partial U_j}{\partial x_i}) \tag{3.6}$$

$$\omega_{ij} = \frac{1}{2}(\frac{\partial U_i}{\partial x_j} - \frac{\partial U_j}{\partial x_i}) \tag{3.7}$$

where S_{ij} is the rate of strain tensor and ω_{ij} is the rate of rotation tensor.

This Poisson equation is solved in many CFD models and it is time-consuming to solve.

The incompressibility approximation is a common technique in SPH method in order to solve for pressure without using the Poisson equation, thinking of pressure as a thermodynamic variable and related to density by an equation of state. The present model uses the following equation of state: [4]

$$P = B[(\frac{\rho}{\rho_0})^\gamma - 1] \tag{3.8}$$

where $\rho_0 = 1000kg/m^3$ is the reference density of water, $\gamma = 7$ is a polytropic constant for equation of state, B is a constant which is chosen based on the speed of sound c_s in slight compressible fluid, $c_s = \sqrt{\frac{\partial P}{\partial \rho}}$, and it is noted that here $c_s = 10u_{max}$ is used to keep Mach number less than 0.1, meaning that the compressibility is negligible; u_{max} is the maximum velocity of particles.

3.2 Large Eddy Simulation: Sub-particle Scheme

3.2.1 Approaches for Turbulent Flows and Breaking Waves Simulation

The study of turbulent flow is very difficult and there is no simple analytic theory. But both numerical models and experimental methods of turbulent flow have progressed in recent decades. This section will focus on the computational approaches.

Direct Numerical Simulation (DNS) solves the Navier-Stokes (N-S) equation for instantaneous velocity and resolves all length scales and timescales, from which all other information can be determined. DNS is the most advanced turbulent model but is computationally expensive, which is increased as Re^3[76]. Therefore, it is applicable for situations with low Reynolds numbers. Due to large computational cost, DNS is used as a supplement for experiments of turbulence, since some properties are impossible to obtain experimentally.

Large Eddy Simulation (LES) solves the N-S equations on a coarse grid for filtered velocity of large-scale turbulent motions and models the effect of small-scale motions as additional terms.

The Reynolds-Averaged Navier-Stokes (RANS) model solves the Reynolds equation to obtain the mean velocity. The turbulent-viscosity model is a widely used model and there are other turbulent Reynolds-stress related models, based on the different closure methods for Reynolds stress. The mixing length model is one of the simplest approaches. Turbulent-viscosity models are based on a turbulent-viscosity hypothesis that assumes the Reynolds-stress term $\overline{u_i' u_j'}$ is determined by the mean velocity gradients $\partial \overline{U_i}/\partial x_j$ [76]:

$$\begin{aligned} \overline{u_i' u_j'} &= -\nu_T \left(\frac{\partial \overline{U_i}}{\partial x_j} + \frac{\partial \overline{U_j}}{\partial x_i}\right) \\ &= -2\nu_T \overline{S}_{ij} \end{aligned} \tag{3.9}$$

where $\overline{S}_{ij}$ is the mean rate-of-strain tensor, analogous to viscous stress $-2\nu S_{ij}$.

In order to capture turbulence during the breaking process, the sub-particle scale

(SPS) method is applied[56][81]. This is equivalent to the sub-grid scale (SGS) in Euler equations and is able to simulate the turbulence at scales smaller than particle scale.

3.2.2 Derivation of Sub-Particle Scheme

The turbulent velocity field can be separated by filtered and residual parts by Filtering Decomposition:

$$< U(x,t) >= \int G(x,t)U(x-r,t)dr$$

$$U(x,t) =< U(x,t) > +u''(x,t) \tag{3.10}$$

where $< U(x,t) >$ is the filtered velocity and $u''(x,t)$ is the residual velocity field.

Continuity Equation:

$$\nabla \cdot U(x,t) = 0 \tag{3.11}$$

because both $< U(x,t) >$,$u''(x,t)$ are divergence free so that:

$$\nabla \cdot < U(x,t) >= 0 \tag{3.12}$$

$$\nabla \cdot u''(x,t) = 0 \tag{3.13}$$

Momentum Equation:

Filter the N-S equation:

$$\frac{DU_i}{Dt} = \frac{\partial U_i}{\partial t} + \frac{\partial (U_j U_i)}{\partial x_j} = -\frac{1}{\rho}\frac{\partial P}{\partial x_i} + \nu \frac{\partial^2 U_i}{\partial x_j \partial x_j} \tag{3.14}$$

Substitute the Filtering Decompositions for U and continuity equation:

$$< U_j U_i > \;=\; < U_j >< U_i > + < u_j'' u_i'' > \tag{3.15}$$

$$\frac{\partial U_i}{\partial x_i} \;=\; 0 \tag{3.16}$$

To obtain the filtered momentum equations:

$$\frac{\overline{D}U_i}{\overline{D}t} = \frac{\partial < U_i >}{\partial t} + < U_j > \frac{\partial < U_i >}{\partial x_j} = -\frac{1}{\rho}\frac{\partial < P >}{\partial x_i} + \nu \frac{\partial^2 < U_i >}{\partial x_j \partial x_j} - \frac{\partial < u_j'' u_i'' >}{\partial x_j} \tag{3.17}$$

Using the Smagorinsky model, which is the simplest residual stress model:

$$\overline{S_{ij}} = -\frac{1}{2}(\frac{\partial < U_i >}{\partial x_j} + \frac{\partial < U_j >}{\partial x_i}) \tag{3.18}$$

$$\tau_{ij}^r = < u_j'' u_i'' >= -2\nu_t \overline{S_{ij}} \tag{3.19}$$

$$\nu_t = (C_s\Delta)^2 \overline{S} \tag{3.20}$$

where $\overline{S_{ij}}$ is the filtered rate of strain, $\overline{S} = (2\overline{S_{ij}S_{ij}})^{1/2}$ is the magnitude filtered rate of strain, ν_t is the eddy viscosity of residual motions, ν is the kinematic viscosity, C_s is a model constant, and Δ is the filter width.

Finally the filtered (resolved-scale) momentum equation is:

$$\frac{\overline{D}U_i}{\overline{D}t} = \frac{\partial < U_i >}{\partial t} + < U_j > \frac{\partial < U_i >}{\partial x_j} = -\frac{1}{\rho}\frac{\partial < P >}{\partial x_i} + (\nu + \nu_t)\frac{\partial^2 < U_i >}{\partial x_j \partial x_j} \tag{3.21}$$

$$\frac{\tau_{ij}}{\rho} = 2\nu_t S_{ij} - \frac{2}{3}k\delta_{ij} \tag{3.22}$$

$$\nu_t = (C_s\Delta l)^2 \|\overline{S}\| \tag{3.23}$$

$$\|\overline{S}\| = (2S_{ij}S_{ij})^{1/2} \tag{3.24}$$

where S_{ij} is SPS strain tensor, k is the SPS turbulence kinetic energy, ν_t is turbulence eddy viscosity, Δl is particle spacing and C_s is Smagorinsky constant.

For a compressible fluid the SPS scaling requires a special averaging: Favre-averaging ($\tilde{f} = \overline{\rho f}/\overline{\rho}$), the filtered equation is similar with incompressible results except the SPS stress tensor is[20][81]:

$$\frac{\tau_{ij}^*}{\overline{\rho}} = (2\nu_t \tilde{S}_{ij} - \frac{2}{3}k\delta_{ij}) - \frac{2}{3}C_I\Delta^2\delta_{ij} \tag{3.25}$$

where $C_I = 0.00066$ is a constant, $\tilde{?}$ means favre-averaging, and $\overline{?}$ is spatial-filtering.

3.3 Numerical Solution for Hydrodynamics Model

3.3.1 Methodology for Numerical Solution in Particle Form

In applying the SPH method, the governing equations have to be converted into the particle approximation form. The following shows the fundamentals to convert the general equations into particle form. This procedure will be applied for derivation of governing equations of the SPH hydrodynamics model.

For the derivation of the SPH formalism, Monaghan set up the 'golden rule' that you should rewrite a formula with the density placed within the operators[62]. The following are the expressions for gradient, divergence and vorticity, respectively:

$$\rho\nabla f \Rightarrow \nabla(\rho f) - f\nabla\rho \tag{3.26}$$

Similarly,

$$\rho\nabla \cdot A \Rightarrow \nabla \cdot (\rho A) - A \cdot \nabla\rho \tag{3.27}$$

$$\rho\nabla \times A \Rightarrow \nabla \times (\rho A) - A \times \nabla\rho \tag{3.28}$$

So we can express them in particle form:

$$\begin{aligned}
\rho_a(\nabla \cdot v)_a &= (\nabla \cdot (\rho v) - v \cdot \nabla\rho)_a \\
&\simeq \nabla \cdot \int_\Omega (\rho v) W(r - r', h) dr' - v \cdot \int_\Omega (\nabla\rho) W(r - r', h) dr' \\
&\simeq \sum_b \frac{m_b}{\rho_b} (\rho v)_b \cdot \nabla W(r_a - r_b, h) - v_a \cdot \sum_b \frac{m_b}{\rho_b} \rho_b \nabla W(r_a - r_b, h) \\
&= \sum_b m_b v_b \cdot \nabla W_{ab} - \sum_b m_b v_a \cdot \nabla W_{ab} \\
&= \sum_b m_b (v_b - v_a) \cdot \nabla W_{ab} \\
&= \sum_b m_b v_{ab} \cdot \nabla_a W_{ab}
\end{aligned} \tag{3.29}$$

Here $v_{ab} = v_a - v_b$ and $W_{ab} = W(r_a - r_b, h)$.

$$\begin{aligned}
\rho_a(\nabla \times v)_a &\simeq \int_\Omega (\nabla \times (\rho v) - v \times \nabla\rho) W(r - r', h) dr' \\
&\simeq \sum_b \frac{m_b}{\rho_b}(\rho v)_b \times \nabla W(r_a - r_b, h) - v_a \times \sum_b \frac{m_b}{\rho_b}\rho_b \nabla W(r_a - r_b, h) \\
&= \sum_b m_b v_b \times \nabla W_{ab} - \sum_b m_b v_a \times \nabla W_{ab} \\
&= \sum_b m_b (v_b - v_a) \times \nabla W_{ab} \\
&= \sum_b m_b v_{ab} \times \nabla_a W_{ab} \qquad (3.30)
\end{aligned}$$

Note that in the last step, the gradient of the kernel with respect to r' has changed to that with respect to r.

3.3.2 Discretized Form

The numerical algorithm for the governing equations is described term by term here:

$$\frac{d\vec{v}}{dt} = -\frac{1}{\rho}\nabla P + \nu\nabla^2\vec{v} + \vec{f} + \frac{1}{\rho}\nabla \cdot \overline{\tau} \qquad (3.31)$$

$$\frac{1}{\rho}\frac{d\rho}{dt} + \nabla \cdot \vec{v} = 0 \qquad (3.32)$$

Pressure gradient force

The pressure gradient force for particle i is expressed by symmetric form for the conservation of linear and angular momentum [62]:

$$(-\frac{1}{\rho}\nabla P)_i = -\sum_j m_j (\frac{P_j}{\rho_j^2} + \frac{P_i}{\rho_i^2})\nabla_i W_{ij} \qquad (3.33)$$

where m_i is the mass of the ith particle, j is the index for neighboring particles, $\nabla_i W_{ij} = \nabla_i W(x_i - x_j)$.

Viscous forces

The viscosity in the SPH method is another numerical issue. There are two kinds of expressions for viscosity currently used in SPH method. One is the artificial viscosity

invented by Monaghan[61] which is designed to stabilize the numerical algorithm.

$$\Pi_{ab} = \begin{cases} \frac{-\alpha\overline{c_{ab}}\mu_{ab}+\beta\mu_{ab}^2}{\overline{\rho_{ab}}}, & \overrightarrow{v}_{ab} \cdot \overrightarrow{r}_{ab} < 0 \\ 0, & \overrightarrow{v}_{ab} \cdot \overrightarrow{r}_{ab} > 0 \end{cases} \tag{3.34}$$

where

$$\mu_{ab} = \frac{h\overrightarrow{v}_{ab} \cdot \overrightarrow{r}_{ab}}{r_{ab}^2 + \eta^2}$$

The average sound speed is $\overline{c_{ab}} = \frac{c_a+c_b}{2}$; average density is $\overline{\rho_{ab}} = \frac{\rho_a+\rho_b}{2}$, $\eta = 0.1h$ is a clipping constant to prevent Π_{ab} from going to infinity, and α and β are constants dependent on the particular case. The former term (α) is the bulk viscosity and the latter term (β) is the Von Neumann-Richtmyer viscosity, which is only used in shock simulations and can be neglected for the small Mach number case.

This artificial viscosity is not used in this study because it is too dissipative. We use the following formulation.

The other expression for viscosity is to calculate the viscous term with velocity derivative using the SPH methodology [92]. This method is related to physical viscosity. Morris *et al.* proposed a better expression in conservative form:

$$(\nu\nabla^2\vec{v})_i = \sum_j \frac{\nu(\rho_i+\rho_j)}{\overline{\rho}_{ij}^2} \frac{r_{ij} \cdot \nabla_i W_{ij}}{r_{ij}^2 + 0.01h^2} v_{ij} \tag{3.35}$$

where $\nu = 10^{-6}m^2/s$ is the kinematic viscosity, h is the smooth length, $v_{ij} = v_i - v_j$ is the velocity difference of particle i and j, $\overline{\rho_{ij}} = (\rho_i + \rho_j)/2$, $r_{ij} = r_i - r_j$.

The viscous term is calculated by the laminar stress improved by Morris *et al.* [67].

$$(\nu\nabla^2\vec{v})_i = \sum_j \frac{\nu(\rho_i+\rho_j)}{\overline{\rho}_{ij}^2} \frac{r_{ij} \cdot \nabla_i W_{ij}}{r_{ij}^2 + 0.01h^2} v_{ij} \tag{3.36}$$

where $\nu = 10^{-6}m^2/s$ is the kinematic viscosity, h is the smooth length, $v_{ij} = v_i - v_j$ is the velocity difference of particle i and j, $\overline{\rho_{ij}} = (\rho_i + \rho_j)/2$, $r_{ij} = r_i - r_j$.

SPS scheme

The SPS scheme is in the form of pressure gradient term with symmetric formulation for momentum conservation, given by Lo and Shao [56].

$$(\frac{1}{\rho}\nabla \cdot \overline{\tau})_i = \sum_j m_j (\frac{\overrightarrow{\tau_i}}{\rho_i^2} + \frac{\overrightarrow{\tau_j}}{\rho_j^2}) \cdot \nabla_i W_{ij} \tag{3.37}$$

where $\overrightarrow{\tau}$ is the SPS stress tensor calculated by the Smagorinsky model[81][56].

Mass of Conservation

The rate of change of density is calculated based on the divergence of velocity.

$$(\frac{d\rho}{dt})_i = \rho_i \sum_j \frac{m_j}{\rho_j} v_{ij} \cdot \nabla_i W_{ij} \tag{3.38}$$

where i is the label of the particle of interest, and j is the label for the neighboring particles.

3.3.3 Predictor-Corrector Method

Numerical integration can be classified into two major types of algorithms. Explicit methods have the several advantages including ease of programming, little memory use and less computation. One downfall is that this method is unstable for a large time step. Implicit methods can use a larger time step and are very stable. The predictor-corrector method is an attempt to combine the best aspects of the two methods[27].

The basic idea behind the 2nd order predictor-corrector method is that the solution for a new time step is predicted using the explicit Euler method, $\phi^{(n+1)*}$ (which is not the final value of the time step t^{n+1}). The final solution is corrected by applying the trapezoid rule of $\phi^{(n)}$ and $\phi^{(n+1)*}$.

$$\begin{aligned} \phi^{(n+1)*} &= \phi^{(n)} + f(t_n, \phi^{(n)})\Delta t \\ \phi^{(n+1)} &= \phi^{(n)} + \frac{1}{2}[f(t_n, \phi^n) + f(t_{n+1}, \phi^{(n+1)*})] \end{aligned} \tag{3.39}$$

There are many other more complicated methods that can be used, which have higher order of accuracy.

3.3.4 Verlet

In molecular dynamics, the most commonly used time integration algorithm is the Verlet algorithm [95]. The basic idea is to write two third-order Taylor expansions

for the positions, one forward and one backward in time. Calling $v(t)$ the velocities, $a(t)$ the accelerations, and $b(t)$ the third derivatives of with respect to t, one has:

$$\begin{aligned} r(t+\Delta t) &= r(t) + v(t)\Delta t + (1/2)a(t)(\Delta t)^2 + 1/6b(t)(\Delta t)^3 + O((\Delta t)^4) \quad (3.40) \\ r(t-\Delta t) &= r(t) - v(t)\Delta t + (1/2)a(t)(\Delta t)^2 - 1/6b(t)(\Delta t)^3 + O((\Delta t)^4) \end{aligned}$$

Adding these together:

$$r(t+\Delta t) = 2r(t) - r(t-\Delta t) + a(t)(\Delta t)^2 + O((\Delta t)^4) \quad (3.41)$$

A better algorithm called the the velocity Verlet Scheme, shows that:

$$\begin{aligned} r(t+\Delta t) &= r(t) + v(t)\Delta t + (1/2)a(t)(\Delta t)^2 \quad (3.42) \\ v(t+\Delta t/2) &= v(t) + (1/2)a(t)\Delta t \\ v(t+\Delta t) &= v(t+\Delta t/2) + (1/2)a(t+\Delta t)\Delta t \end{aligned}$$

The Verlet algorithm uses positions and accelerations at time t and the positions from time t-dt to calculate new positions at time t+dt. The Verlet algorithm uses no explicit velocities. The advantages of the Verlet algorithm are: i) it is straightforward, and ii) the storage requirements are modest. This algorithm is more accurate than the simplest predictor-corrector method.

3.3.5 Shephard Filter

The Shephard filter is used in order to increase the model stability with the Verlet algorithm [8] [20].

$$\rho_i = \frac{\sum_j \rho_j W_{ij} V_j}{\sum_j W_{ij} V_j} \quad (3.43)$$

3.4 Numerical Wave Tank

Numerical Wave Tank (NWT) refers to computer codes that are able to reproduce the physical wave basin or flume as closely as possible. The program very

accurately accounts for free surface wave generation, propagation, breaking, current, sediment transport, floating body interaction, wave loading on structures, and several other applications. The typical numerical methods used for NWT simulation are the boundary element method (BEM), finite element method (FEM) and finite volume method (FVM). In this study, we will set up NWT with the SPH method in order to validate the SPH simulation.

The water body is simulated by Lagrangian smoothed particles whose motion is governed by N-S equation. The boundaries of the domain are bounded by particles. The wavemaker is composed of boundary particles with given position and velocity at each time step. The boundary condition for sediment concentration model will be discussed in the next chapter.

3.4.1 Wavemaker

In order to create different wave types, we have developed several kinds of wavemakers including sinusoidal wave, solitary wave, cnoidal wave, and other shallow water wavemaker. The wavemaker is composed of moving boundary particles with given trajectories in time. They interact with water particles as a result of pressure or boundary forces, depending on the boundary condition used in the model. Some formulation and theoretical background are presented to show how to implement the wavemaker in SPH modeling. Most of the test cases use shallow water waves, so we only discuss the piston wavemaker here.

Sinusoidal Wavemaker

This is the simplest wavemaker. At each time step, the displacement of wavemaker particles is given by a sinusoidal function, and its velocity equals to its derivative.

$$\begin{aligned} x_p(i) &= x_0(i) + S(1. + \cos(\omega t - \pi)) \\ u_p(i) &= -S\omega \sin(\omega t - \pi) \end{aligned} \tag{3.44}$$

where x_p and u_p are the position and velocity of wavemaker particles, respectively. i is the identity or index of particles, x_0 is the initial position of wavemaker particles,

S is the stroke of the wavemaker that is related to wave height and water depth (refer to wavemaker theory for details in Dean and Dalrymple's book[21]), ω is the angular frequency and t is the time. The phase shift is intended to start the wavemaker at zero velocity, otherwise it could cause some instability.

Solitary Wavemaker

Solitary waves and cnoidal waves are typically used to represent the characteristics of tsunamis. Both of these wavemakers are programmed by the Goring wavemaker theory [35]. The Goring wavemaker formula eliminates the unacceptable trailing waves by matching the velocity of the wavemaker with the corresponding velocity of the water particles. Based on theoretical analysis, Goring proposed the formula for a solitary wavemaker:

$$\frac{\xi}{S} = \frac{1}{2}\{1 + \tanh 2[(3.80 + \frac{H}{h})(\frac{t}{\tau} - \frac{1}{2}) - \frac{H}{h}(\frac{\xi}{S} - \frac{1}{2})]\} \tag{3.45}$$

where ξ is the displacement of the wavemaker from $x = 0$.
The following parameters are needed:

$$\begin{aligned} \kappa &= \sqrt{\frac{3H}{4h^3}} \\ S &= \frac{2H}{\kappa h} = \sqrt{\frac{16H}{3h}}h \\ c &= \sqrt{g(h+H)} \\ \tau &= 2t_0 + S/c = \frac{2}{\kappa c}(3.80 + \frac{H}{h}) \end{aligned} \tag{3.46}$$

where H is the wave height, h is water depth, κ is equivalent to wave number, S is the stroke of the wavemaker, c is the phase speed of wave, and τ is the duration of wavemaker motion.

The SPH model uses the normalized form of generation equation 3.45 for solitary wavemaker.

Cnoidal Wavemaker

Zelt [100] wrote the code based on Goring's wavemaker theory that produces the control signal of wave paddle. Ting and Kirby also used this in their experimentation

on spilling and plunging breakers. The code is modified and adopted for use in the SPH model. The parameters of wave train and generation equations are listed as the following:

$$\begin{aligned}
\eta &= (y_t - h) + Hcn^2\{2K(\frac{x}{L} - \frac{t}{T})|m'\} \\
y_t &= \frac{H}{K(1-m')}(K-E) + h - H \\
\frac{HL^2}{h^3} &= \frac{16}{3}K^2(1-m') \\
c &= \frac{L}{T} = \sqrt{gh}\{1 + \frac{H}{h}[(\frac{2}{1-m'}) - (\frac{3E}{(1-m')K})]\}
\end{aligned} \tag{3.47}$$

where h is the depth, H is the wave height, K and E are the first and second complete elliptic integrals respectively (for the details about the calculation refer to the Appendix of Goring's thesis). y_t is the distance to the trough from the bottom, L is the wave length, and T is the wave period, m' and m are the elliptic parameter and $m = 1 - m'$.

The non-dimensional form is:

$$\begin{aligned}
\frac{y_t}{h} &= \frac{H/h}{m}(1 - \frac{E}{K}) + 1 + \frac{H}{h} \\
\theta_0 &= cn^{-1}(\sqrt{\frac{1 - y_t/h}{H/h}}|m) \\
\frac{\xi_{max}}{L} &= \frac{1}{2K}\{(y_t/h - 1)\theta_0 + \frac{H/h}{m}[E(\theta_0|m) - m'\theta_0]\} \\
\frac{c}{\sqrt{gh}} &= 1 + \frac{H}{h}(\frac{2}{m} - \frac{3E}{mK}) \\
\frac{S}{h} &= \frac{2\xi_{max}}{h} = 2\frac{\xi_{max}}{L} * \frac{L}{h} \\
T^* &= \frac{L/h}{c/\sqrt{gh}} \\
\frac{\xi}{S} &= \frac{L/(2\xi_{max})}{2K}\{(y_t/h - 1)\theta + \frac{H/h}{m[E(\theta|m) - m'\theta]}\}
\end{aligned} \tag{3.48}$$

We then use the Newton-Ralphson method to solve the generation equation and find the trajectory of the wavemaker.

For the real implementation, we generate the trajectory of the cnoidal wavemaker and save it as the external data file. The SPH model reads the data and interpolates

for each time step. It is noted that we add the ramp function to avoid the impulse motion of the wavemaker. The figure 3.1 shows the wavemaker trajectory by solitary wave and cnoidal wave.

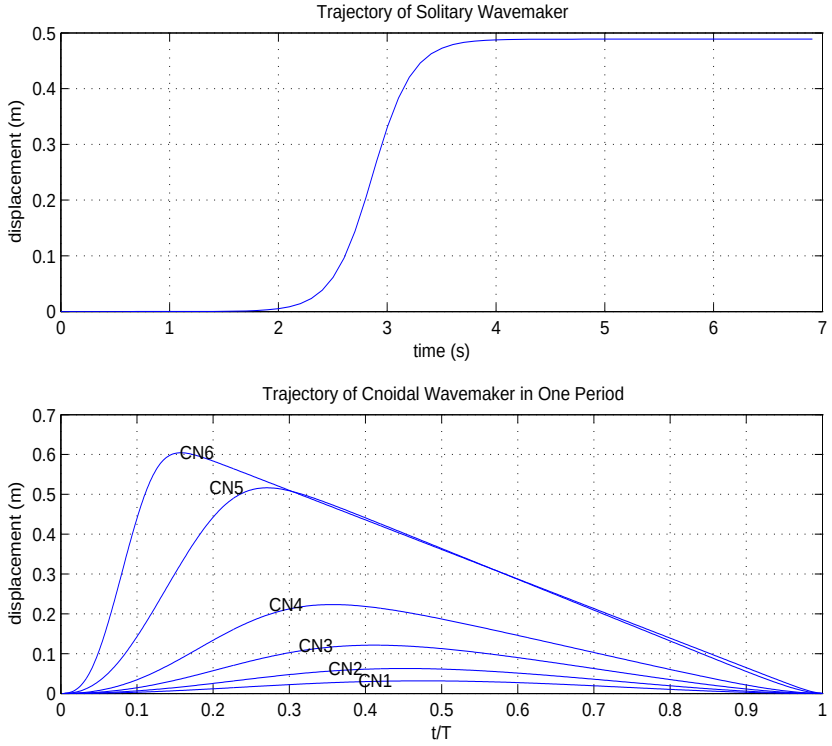

Figure 3.1: Examples of trajectory of wavemaker: above, solitary wavemaker; below, periodic cnoidal wavemaker.

3.4.2 Boundary Condition

As mentioned before, the link between water particles and boundary particles depends on the kind of boundary condition. There are two kinds of boundary conditions for SPH hydrodynamics model used in this study, classified by its action force: pressure and boundary force boundary condition.

The *pressure boundary condition*: It is also referred to as particle boundary condition, proposed by Dalrymple *et al.*[19]. Particles are put along the boundary position in two staggered rows for the purpose of reducing the error caused by cut off of in-

tegration. They are involved in all calculations as the water particles for velocity, pressure and density, but without updating their positions. When the water particle approaches the boundary particles, the density becomes larger than the reference density, which generate a positive pressure according to the equation of state. This pressure force prevent them from getting closer and the force applied to the water particles appear as the pressure gradient term in N-S equation. This boundary condition is locally in equilibrium and natural, because there is no obvious gap between water particles and boundary particles. But in some cases, if the water particle manage to pass through the boundary, the instabilities can result in the domain of computation has to expand.

The *boundary force boundary condition*: The boundary particles that are placed along the boundaries indicate the boundary position. They are not involved in the calculation for velocity or pressure, but provide a means to note distance. The water particles near the boundary are affected by the boundary force from boundary particles, depending upon the distance between them. The boundary forces acting on water particles appear as the external force terms in the N-S equation. This boundary condition is good for uniformly shaped boundaries and can prevent the water particles from passing through. But it is hard to determine the proper relation of magnitude of force and distance for irregular shape or slope. Usually it needs adjustment by a correction function.

The proper boundary force is crucial for the simulation of waves near the shoreline. In order to accurately model the run-up of water waves along the beach slope, the boundary force near the shoreline should be treated carefully. The figure 3.2 shows an example of the different results due to the use of different correction functions.

The repulsive boundary force with improved correction function from Rogers and Dalrymple[81] is:

$$\overrightarrow{f}(x,y) = \epsilon_Z(y)P(x)R(y)\overrightarrow{n} \tag{3.49}$$

$$\epsilon_Z(x,y) = \begin{cases} 1 & \text{if } h_* \geq 1.0 \\ 0.2 + p_* & \text{if } 0.1 \leq h_* < 1.0 \\ 0.2 + h_* + p_* & \text{if } h_* < 0.1 \end{cases} \tag{3.50}$$

where $h_* = y/h_0$ is the non-dimensional water depth of (x,y), h is the total water depth, $p_* = (u^2 + v^2)/\sqrt{2gh}$ is the non-dimensional dynamic pressure.

The pressure boundary condition is used as non-slip boundary condition and boundary force boundary condition as slip boundary condition.

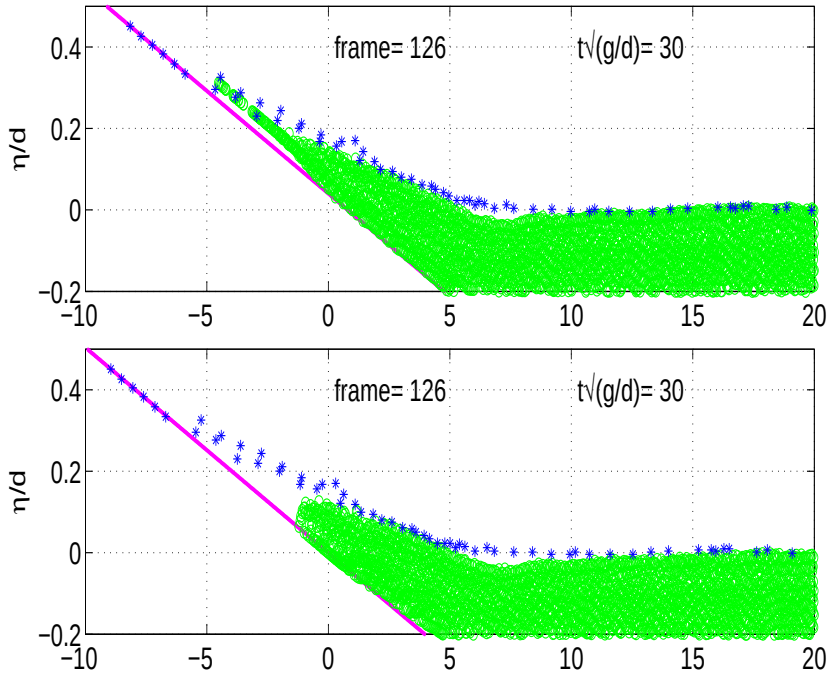

Figure 3.2: An example of different correction function for boundary force boundary condition: above with improved correction function; below, old boundary condition

3.5 Validation of Hydrodynamics Model

The run-up of waves on beaches is a difficult subject due to the breaking and bore propagation process. This includes the transition of unbroken waves to the bore as they approach the shore. The Dalrymple research group has validated the SPH model

for giant waves and impact of fluid-structure interaction[34][33]. In this study, the quality of the SPH model to predict the wave propagation, breaking, bore propagation and run-up of waves on a beach slope is tested, numerical results are compared with laboratory data of Synolakis (1986, 1987) [91] [90] for the run-up of solitary waves.

3.5.1 Experiment Setup

To evaluate the coastal effects of tsunamis, Synolakis (1986) performed a theoretical and experimental investigation of the run-up of long waves on a plane beach. We briefly described the experiment setup here. For the details on experimental apparatus and procedures, please refer to Synolakis's thesis [91]. The experiments were performed in the 40m wave tank facility located at the W. M. Keck Laboratory of the California Institute of Technology. The dimensions of the wave tank are 37.73m $\times$ 0.61m $\times$ 0.39m. There is a ramp installed at one end of the tank, which models the plane beach and has a slope of 1:19.85. It is constructed of an aluminum plate that is hydrodynamically smooth. At the other end a piston functions as the wave generator. The distance between the toe of the ramp and piston is 14.95m.

3.5.2 Comparison of Results

Two different waves were compared with the numerical model: $H/d = 0.04$ and $H/d = 0.28$. The selection of these two cases is based on the observations of Synolakis. Breaking did not occur for the $H/d = 0.04$ wave, while the $H/d = 0.28$ wave broke strongly during both of the run-up and run-down processes.

Non-breaking Case: $H/d = 0.04$

Figures 3.3 3.5 show the comparison of free surface profiles between the SPH model and experiment data at different time instances. It is noted that the figures show the entire slope, the toe of the slope is located at $x/d = 19.85$. At time $t\sqrt{g/d} = 26$, 32 and 36, the incident wave approaches the shoreline and just starts to run up the plane beach. The SPH model results slightly underestimate the peak and overestimate the water level near the toe of the slope. This mismatch is likely caused by the vertical resolution because the wave height is only 4% of the water depth. At time $t\sqrt{g/d} =$

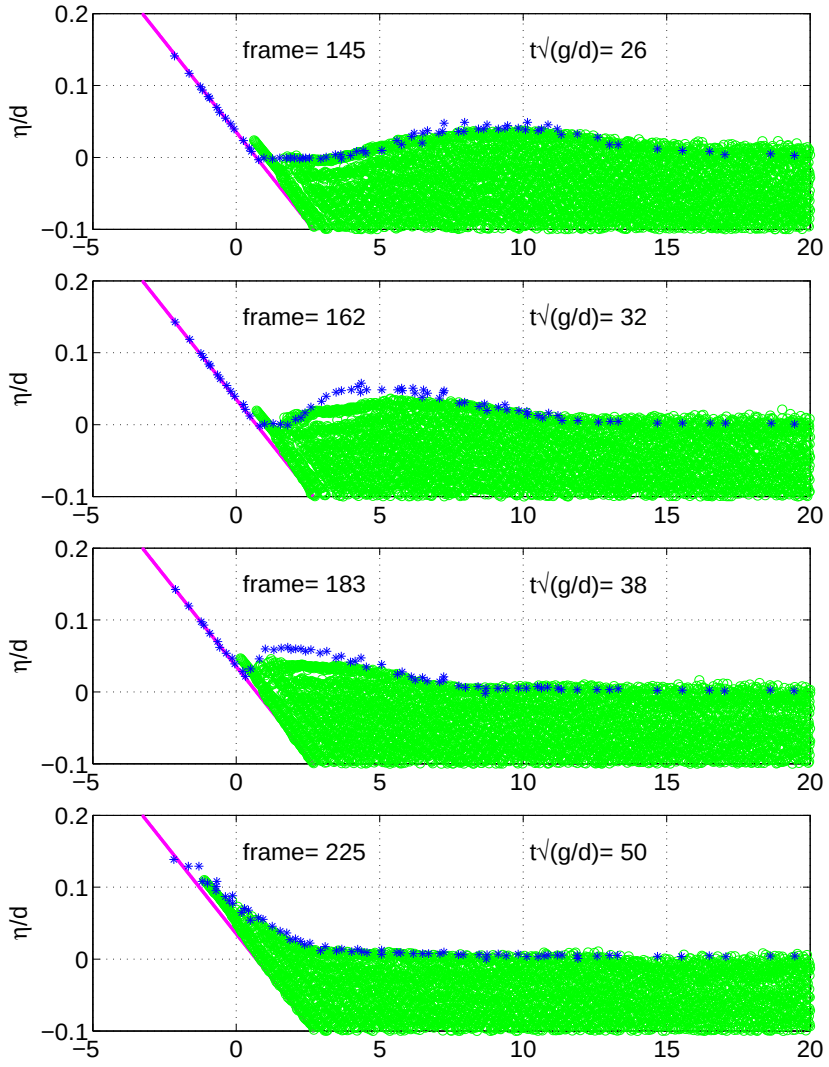

Figure 3.3: Comparison of non-dimensional free surface profiles for the non-breaking case $H/d = 0.04$ solitary wave at non-dimensional time $t\sqrt{g/d} = 26, 32, 36, 38, 50, 56, 60, 62, 66, 72, 78$; open circles, SPH model; star symbols, experiments (Synolakis(1987))

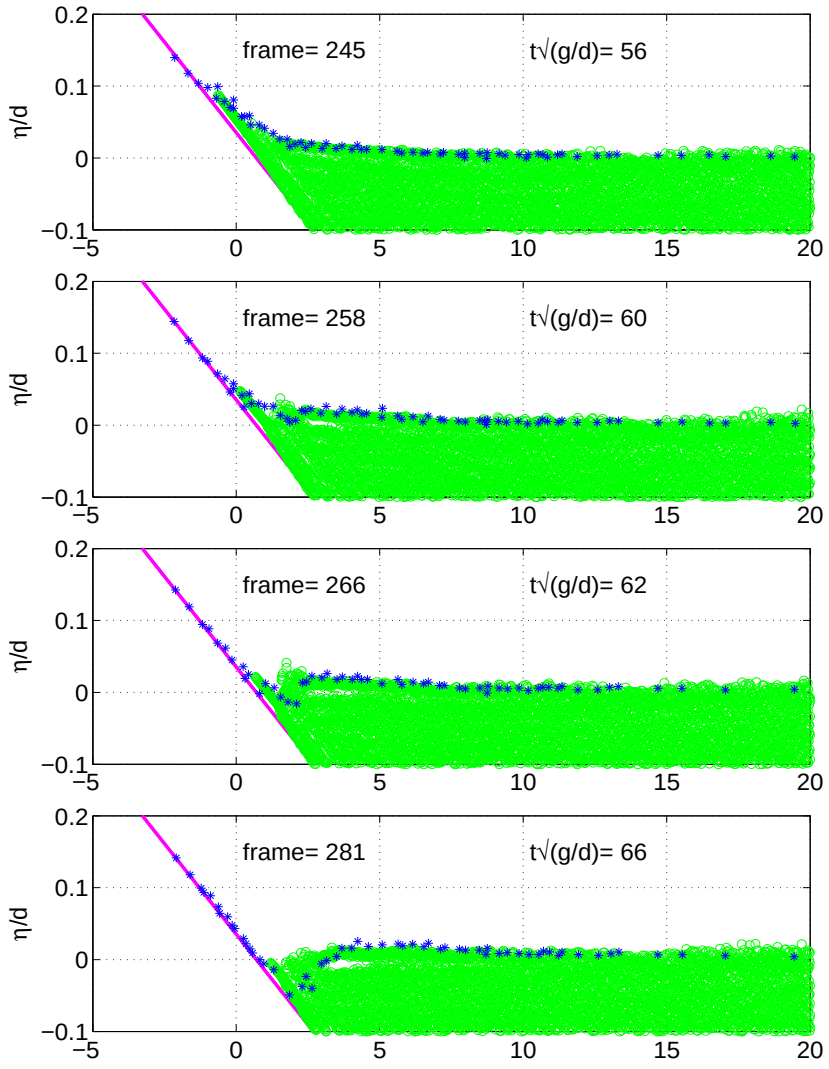

Figure 3.4: continued

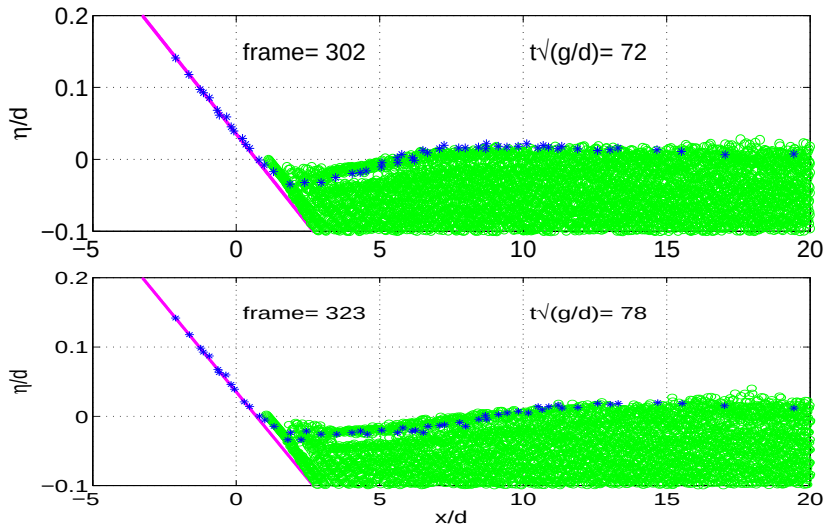

Figure 3.5: continued

38,50,56, figures show the run-up process. Model results can predict not only the shoreline elevation but also the run-up tongue thickness, which is represented very well. At the latter time, figures show the run-down of the wave. The comparison shows that the model results overestimate the shoreline elevation. The reason is not very clear and requires further study. In general, although the SPH model result does not agree with the experimental data perfectly, it does predict reasonable estimates for free surface profiles and maximum run-up.

Breaking Case: $H/d = 0.28$

Figures 3.6 3.9 show the comparison of free surface profiles of the SPH model results with experiment data for larger amplitude $H/d = 0.28$ solitary wave. At the time $t\sqrt{g/d}$ = 10,15,20,21, the wave approaches the shoreline. The front face of the wave becomes steeper as it nears the shoreline and finally forms the triangular bore. The SPH model results can predict these observations very well. At the time $t\sqrt{g/d}$ =22,23,24,25, they show the collapse and propagation of the bore along the slope. The numerical results predict this process almost perfectly in shape, size and speed. The SPH model is able to predict the maximum run-up and run-up tongue thickness very accurately. This model matches the time well. After the wave

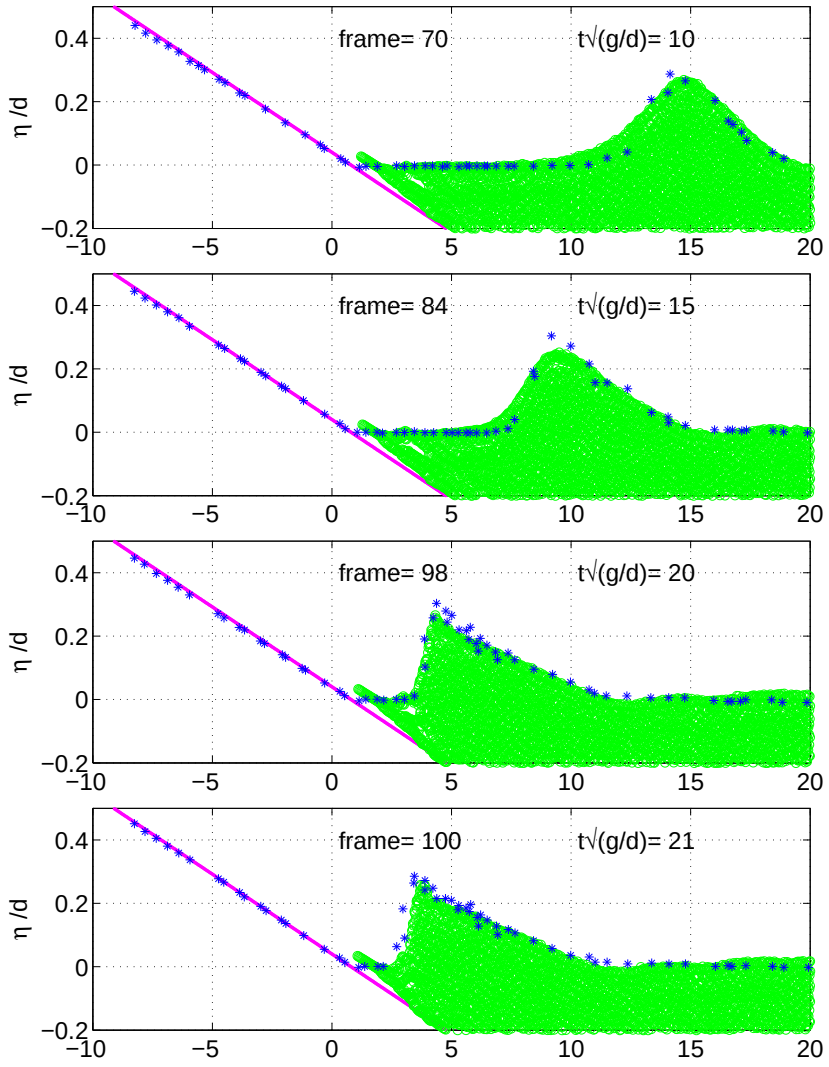

Figure 3.6: Comparison of non-dimensional free surface profiles for the breaking case $H/d = 0.28$ solitary wave at non-dimensional time $t\sqrt{g/d} =$ 10,15,20,21,22,23,24,25,26,27,28,29,30,45,50,55,60,65,70,80; open circles, SPH model; star symbols, experiments (Synolakis(1987))

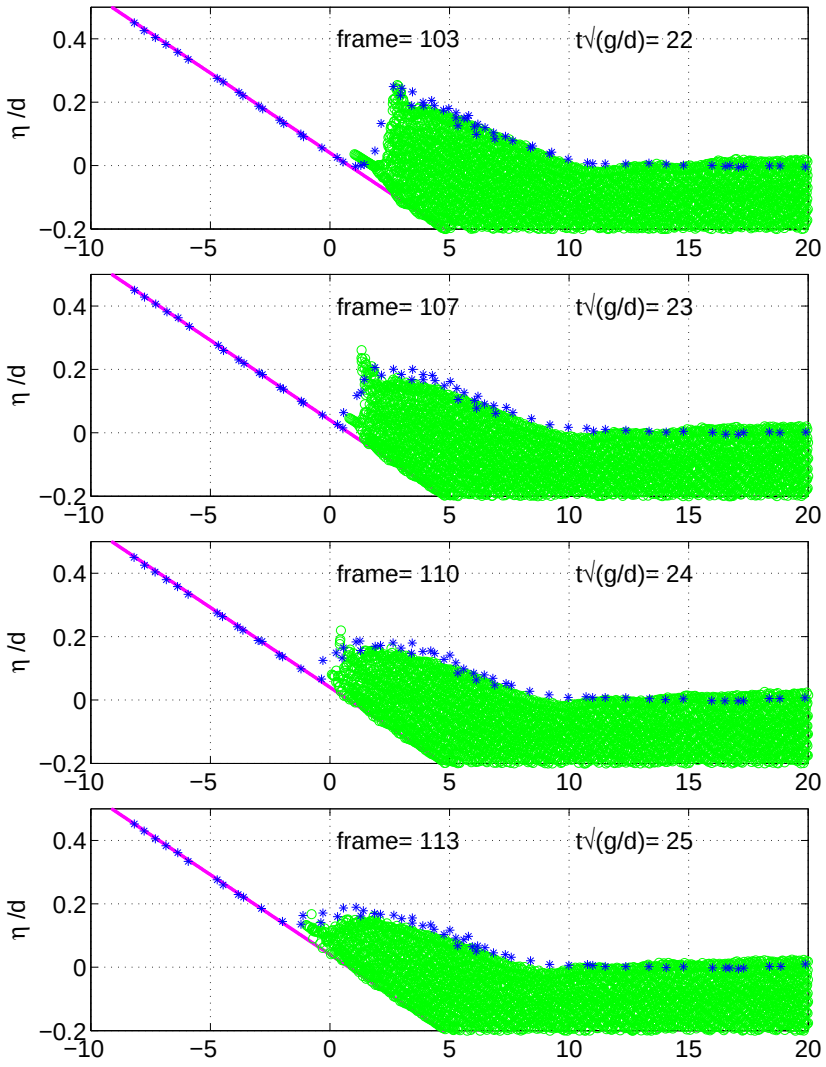

Figure 3.7: continued

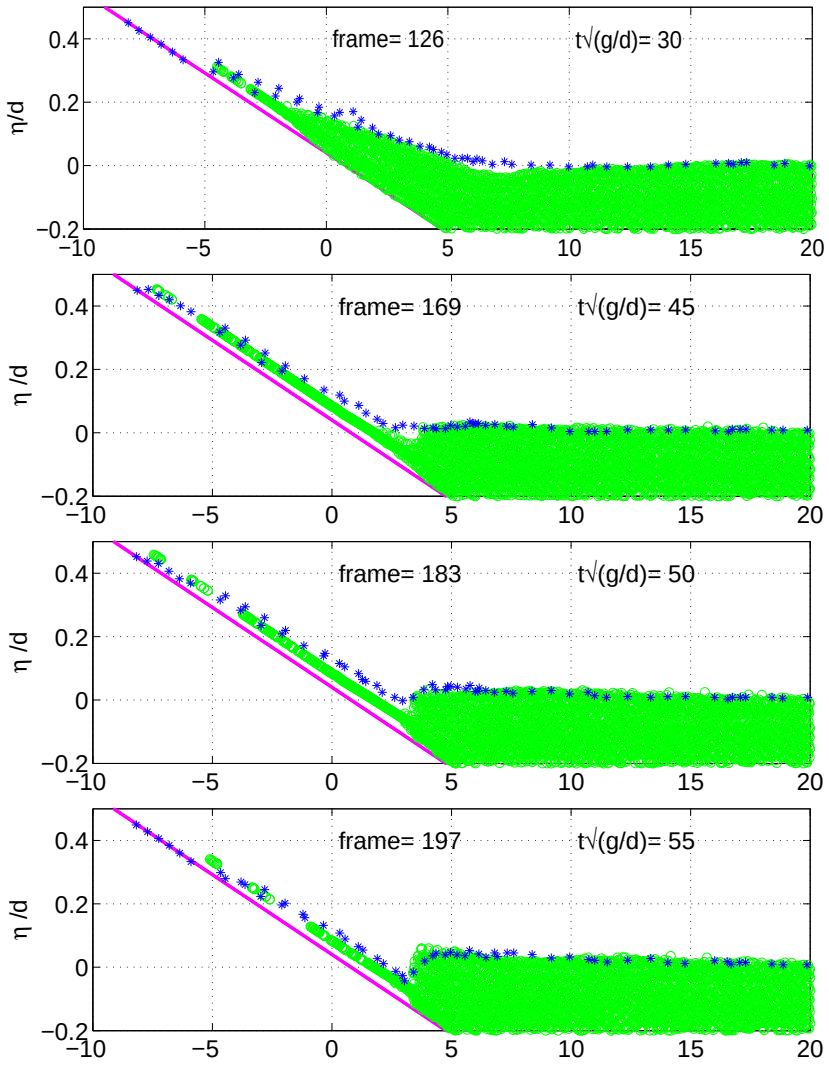

Figure 3.8: continued

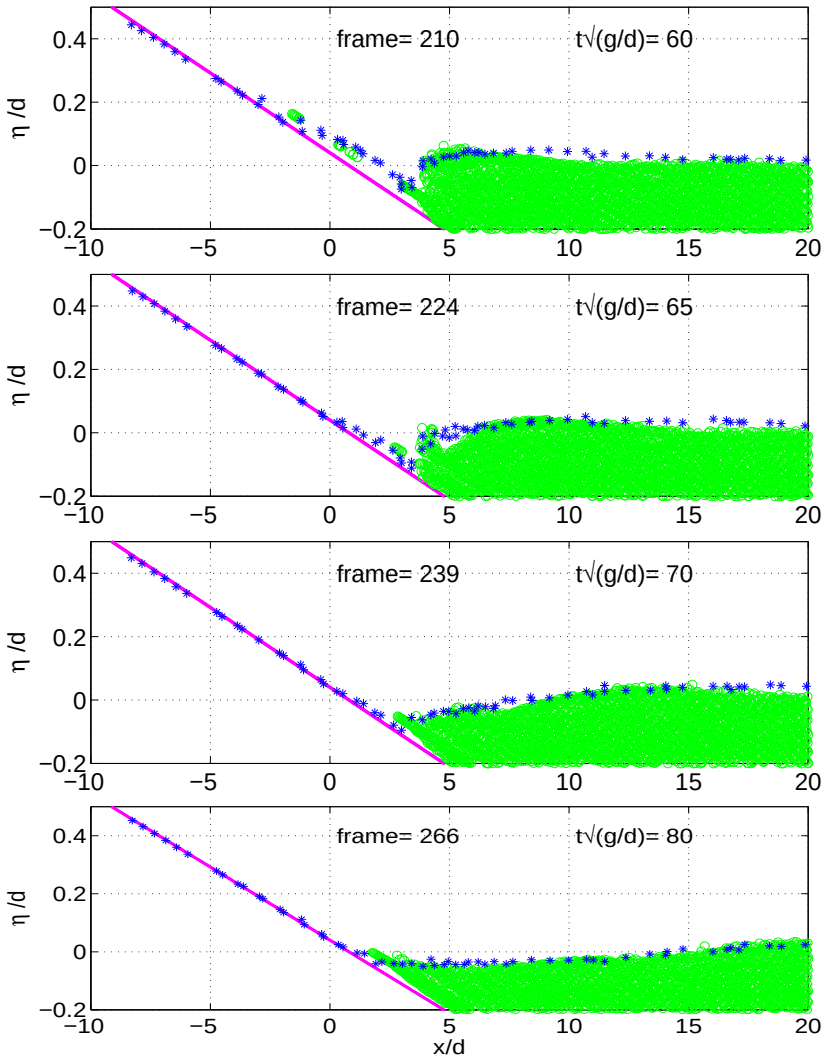

Figure 3.9: continued

reaches the maximum run-up, it begins to run down and reflect from the beach. The agreement of prediction is much better than the small amplitude ratio $H/d = 0.04$ case.

3.6 Summary

The SPH hydrodynamics model is used to reproduce the experiments for the run-up of both non-breaking and breaking solitary wave on a plane beach. The numerical results can predict the free surface profile, maximum run-up, run-up tongue thickness, and shoreline elevation very accurately, compared with experiment data.

The algorithm in the SPH model is consistent and robust to resolve the complicated physics in the processes of shoaling, breaking, formation and collapse of bore. Some other numerical model, such as the Boussinesq model (Zelt 1991, Svendsen 1987)[100], need specific algorithms and numerical techniques to treat the breaking and calibrate the bottom friction to determine the correct energy dissipation.

Chapter 4

SPH Sediment Transport Model

In this chapter, the governing equation and numerical solution for SPH sediment transport model will be discussed. First, the SPH numerical schemes will be tested term by term by comparing with finite difference schemes and analytical solution. Then the SPH sediment transport model are validated by reproducing experiments on sediment suspension over several bed configurations including flat and wave-generated ripples with parabolic and sinusoidal profiles. Finally the model results will be compared with experimental data to see if this model can capture the physical characteristics of the sediment suspension around the ripples.

4.1 Suspended Sediment Model

4.1.1 Introduction

Sediment transport is typically divided into three modes: bed load, suspended load and wash load. Because the wash load is composed of very fine sediment and usually does not involve the evolution of the bed, it can always be neglected in morphological studies. There is no precise distinction between bed load and suspended load. The motion of the bed load is limited in the region of $2d$, where d is the size of sediment in the bed. It is driven mainly by skin friction or bed shear stress. The motion of the suspended load occurs over the entire water column. The driving force is the fluid

turbulence. In the morphological study, which one is more important, bed load or suspended load? The answer depends on the region of study, fluid dynamics and the property of the sediment. In bay areas, with mud or fine sediment, the suspended load is the dominant factor in bathymetry evolution and the main driving force is the tidal flow. For sandy beaches, the wave and its resulting currents are the main driving forces and both suspended and bed loads are important. In fluvial area, the bed load is more important for pebble beds. Here we focus on the suspended load for numerical models. The bed load is commonly calculated by empirical formulas. Suspended sediment has been modeled by two ways numerically: one is to use a sediment concentration model, which is the most commonly used method; the other is discrete particle method, in which solid particles are put in the fluid domain and the particle motion is determined by interaction.

The concentration model is the most widely used model for chemical engineering, water quality, and heat transfer problems. It is also used for suspended sediment in river and coastal engineering. It can be used for engineering scales or lab scales. Celik and Rodi [10] present a mathematical model for calculating suspended sediment transport in unidirectional channel flow under general, non-equilibrium conditions. The model consists of a hydrodynamic component for calculating the flow field and the turbulence characteristics and a scalar transport model for calculating the distribution of sediment concentration. The former component provides the driving force and inputs for the latter. The combined hydrodynamic-sediment transport model was applied to several flume experiments in equilibrium, net-deposition, net-entrainment situations and yields fairly close agreement with experiments. In conjunction with the bed-load formula, the model can be used for predicting the river-bed morphology. Duy and Shibayama [23] developed a model to simulate the temporal and spatial distributions of suspended sediment in the surf zone. The hydrodynamic model is based on the Reynolds equation of motion and the sediment concentration is determined by solving the convection-diffusion equation of sediment mass. They found that turbulence generated by broken waves is considered the main mechanism for the flow structure as well as the transport of sediment in the surf zone. They also discovered that the convection and diffusion play equally important roles in the mixing process

of suspended sediment under broken waves.

With the advantages of SPH method for hydrodynamic model, how can this method be used to simulate the sediment transport? Currently there are two ways to apply the particle method for flow-sediment interaction. One is the SPH method and another is the discrete particle method. Gotoh and Fredsoe [36] used the MPS method to model the flow-sediment two phase flow for dredge spoil and reproduce details of the deposition and diffusion process. They captured the existence of twin peaks in the time series of sediment concentration, which is not easily simulated by ordinary Eulerian models. Drake and Calantoni [22] presented a discrete particle model to simulate sediment transport. The basic idea of this model is that every sediment particle is simulated by a discrete spherical particle; the velocities and positions of each particle are obtained by integrating Newton's equations of motion at every time step; the forces are generated by direct particle-particle contact and fluid-particle interactions including buoyancy, drag, added mass, pressure gradient and gravitational forces. The hydrodynamic model is a discrete fluid model in which the pressure gradient forces accelerate a stack of horizontal layers of fluid and the spherical particles embedded within them.

Both flow-sediment of two-phase SPH method and discrete particle method are very precise in physics but are limited in their applicability to small scale problems in the order of centimeter. But the dimensions of practical applications are generally up to 10 meters, even up to 1000 meters. Here the combination of the SPH method for the hydrodynamics and a scalar transport model (concentration model) for sediment transport is proposed. Each fluid particle carries a sediment concentration, determined by the scalar transport equation, which is the most widely used model.

In the present study, we use the SPH method to simulate sediment deposition, suspension and bed changes with a concentration model. With a similar formulation, neglecting the fall velocity of the sediment, the solute transport problem, such as contaminant diffusion, can also be handled by the SPH method.

4.1.2 Governing Equations and Boundary Conditions

Governing Equation

The concentration model is based on the sand mass conservation and mixing length theory. Peter Nielsen (1992) explained this very clearly in his book[69]. Considering a horizontally uniform sediment concentration field and finite volume, the change rate of local concentration $\frac{\partial c}{\partial t}$ depends on the total sediment flux in the vertical direction $\frac{dq_z}{dz}$.

$$\frac{\partial c}{\partial t} = -\frac{dq_z}{dz} \tag{4.1}$$

The total vertical sediment flux includes gravitational settling $-w_s c$ (downward) and the combination of convection q_c and diffusion q_d (upward or downward).

$$q_z = -w_s c + q_d + q_c \tag{4.2}$$

In the Eulerian coordinate system, the rate of change of local sediment concentration is determined by gradients of vertical sediment flux, showed in the figure 4.1.2. But for Lagrangian coordinate system, the convection flux is resolved by the total acceleration term.

Eulerian System:

$$\frac{\partial c}{\partial t} = w_s \frac{\partial c}{\partial z} - \frac{\partial q_d}{\partial z} - \frac{\partial q_c}{\partial z} \tag{4.3}$$

Lagrangian System:

$$\frac{dc}{dt} = w_s \frac{\partial c}{\partial z} - \frac{\partial q_d}{\partial z} \tag{4.4}$$

Following the concepts of mixing length theory, the diffusive sediment flux can be expressed by gradient diffusion as:

$$q_d = -\epsilon_s \nabla c \tag{4.5}$$

where ϵ is the diffusivity coefficient, which has the same dimension as eddy viscosity or kinematic viscosity (m^2/s). It means the sediments diffuse from high concentration region to low concentration region by turbulence fluctuation in terms of random walk. So the diffusion coefficient can be taken as eddy viscosity roughly, β is constant:

$$\epsilon_s = \beta \nu_t \tag{4.6}$$

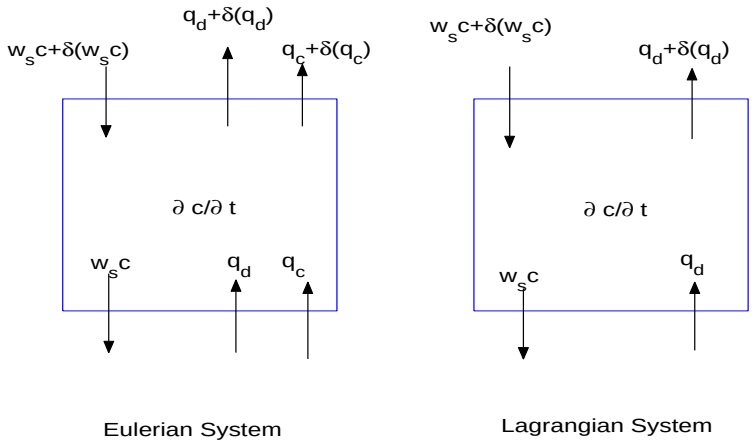

Figure 4.1: Considering horizontally uniform case, the rate of change for sediment concentration depends on the vertical sediment flux. (Left, Eulerian Finite Volume; Right, Lagrangian Finite Volume)

So the governing equation for concentration model can be expressed by the convection-diffusion equation (also called transport equation) to simulate the transport of sediment:

$$\frac{dC}{dt} = w_s \frac{\partial C}{\partial z} + \nabla \cdot (\epsilon_s \nabla C) \tag{4.7}$$

where C is sediment volumetric concentration, w_s is sediment fall velocity, and ϵ_s is a diffusion coefficient. The last term in the above equation is the diffusion term, which is challenging problem for the SPH particle method. The details about the numerical scheme will be presented later.

The vertical flux of sediment above bed can be expressed by sediment settling $q_s = -w_s c$ and diffusive flux $q_d = -\epsilon_s \frac{\partial c}{\partial z}$. Near the bed, these vertical sediment fluxes should be equal to the amount of sediment eroded from $q_s = D$ or deposited to $q_d = E$ the bed. For the steady and equilibrium case, the net flux is zero, which is also called the Equilibrium Boundary Condition:

$$(-w_s c - \epsilon_s \frac{\partial c}{\partial z})|_{z=2d} = E - D = 0 \tag{4.8}$$

Derivation of Sub-Particle Scheme

Filter the convection-diffusion equation:

$$\frac{DC}{Dt} = \frac{\partial C}{\partial t} + \frac{\partial (U_j C)}{\partial x_j} = w_s \frac{\partial C}{\partial x_i} + \epsilon \frac{\partial^2 C}{\partial x_j x_j} \tag{4.9}$$

Substitute the nonlinear term by Filtering Decomposition:

$$\begin{aligned} U_j &= < U_j > + u_j'' \\ C &= < C > + c'' \\ < U_j C > &= < U_j >< C > + < u_j'' c'' > \end{aligned} \tag{4.10}$$

To obtain the filtered (resolved-scale) equation for convection-diffusion:

$$\frac{\overline{D}C}{Dt} = \frac{\partial < C >}{\partial t} + < U_j > \frac{\partial < C >}{\partial x_j} = w_s \frac{\partial < C >}{\partial x_i} + \epsilon \frac{\partial^2 < C >}{\partial x_j x_j} \tag{4.11}$$

$$\frac{\overline{D}C}{\overline{D}t} = w_s \frac{\partial < C >}{\partial x_i} + \epsilon \frac{\partial^2 < C >}{\partial x_j x_j} - \frac{\partial < u_j'' c'' >}{\partial x_j x_j} \tag{4.12}$$

In order to close the problem, the model for scalar flux term in sub-grid scale is needed. There are four models for the scalar flux term, including eddy diffusivity (Smagorinsky), scale similarity, mixed model and dynamics structure model. The simplest Smagorinsky (eddy diffusivity) model is expressed as:

$$\overline{S_{ij}} = -\frac{1}{2}\left(\frac{\partial < U_i >}{\partial x_j} + \frac{\partial < U_j >}{\partial x_i}\right) \tag{4.13}$$

$$\sigma_{ij}^r = < u_j'' c'' > = -2\epsilon_t \frac{\partial < C >}{\partial x_j} \tag{4.14}$$

$$\epsilon_t = -C_c \Delta^2 \overline{S} \tag{4.15}$$

where $\overline{S_{ij}}$ is the filtered rate of strain, $\overline{S} = (2\overline{S_{ij}S_{ij}})^{1/2}$ is the magnitude filtered rate of strain, ϵ_t is the eddy diffusivity of residual motions, C_c is a model constant, and Δ is the filter width.

Finally the governing equation of the sediment transport for mean flow:

$$\frac{DC}{Dt} = w_s \frac{\partial C}{\partial x_i} + \epsilon_{eff} \frac{\partial^2 C}{\partial x_j x_j} \tag{4.16}$$

where ϵ_{eff} is the effective diffusivity, the $<>$ is omitted for convenience.

Boundary Conditions

In unsteady flow, there are two kinds of boundary conditions:

The first is the Bottom Reference Concentration Boundary Condition, proposed by Englund and Fredsoe [25], which relates the instantaneous bed concentration at $z = 2d$ to Shields parameter θ as follows [47]:

$$C_b = C_0(1 + \frac{1}{1+\lambda_b})^{-3} \tag{4.17}$$

where C_b is the bottom reference concentration, λ_b is the so-called linear concentration related to the real volumetric concentration, C_0 is the maximum value for the volumetric concentration.

$$\lambda_b^2 = \frac{0.4\kappa^2}{0.013s\theta}(\theta - \theta_c - \frac{\pi}{6}\mu_d p) \tag{4.18}$$

$$\theta = \frac{\tau_b}{\rho g(s-1)d} = \frac{u_*^2}{(s-1)gd} \tag{4.19}$$

$$\theta_c = 0.05 \tag{4.20}$$

where κ is a constant, $s = 2.65$ is the relative density of sediment, θ, θ_c are the instantaneous and critical Shields parameter (non-dimensional stress due to skin friction) respectively, $\mu_d = \tan(\phi_d)$ is the dynamic friction determined by the dynamics friction angle of bed load sediment ϕ_d, p is a certain fraction or probability of the moved particles on the single layer of bed surface.

Zyserman and Fredsoe suggested a simpler empirical formula for the bottom reference concentration:

$$C_b = \frac{0.331(\theta - \theta_c)^{1.75}}{1 + \frac{0.331}{C_m}(\theta - \theta_c)^{1.75}} \tag{4.21}$$

where $C_m = 0.32$ is the maximum sediment concentration. Theoretically maximum concentration can be as large as 0.65, but this corresponds to firm packing and does not allow free motion of the particles.

The second is the Gradient (Flux) Boundary Condition. Nielsen suggested that the sediment entrainment and deposition should be considered as independent processes and the rate of sediments entrained from the bed is estimated in terms of the pick-up function, [69], in which the net flux between interfaces is determined by the local flow conditions.

Van Rijn recommended the following formula for the pick-up function in steady flow based on experimental data and analysis on the previous study on steady bed load transport:

$$\frac{p}{\sqrt{(s-1)gd}} = 0.00033(\frac{\theta - \theta_c}{\theta_c})^{1.5}(\frac{(s-1)gd^3}{\nu^2})^{0.1} \tag{4.22}$$

where p is the rate of pick-up of sediment, $g = 9.81m^2/s$ is the gravity acceleration, d is the diameter of sediment, and ν is the kinematic viscosity. It is assumed that this formula can be applied instantaneously for unsteady flow.

In our SPH model, we use the Gradient (Flux) Boundary Condition.

4.1.3 Sediment Flux and Morphological Model

Changes in the bed elevation are given by the following equation, which is based on the mass transfer between the fluid and sandy bed:

$$(1-n)\,\frac{\partial z_b}{\partial t} = D - E \tag{4.23}$$

where z_b is the bed elevation, n is porosity, D and E are the deposition and erosion fluxes at the boundary.

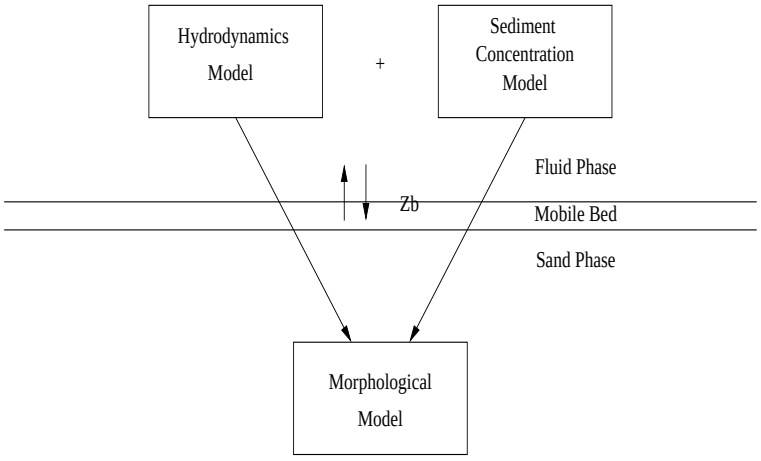

Figure 4.2: Structure of sediment transport and morphological numerical model

4.1.4 Numerical Solution for Sediment Transport Model

The numerical solution the the convection-diffusion equation is discussed term by term.

$$\frac{dC}{dt} = w_s \frac{\partial C}{\partial z} + \nabla \cdot (\epsilon_s \nabla C) \tag{4.24}$$

Settling Term: $-w_s \frac{\partial c}{\partial z}$

The settling term, which is a convective term, must be handled carefully. Most classic books on numerical methods discuss the different numerical algorithms for convective term. Fletcher[29] spent several chapters discussing the algorithm for the convective term. A good numerical scheme for the convective term should not introduce non-physical dissipation. Nor should it change the speed of wave propagation. So it is important to reduce the numerical dissipation and dispersion. Before the derivation of the SPH numerical scheme for convection term, let us review some important concepts such as numerical dissipation, numerical dispersion and artificial diffusivity, and techniques to solve these problems in finite difference method which is helpful to derive the right schemes in SPH method.

The convection equation, also called the advection equation, is classified as a conservative hyperbolic equation.

$$\frac{\partial C}{\partial t} + w_s \frac{\partial C}{\partial x} = 0 \tag{4.25}$$

Its general analytical solution $C = f(x - w_s t)$ represents a wave moving in the positive x-direction with the velocity w_s. The stability of numerical solution requires the Courant-Friedrichs-Lowy condition (CFL) less than one,

$$c_{CFL} = \frac{|w_s|\Delta t}{\Delta x} \leq 1$$

Numerical dissipation is the attenuation of the amplitude of plane waves introduced by a particular computational algorithm, associated with even-ordered derivatives multiplied by coefficients of alternating sign. This is called artificial diffusivity. Numerical dispersion is the propagation of plane waves of different wave number at

different speeds, associated with the truncation error as odd-ordered spatial derivatives. The modified equation approach analysis is an important tool to investigate the consistency and the order of accuracy of the computational algorithm, and it can also help to construct the new numerical scheme to reduce or eliminate the numerical dissipation or dispersion.

$$L(C) = L_a(C) - E_j^n(C) = 0 \tag{4.26}$$

where $L(C) = 0$ is the differential equation to be solved, L_a is the approximate solution, and E_j^n is the truncation error. So the modified equation is the differential equation that the algebraic equation actually solves:

$$L_a(C) = L(C) + E_j^n(C) = 0 \tag{4.27}$$

In order to develop the right algorithm for the settling term, two numerical schemes are proposed: the SPH-upwind and SPH-modified-upwind scheme. The propagation of a sine wave is chosen as a benchmark test case to illustrate the different numerical schemes including three finite difference schemes and two SPH schemes.

SPH-upwind Scheme

In the SPH-upwind scheme, only the particles above particle i are integrated when calculating the convection term. Figure 4.3 shows how to use this special scheme by particle method. However, the upwind particle scheme introduces numerical diffusion, or artificial (numerical) diffusivity[29]. It has the first order accuracy. Further studies on a better scheme are needed.

Calculating the convection term by this scheme should be corrected by normalization of the kernel with corrective SPH to eliminate the boundary effect due to partial integration, expressed as the following [12]:

$$w_s \frac{\sum_j \frac{m_j}{\rho_j}(C_j - C_i)\frac{\partial W_{ij}}{\partial z}}{\sum_j \frac{m_j}{\rho_j}(z_j - z_i)\frac{\partial W_{ij}}{\partial z}} \tag{4.28}$$

SPH-modified upwind scheme

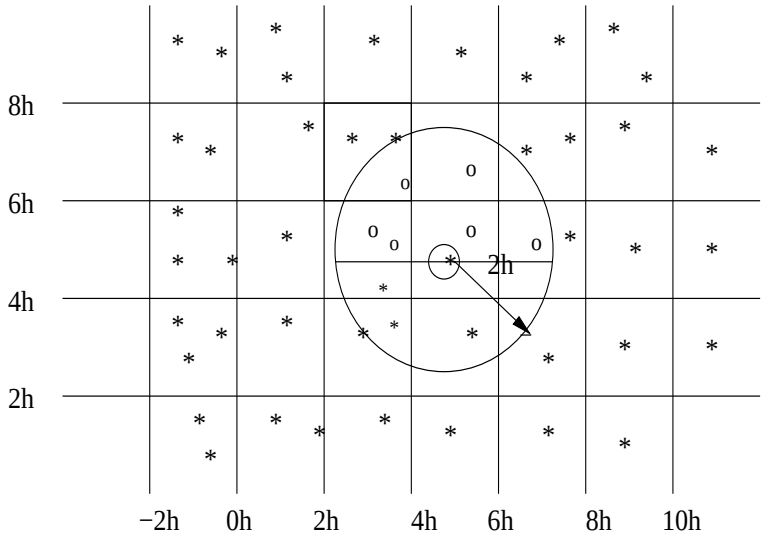

Figure 4.3: " Up-winding " particle scheme for particle i in the center of circle, $2h$ is the range of kernel, small open circles are the particles integrated for upwind scheme.

In finite difference method, the upwind scheme:

$$\frac{T_j^{n+1} - T_j^n}{\Delta t} + u\frac{(T_j^n - T_{j-1}^n)}{\Delta x} = 0 \tag{4.29}$$

can be expressed as:

$$T_j^{n+1} = (1 - C)T_j^n + CT_{j-1}^n \tag{4.30}$$

Taylor expansion of T_j^{n+1} and T_{j-1}^n at T_j^n, and substitute into above equation and get:

$$\frac{\partial T}{\partial t} + u\frac{\partial T}{\partial x} + 0.5\Delta x\frac{\partial^2 T}{\partial x^2} + O(\Delta t^2, \Delta x^2) = 0 \tag{4.31}$$

It can be rewritten as:

$$\frac{\partial T}{\partial t} + u\frac{\partial T}{\partial x} - 0.5u\Delta x(1 - C)\frac{\partial^2 T}{\partial x^2} + O(\Delta t^2, \Delta x^2) = 0 \tag{4.32}$$

Because of

$$\frac{\partial T}{\partial t} = -u\frac{\partial T}{\partial x}$$

and

$$\frac{\partial^2 T}{\partial t^2} = u^2\frac{\partial^2 T}{\partial x^2}$$

In the finite difference scheme, the truncation error for the upwind scheme introduces an artificial diffusivity $\epsilon' = 0.5u\triangle x(1-C)$. In order to achieve the higher order scheme, the modified equation analysis is applied for this convective term $(\epsilon+\epsilon')\nabla^2 c$ for SPH-modified upwind scheme.

$$\frac{\partial T}{\partial t} + u\frac{\partial T}{\partial x} + \epsilon'\frac{\partial^2 T}{\partial x^2} = O(\Delta t^2, \Delta x^2) \tag{4.33}$$

Where u is the convection velocity, $\triangle t$, $\triangle x$ are time step and grid spacing, and $C = u\triangle t/\triangle x$. In the SPH method, $\triangle x$ is replaced by smoothed length h.

The following schemes are the Finite Difference Method (FDM) schemes for convection equation $\frac{\partial T}{\partial t} + u\frac{\partial T}{\partial x} = 0$, which are used for comparison.

FDM-1st upwind scheme

The first order upwind scheme:

$$\frac{T_j^{n+1} - T_j^n}{\Delta t} + u\frac{(T_j^n - T_{j-1}^n)}{\Delta x} = 0 \tag{4.34}$$

The spatial derivative is discretized as a forward-difference or backward-difference scheme that depends on the convection velocity. The approximation is first order accurate, which is very inaccurate with the truncation error that has the effect of false diffusion.

FDM-2nd upwind scheme

The second order upwind scheme:

$$\frac{T_j^{n+1} - T_j^n}{\Delta t} + u[\frac{T_{j+1} - T_{j-1}}{2\Delta x} + \frac{0.5(T_{j-2} - 3T_{j-1} + 3T_j - T_{j+1})}{3\Delta x}] \tag{4.35}$$

This is a higher order of upwind scheme which is similar with four points centered finite difference. This modification can counteract some of the truncation error and produce a more accurate solution.

FDM-Lax-Wendroff scheme

The second order scheme in both time and space:

$$\frac{T_j^{n+1} - T_j^n}{\Delta t} - 0.5uC\Delta x L_{xx} + uL_x T_j^n = 0 \tag{4.36}$$

where $L_x T_j^n = (T_{j+1}^n - T_{j-1}^n)/\Delta x$ and $L_{xx} T_j^n = (T_{j+1}^n - 2T_j^n + T_{j-1}^n)/\Delta^2 x$. This is a second order accuracy scheme and needs two time levels. It can be derived as the combination of the Lax-Friedrichs and the Leapfrog schemes.

The figures 4.4 4.5 show the different results of above schemes for the linear convection of a truncated sine wave:

$$\frac{\partial T}{\partial t} + u\frac{\partial T}{\partial x} = 0 \tag{4.37}$$

with the initial condition and boundary condition as:

$$T(x,0) = \begin{cases} \sin(10\pi x) & \text{for } 0 \le x \le 0.1 \\ 0 & \text{for } 0.1 \le x \le 1.0 \end{cases}$$

$$\begin{aligned} T(0,t) &= 0 \\ T(1,t) &= 0 \end{aligned} \tag{4.38}$$

The exact solution should be the sine wave that propagates with no reduction in amplitude at a speed u, which is shown in the figures4.4 4.5. The schemes are implemented in the SPH and Finite Difference codes. A computational solution is obtained with 41 equally spaced points in range of $0 \le x \le 1.0$. It is concluded that:

The solution for SPH upwind (SPH-uw)) and FDM first upwind (uw-1) are first order schemes and have diffused due to the numerical diffusion, compared with the exact solution; the SPH-uw is consistent with the travel speed but uw-1 has a little mismatch; The solution for SPH modified upwind (SPH-mod), FDM second upwind (uw-2) are second order in space, Lax-Wendroff is second order schemes in both space and time; All of the second order schemes have some numerical dispersion effect in which there are wakes behind the primary wave.

Diffusion Term: $\epsilon\nabla^2 c$

The diffusion term is a second derivative. It is easy for finite difference schemes. The SPH scheme is adopted from the one proposed by Brookshaw[9] and is used for heat conduction problems[15].

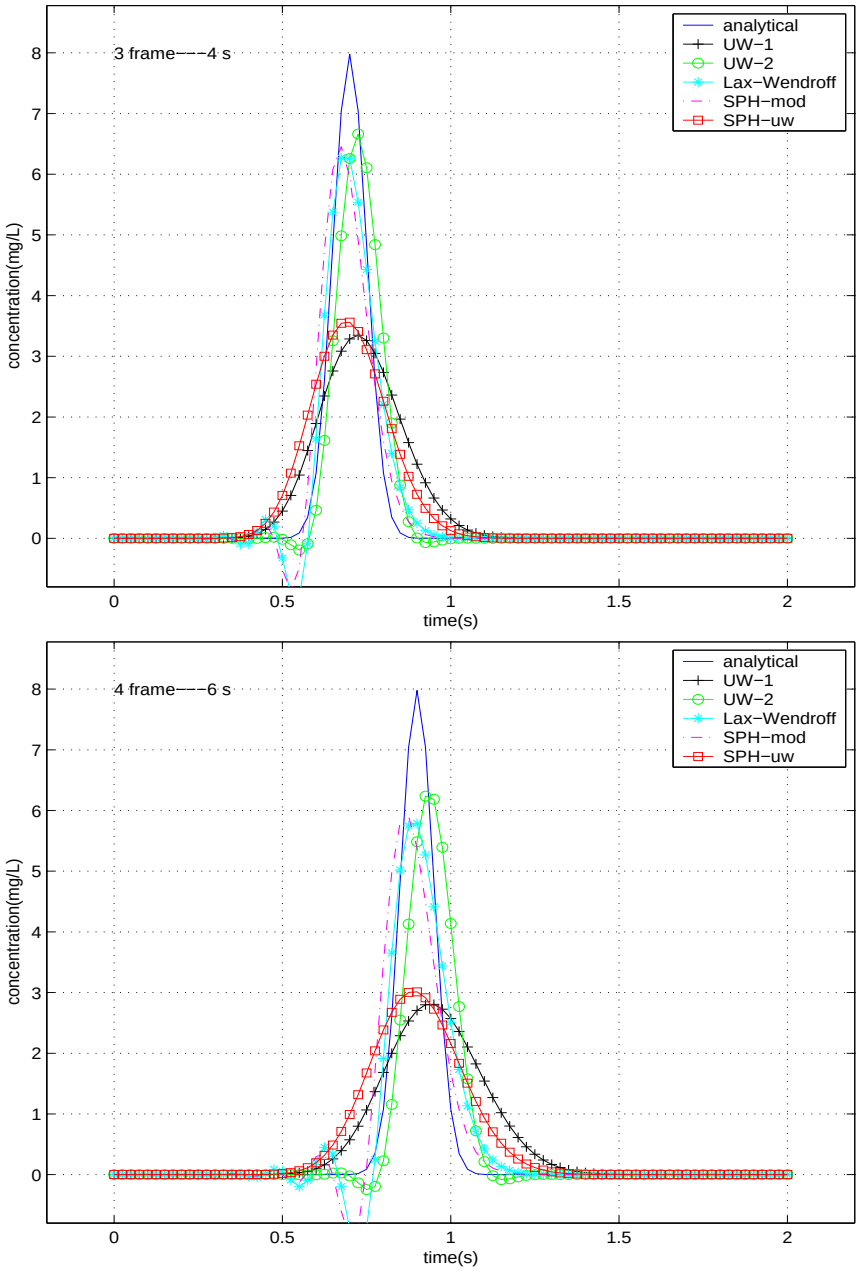

Figure 4.4: Comparison of the SPH schemes for the convection term with other numerical schemes at different time (1)

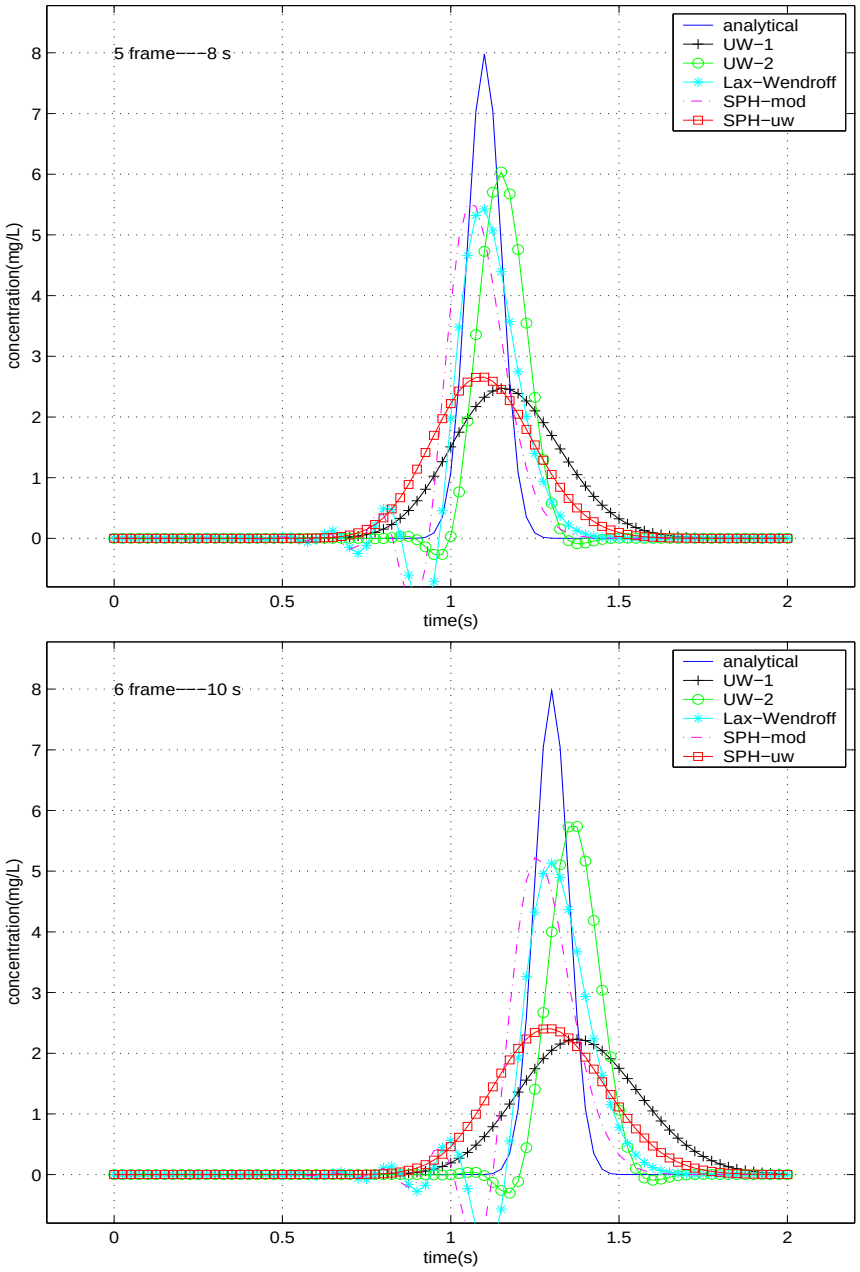

Figure 4.5: Comparison of the SPH schemes for the convection term with other numerical schemes at different time (2)

SPH-diffusion term

The second derivative of SPH particle form is adopted from Cleary and Monaghan's paper about the heat conduction[15] .

$$(\epsilon\nabla^2 T)_i = \sum_j (\frac{m_j}{\rho_j})(\epsilon_i + \epsilon_j)(T_i - T_j)\frac{\vec{r_i} - \vec{r_j}}{|\vec{r_i} - \vec{r_j}|^2 + \eta^2} \cdot \nabla_i W_{ij} \tag{4.39}$$

where j represents the neighboring particles for i, and η is the clip parameter to prevent the singularity.

FDM-forward time centered space (FTCS)

The typical finite difference scheme for one dimensional diffusion equation

$$\frac{\partial T}{\partial t} - \alpha\frac{\partial^2 T}{\partial x^2} = 0$$

Using forward in time and central in space (FTCS) scheme gives the following algorithm:

$$\frac{T_j^{n+1} - T_j^n}{\nabla t} - \frac{\alpha(T_{j-1}^n - 2T_j^n + T_{j+1}^n)}{\nabla x^2} = 0 \tag{4.40}$$

which can be rewritten as:

$$T_j^{n+1} = sT_{j-1}^n + (1-2s)T_j^n + sT_{j+1}^n \tag{4.41}$$

where $s = \alpha\Delta x/\Delta t$.

The Laplace Transform and Separation Variables are the common methods to solve the diffusion equation. In order to test the schemes, the following problem is solved numerically.

Governing equation:

$$\frac{\partial C}{\partial t} = D\frac{\partial^2 C}{\partial x^2} \tag{4.42}$$

initial condition and boundary condition:

$$\begin{aligned} C(x,0) &= 0; \\ C(0,t>0) &= C_0; \\ C(\infty,t) &= 0. \end{aligned} \tag{4.43}$$

The analytical solution of concentration and flux is:

$$C(x,t) \;=\; C_0(1 - erf\{\frac{x}{\sqrt{4Dt}}\}) = C_0 erfc\{\frac{x}{\sqrt{4Dt}}\} \tag{4.44}$$

The results are shown in the figures 4.6. Both of the schemes have very good accuracy.

4.2 Test Cases for Numerical Schemes

In this section we will apply the above SPH schemes into the SPH concentration model. The first test case is for mobile bed under the oscillatory flow that will be tested for both of the concentration and morphological model. The second test case is for the artificial size ripple under the oscillatory flow to see if the model can capture some basic physics in this phenomenon. Both of these test cases show the feasibility of the concentration model.

We applied the above models in three test cases to show the feasibility of simulating the sediment transport problem by the SPH method.

- sediment settling
- sediment suspension in oscillatory flow over flat bed
- sediment suspension in oscillatory flow over a sand ripple

Case 1.

Put a block of sediment in stagnant water and let it fall freely. Actually give the square area of fluid particles with initial concentration with 0.05 (volumetric concentration). Assume the constant diffusion coefficient for simplification. The bed level change is calculated from flux between the interface of water and bed. The result shows that:

1. the bed level increases with sediment deposition
2. numerical diffusion can be observed in the upwind scheme
3. the mass of sediment is conserved during the process

The figure 4.8 is the snapshot of the simulation for settling case. The lower figure shows the exchange of volume flux between the interface.

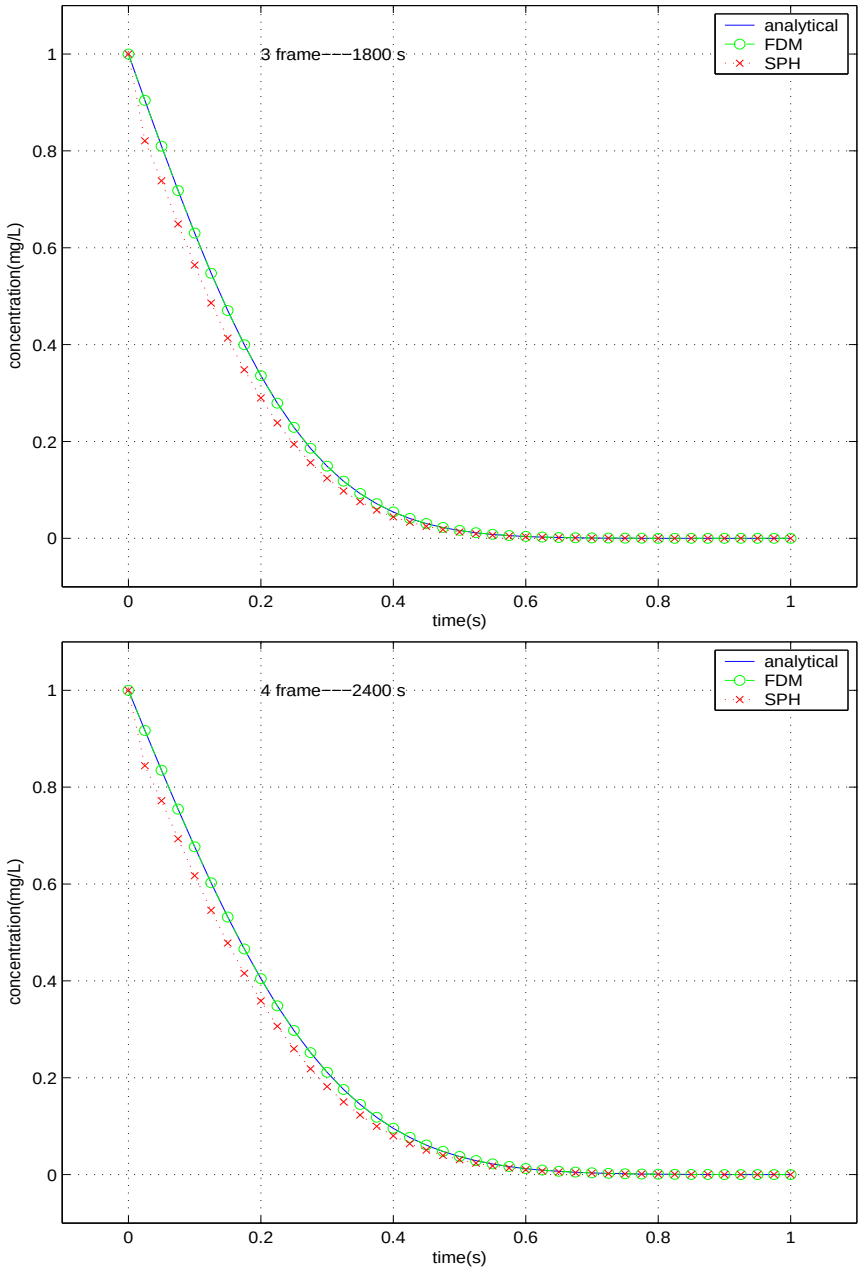

Figure 4.6: Comparison of SPH schemes for diffusion term with other numerical schemes

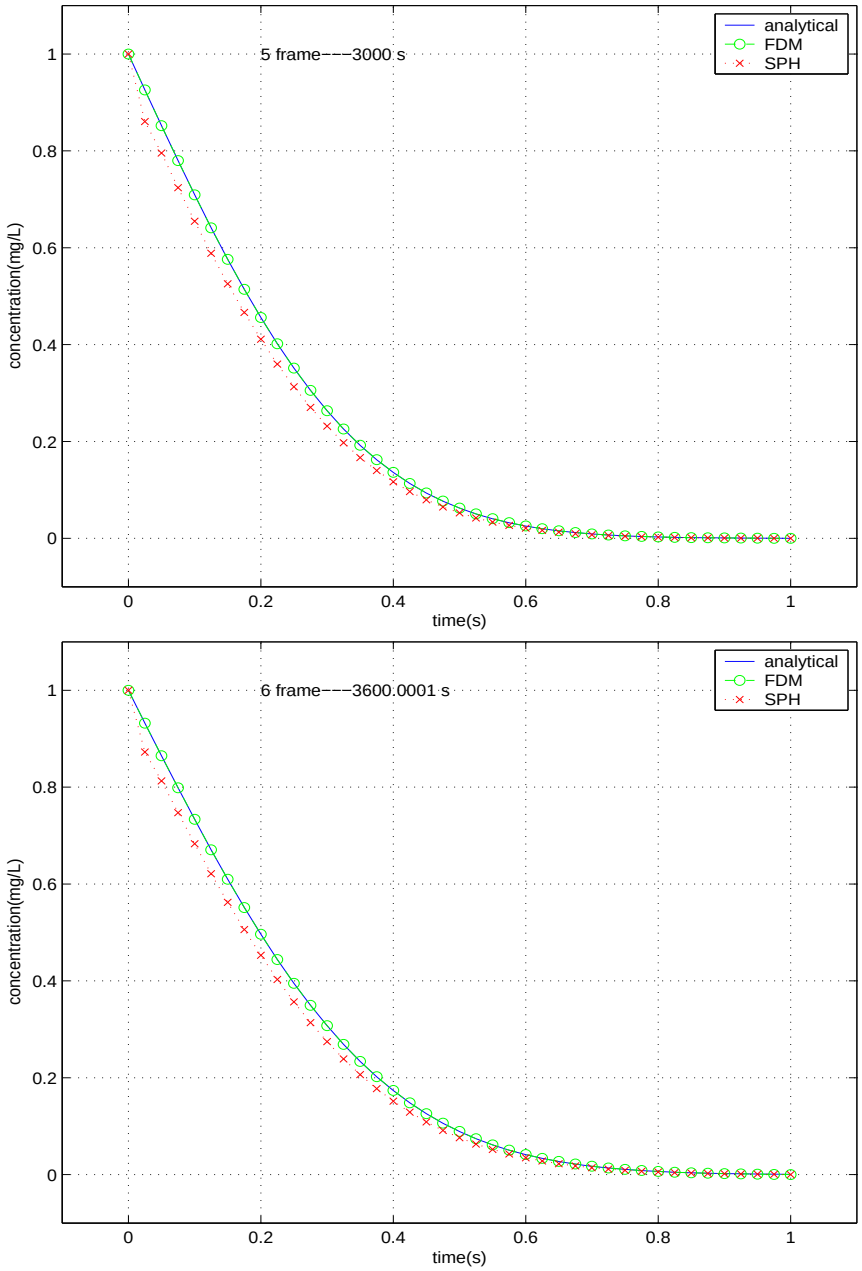

Figure 4.7: Comparison of SPH schemes for diffusion term with other numerical schemes(continued)

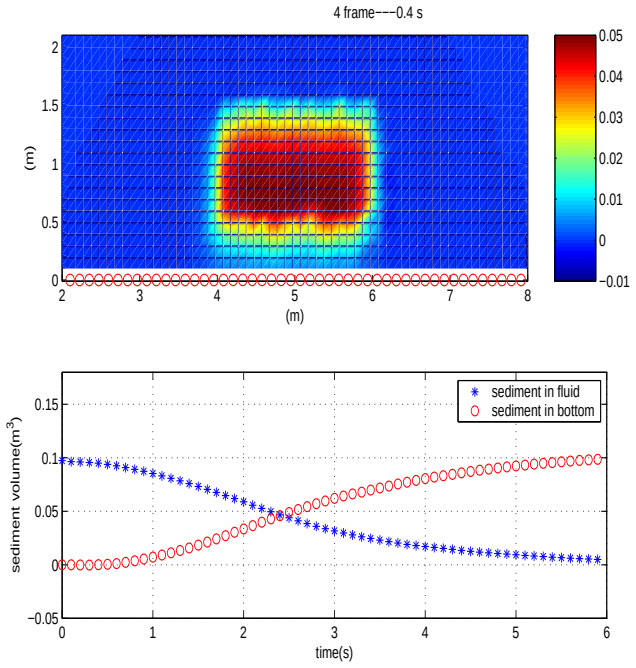

Figure 4.8: Snapshot of settling case and mass exchange between fluid and bottom

Case 2.

In order to produce the oscillatory flow to test the sediment suspension, a tube with a piston at each end is set up similar to the facilities of Horikawa's experiment [46] and Delft's oscillating water tunnel. The piston motion is given and they move in phase. The middle part of the bed is the test section with a mobile bed; it is away from the effect of pistons. The Figure 4.9 show the scheme of setup of this numerical experiment.

The experimental condition is the same as the experiment as that performed by Ribberink and Al-Salem (1995). In their experiment, the phase lag between stream velocity and concentration is about 0.8s and 0.7s, respectively.

The Figure 4.10 is the snapshot of the simulation for settling case. The lower figure shows the bed level change in test section.

The results has following features:

1. bed level changes periodic with oscillatory flow

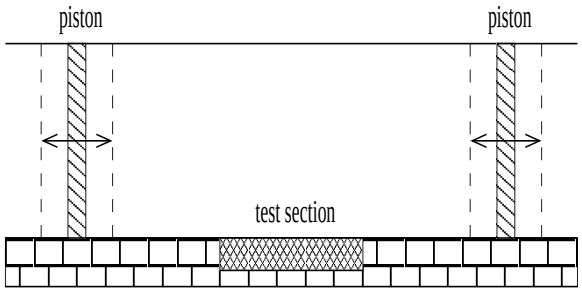

Figure 4.9: Setup of numerical oscillating water tube

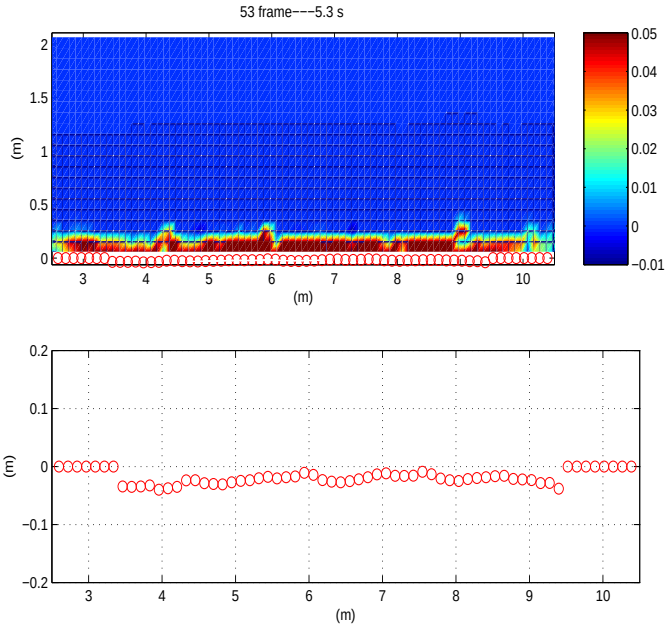

Figure 4.10: Snapshot of sediment suspension over flat bed (above) and mobile bed change in the test section

2. two ends of test section eroded more than other area, which is reasonable

3. the phase lag between stream velocity and sediment concentration agrees with experiment data. See figure 4.11.

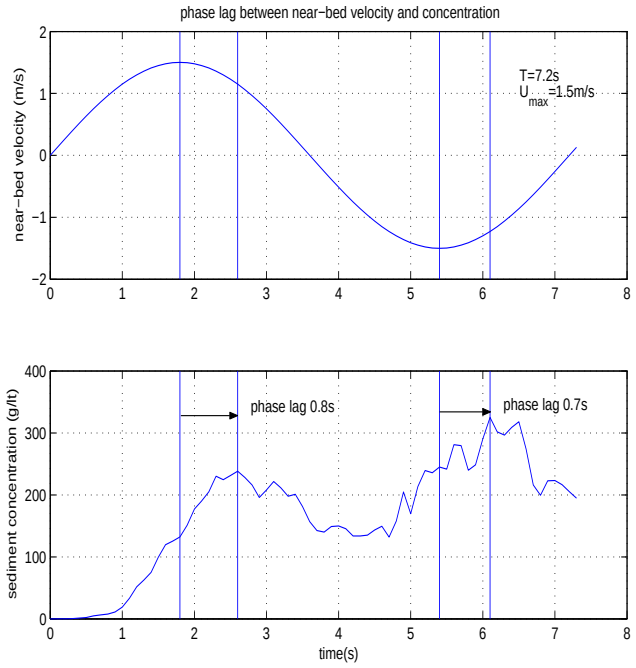

Figure 4.11: Phase lag between stream velocity and concentration

Case 3.

The last numerical experiment is about the sediment suspension over the artificial sand ripple in order to check if the model can produce some qualitative results. The sand ripple is placed in the numerical oscillating water tube, and the piston is programmed to produce the sinusoidal oscillatory flow.

The results are encouraging and we can get the following features:

1. in the initial stage the sediment is suspended near the upstream peak of ripple

2. after while a vortex is formed in downstream of ripple

3. at the beginning of the stream velocity reverse, there is a upward lift current just above the peak of the ripple

4. the center of downstream vortex moves with the intensity of oscillatory flow

The table of figures 4.12 includes the snapshots of the simulation for sediment concentration and velocity vector plot around the sand ripples.

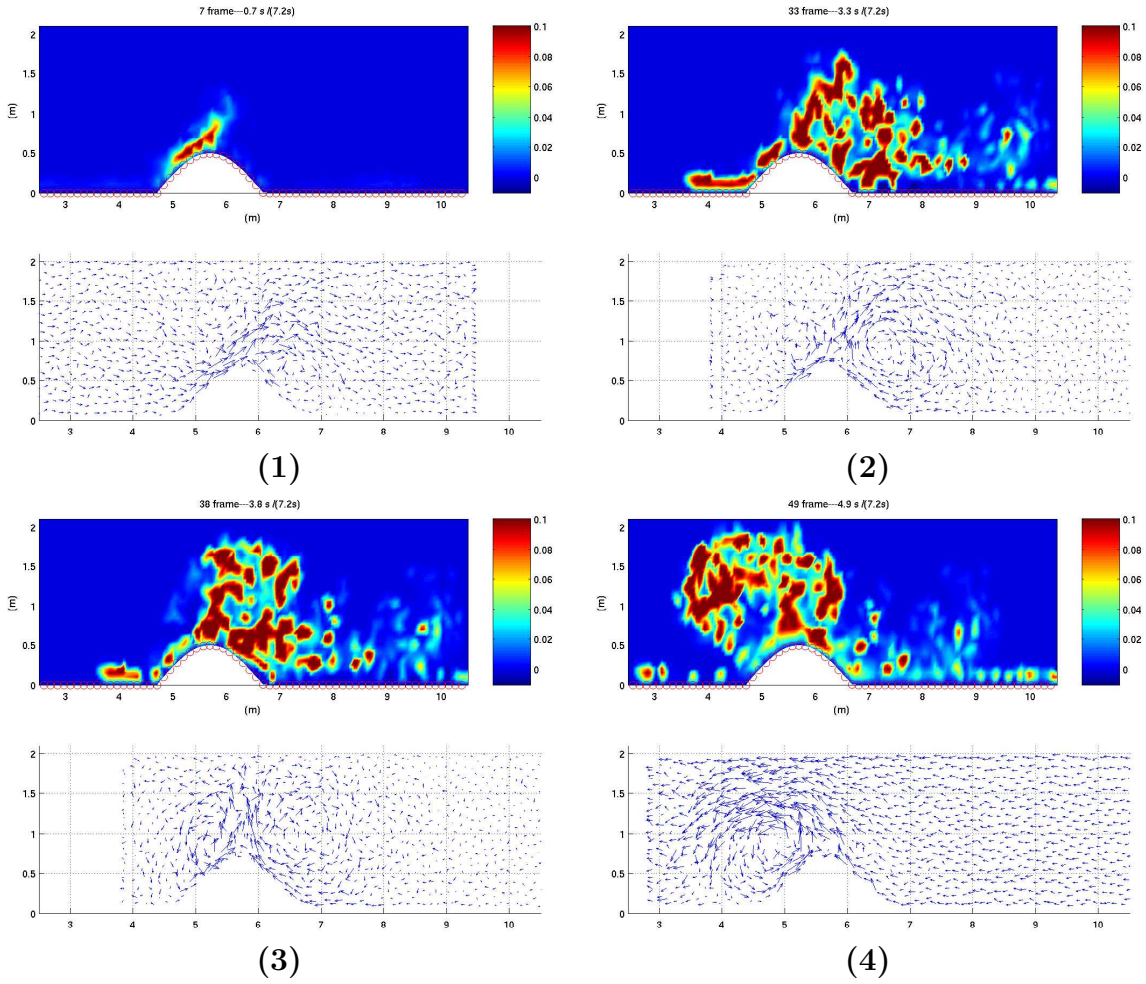

Figure 4.12: Snapshots of sediment suspension of concentration and velocity vectors

4.3 Validation of Sediment Suspension Model

4.3.1 Simulation of Oscillatory Flow over Ripples

Introduction

In river mechanics, the sediment transport and bed forms relate to the stream power, which is the time rate of at which either work is done or energy is expended. The stream power is expressed per unit area, length, mass or weight[28]. For example, the stream power per unit mass of water is

$$\omega_m = gVS \tag{4.45}$$

where g is the gravity acceleration, V is the mean velocity (m/s) in the stream cross section, S is the slope of the stream. ω_m has the unit of m^2/s^3 or $watts/kg$.

A plane stream bed will change bed configurations with increasing intensity of flow: ripples, dunes, plane bed, and anti-dunes. The shape of ripples or dunes is roughly triangular with a mild and slightly curved upstream surface and a downstream slope approximately equal to the angle of repose. Flow separates from the ripple near the crest and reattaches to the bed in the trough. A vortex is formed at the lee side of the ripple, which is a low energy region that experiences some sediment deposition. The zone above it has free turbulence. So the flow-sediment interaction pattern is that the shear stress moves the sediment particles from the upstream side of ripple until the sediments pass the crest and deposit on the lee side. These processes make the ripples or dunes move in a slow and continuous pattern.

For increased stream power, the dunes become longer and flatter. Finally the bed changes to a flat bed. Further increases in stream power leads from transition of flat bed to anti-dunes which move upstream[26] because the the free surface changed by bed form dramatically and possible breaking occurs. And bed shear stress increases along the downstream side of the bed form to a maximum just downstream of the trough with resulting erosion along this interval. Bed shear stress along the upstream side of the bed form reduces to a minimum till the crest with resulting deposition along this interval. Thus the bed form migrate upstream.

In coastal areas, the wave-generated bed forms are quite different from those in unidirectional flow. The shape of ripples is more symmetric than those caused by unidirectional flow because of oscillatory changes of flow strength and direction due to waves. The scale of wave-generated ripples depends on wave conditions. The ripples occur in two groups: rolling grain ripples and vortex ripples, which are formed by low and high Shields parameters respectively. The rolling grain ripples are formed at low Shields number not much larger than twice of the critical Shields number, which have small ripple height and there is no real vortex forms downstream from the ripple crest. The vortex ripples have higher height, formed at higher Shields number, and the vortex motion is important in the flow near the ripples[47].

The formation of ripples is due to the interaction between flow and granular beds. As flow starts a cycle in the oscillatory flow, the fine sediments start to move with the flow and weak turbulence structures form. With the increase of flow intensity, the turbulence becomes more organized and the sand starts to move in bed load close to the bed. At a certain stage, some sand grains are picked up and suspended by turbulence fluctuations, forming ripples. The change in the bed changes the hydrodynamics. For example, in flat beds the bed skin friction is a dominant force but the drag friction is more important after the formation of ripples. If the intensity of flow is increased further until sheet flow conditions, the ripples will be erased by the strong suspension and transport. When the flow reverses the process is repeated but in the other direction.

At the stage of steady or quasi-steady sand ripples, the pattern of flow and sand transport interaction is much more complicated than that for the flat bottom. The flow-sediment pattern for oscillatory flow is that: after the flow has turned to the right, a separation eddy develops downstream from the crest. This eddy expands with time and will be released from the bed when the pressure gradient reverses. The released eddy gradually loses its strength and this vortex is able to move considerable amounts of sediment away from the bed, which means that the presence of ripples increases the amounts of sediment in suspension [26].

As early as 1910, Ayrton found that the formation of sand ripples on the sea bed is related to the existence of vortices due to the alternate directions in wave cycle and

the vortex structure plays crucial role in sediment transport [7]. Nielsen proposed two mechanisms for sediment suspension around sand ripples based on experimental observation [69]: in the first half of the wave cycle, the flow separates at the lee side of ripple, the sediments are trapped in the vortex structure generated by this separation; in the second half wave cycle, the vortex structure is no longer reinforced when the flow reverses, the vortex structures are convected by local velocity. At the same time the sediments are carried into suspension far from the point where they are picked up. They are released into the water column as the vortices decay.

There are some attempts to study this phenomenon using numerical model, but most of them focus on the hydrodynamics instead of the prediction of sediment motion. Longuet-Higgins [57] used a discrete vortex method to study the oscillatory flow over steep ripples with the assumption that sand-water interface is fixed. Barr and Slinn et.al [3] solved the three-dimensional time-dependent Navier-Stokes equations on curvilinear grids in a horizontally periodic domain and examined the turbulent oscillatory flow over sand ripples of various shapes. They did some numerical experiments and showed how the flow dynamics adjust in the presence of ripples topography. But there is no sediment transport and experiment data comparison in the study.

There is few literatures on the flow and sediment interaction over the sand ripples using the numerical simulation. Blondeaux and Vittori [7] studied the oscillatory flow over a ripple bed by solving the vorticity equation and Poisson equation using a new numerical approach based on spectral methods and finite difference approximations. Using the computed flow field they formulate a numerical model to provide a description of the dynamics of sediment grains in suspension. The numerical results are compared with the instantaneous experimental visualizations. Hansen *et al.*[41] describes the sediment suspension over wave-generated ripples by use of a discrete vortex model using cloud in cell concepts.

The cloud-in-cell method is an high order interpolation algorithm for Lagrangian motion in Eulerian system. In this algorithm the known vortices are described by positions and strengths. At every time step a grid vorticity is generated by smoothing the vorticity of known vortices onto the four neighboring grid points. This grid vorticity then used to generate the grid stream function by solving Poisson equation.

The stream function can be differenced on the grid to produce the velocity field, which is finally interpolated back to the vortex positions. The details refer to Christiansen's paper[14].

The model is summarized here because the SPH model will be used to reproduce the same experiments that are simulated by this model.

The hydrodynamics model is based on the Navier-Stokes equation for a two-dimensional incompressible flow and transport equation for vorticity. The N-S equation can be expressed in Poisson equation by introducing stream function by eliminating pressure:

$$\frac{\partial^2 \psi}{\partial x^2} + \frac{\partial^2 \psi}{\partial y^2} = \omega \tag{4.46}$$

and the transport equation for vorticity

$$\frac{d\omega}{dt} = \nu \nabla^2 \omega \tag{4.47}$$

where ψ is stream function, ω is vorticity, ν is kinematic viscosity.

The stream function and vorticity are defined by velocity field:

$$u = \frac{\partial \psi}{\partial y} \tag{4.48}$$

$$v = -\frac{\partial \psi}{\partial x} \tag{4.49}$$

$$\omega = \frac{\partial u}{\partial y} - \frac{\partial v}{\partial x} \tag{4.50}$$

The Poisson equation is solved by finite differences on a grid and the strength of vortices in each grid cell is distributed as vorticity in the four grid points at the corners of the cell. The vorticity generated in the boundary layer is solved by Von Karman's momentum equation includes with the assumption that the velocity profile in the turbulent boundary layer is logarithmic.

The suspended sediment model is described by the turbulent diffusion equation, which is the same as the convection-diffusion equation mentioned before. But the individual suspended grains are followed with a Lagrangian formulation.

The near-bed boundary condition is formulated by the approach of Englund and Fredsoe [25]. The agreement between the time-averaged simulated concentration profiles and the experimental data is satisfactory.

Experiments for Sand Ripples

In order to validate the sediment transport model, the SPH model is applied to simulate the suspended sediment over ripples. Obtaining the correct results for sediment requires a detailed description of the flow. The motion of the water particle will show the turbulent structure by the SPS scheme which can resolve the turbulence structure that is smaller than the particle size.

There are two experiments that will be reproduced from the Hansen *et al.* paper: experiment A and experiment B. The conditions of oscillatory flow is listed in the following table 4.1. where U_{1m} is the amplitude of velocity, T is the period of oscil-

experiment	$U_{1m}(m/s)$	$T(s)$	$a(m)$	$\lambda(m)$	$\eta(m)$	shape
A	0.35	5	0.28	0.252	0.03	parabolic
B	0.90	4	0.57	0.83	0.125	sinusoidal

Table 4.1: Oscillatory flow conditions, ripple size and shape for the experiments

latory flow, $a = \frac{U_{1m}T}{2\pi}$ is the amplitude of oscillatory motion, λ is the ripple length, η is the ripple height.

The experimental data of sediment concentration over sand ripples was obtained by Ribberink and Al-Salem [78], who used the Large-scale Oscillating Water Tunnel in Delft. There are a total 28 experiments that were presented. The experiment A is test 4 and experiment B is the test 18. The size of bed sediment is characterized by the parameters $d_{10} = 0.15mm$, $d_{50} = 0.21mm$, $d_{90} = 0.32mm$, where d_n is statistic size of sediment, for example, $d_{90} = 0.32mm$ means that 90% of sediments are finer than 0.32 by weight.

The configurations of simulation are adopted from Hansen's paper[41]. In the simulation of experiment A, the ripples are represented by parabolas and in the experiment B the sinusoidal bed forms are simulated. These two experiments are selected as the Shields parameter $\theta = 0.15$ for typical vortex ripple bed and $\theta = 0.82$ which is the upper limit for the formation of ripples. The figure 4.13 shows the schematic sketch of the shapes of two kinds of ripples. The difference from Hansen's paper is that used the only one ripple in the simulation then copy it to both sides.

In our simulation three ripples are used and found that the motion above each ripple is not exactly same due to the random 'Brownian motion' of SPH particles, but the difference is very small.

To obtain sufficient resolution to model ripples of realistic size instead of artificial ripple as the last section, a parallel version of the model was developed. The details of parallel computing will be discussed in the Appendix A. At two ends of the tube a periodic condition is used because there are many particles wasting the computation in the range of stroke if using pistons as before. In the periodic boundary condition, when a particle exits the right boundary at a time, it enters the left boundary. The figure 4.14 shows the implementation. The periodic boundary condition for particle method is more complicated than the traditional grid method due to the change of number of particles passing the boundary at each time step.

As discussed in the previous sections, the sediment suspension includes two mechanism: diffusion and convection. The diffusion process caused by turbulent fluctuations describes the suspension close to the bottom. Turbulent fluctuations with dimensions smaller than the SPH particle size are resolved by the sub-particle scheme, which is equivalent to the sub-grid scheme in the grid method. The convection process is the dominant transport mechanism away from the bed due to the large organized eddies in the main stream.

In the SPH simulation there is no boundary layer theory incorporated in the SPH hydrodynamics model because the size of particle could be larger than the boundary layer thickness. So the prediction of this SPH model in the boundary layer is poor. One must be careful to apply this method to the case in which the boundary layer effect is important.

The pick-up function is related to the Shields parameter and the critical Shields parameter $\theta_c = 0.05$ is used in the simulation. The Shields parameter is calculated by the following equations.

$$\begin{aligned} \theta &= \frac{f_w}{2}\frac{U_{1m}^2}{(s-1)gd} \\ f_w &= 0.04(\frac{a}{k_N})^{-1/4} \\ k_N &= 2.5d_{50} \end{aligned} \tag{4.51}$$

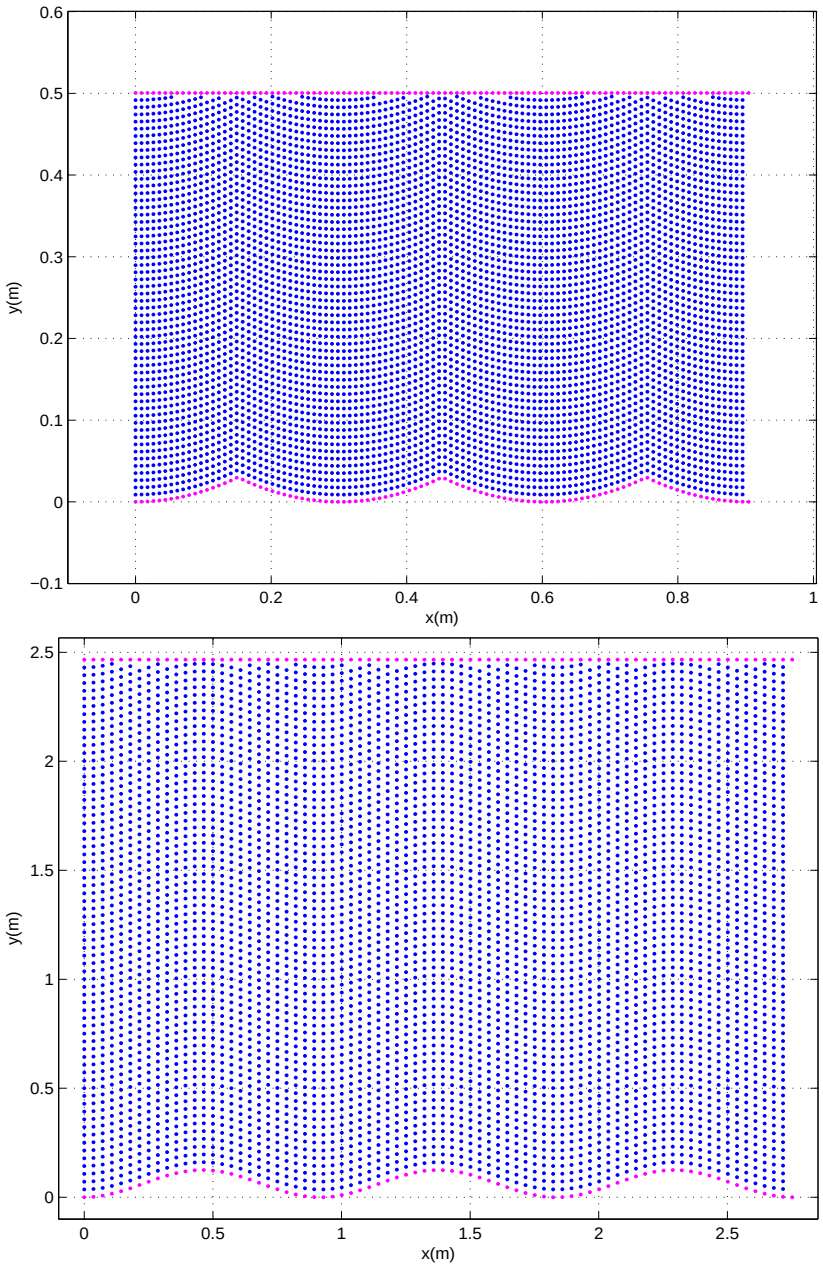

Figure 4.13: Schematic sketch of parabolic and sinusoidal ripples, showing initial SPH particle position

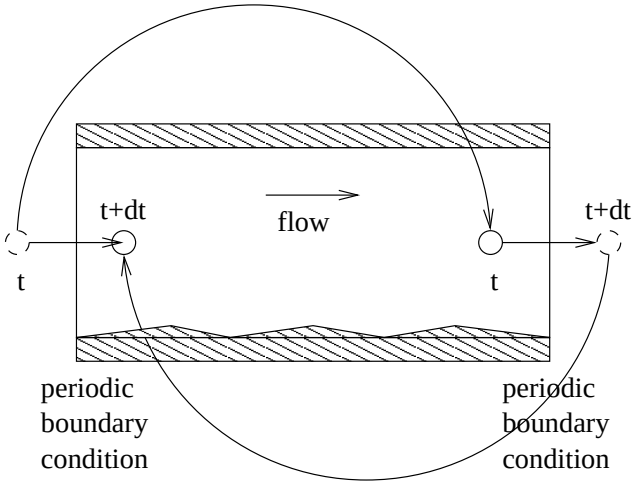

Figure 4.14: Schematic sketch of periodic boundary condition

where θ is Shields parameter, f_w is the friction factor, $s = 2.65$ is the relative density, $d = d_{50}$ is the diameter of sediment, $g = 9.81$ is the gravity acceleration, k_N is the surface roughness.

The experiments are presented by Ribberink and Al-Salem [78] and conducted in the Large-scale Oscillatory Water Tunnel (LOWT) in Delft Hydraulics. The SPH simulations reproduce the same setup as the cases presented in Hansen's paper.

Experiment A

The SPH simulation has 5864 particles and the dimensions of the computational domain are $0.9m \times 0.5m$. Smoothing length $h = 1.3\Delta x = 0.0114m$, where Δx is the particle spacing, time step is $\Delta t = 0.00001s$.

The shape of ripples is parabolic shaped troughs. The crest of the ripples are connected smoothly. The shape equations are $y = \frac{4\eta}{\lambda^2}x^2 + \frac{4\eta}{\lambda}x + \frac{\eta}{2}$ and $y = \frac{4\eta}{\lambda^2}x^2 - \frac{4\eta}{\lambda}x + \frac{\eta}{2}$, where η is the ripple height from trough to crest, λ is the ripple length, and the origin is located under the crest, where the surface elevation corresponds to the half of the ripple height.

The model results for flow and suspended sediment concentration at different times are shown in figures 4.15 and 4.16. The animation shows the flow and sediment suspension pattern: In the first wave cycle, the sediments are suspended from

upstream side of ripple and transported to downstream by main stream flow until the flow reversal. The separation occurs at the lee side of ripple crest, its vortex structure is reinforced and developed with the strength of main stream; the flow in the trough region is to the left while the main stream flow is directed to the right, which is different from the case of artificial ripple; at the beginning of flow reversal, the vortex structures become weak and diffuse into the flow, and there is phase lag between main stream flow and flow in the trough. After the flow reversal, the sediment cloud uplifted from the bed. Finally the sediments are released into the water by the vortex and its suspension is balanced by turbulence and gravity settling. The simulation results confirm the experimental observations.

After several periods, the sediment concentration of suspended load reaches the steady state due to the balance between gravity and turbulent diffusion. The period-averaged sediment concentration profile is shown in the figure 4.17. The agreement is satisfactory.

Experiment B

The SPH simulation has 5264 particles and dimensions of the computational domain $2.75m \times 2.47m$. Smoothing length $h = 1.3\Delta x = 0.0465m$, where Δx is the particle spacing, and time step is $\Delta t = 0.00001s$.

This case is for high Shields number calculated for plane bed conditions $\theta = 0.82$, which is close to the upper limit for the formation of wave ripples. In the experiments the bed forms were observed to be very irregular: the ripple heights are in the range of 0.04 m to 0.175 m, the ripple lengths varied from 0.53 m to 1.29 m. Hansen et. al. used the mean value of ripples and represented the bed forms with a sinusoidal bed. The shape equations are $y = \frac{\eta}{2}\sin(\frac{2\pi x}{\lambda})$, where η is the ripple height from trough to crest, λ is the ripple length.

The model results of flow and suspended sediment concentration at different time instances are shown in the figure 4.18. The animation shows the similar flow and sediment suspension pattern. There are several differences defined in the following instances: during the time of the flow reversal, the non-dimensional height of vortex uplifted (ratio of suspended height to the sand ripple's height) is smaller than experiment A, which is related to the shape of ripple and the strength of flow; the

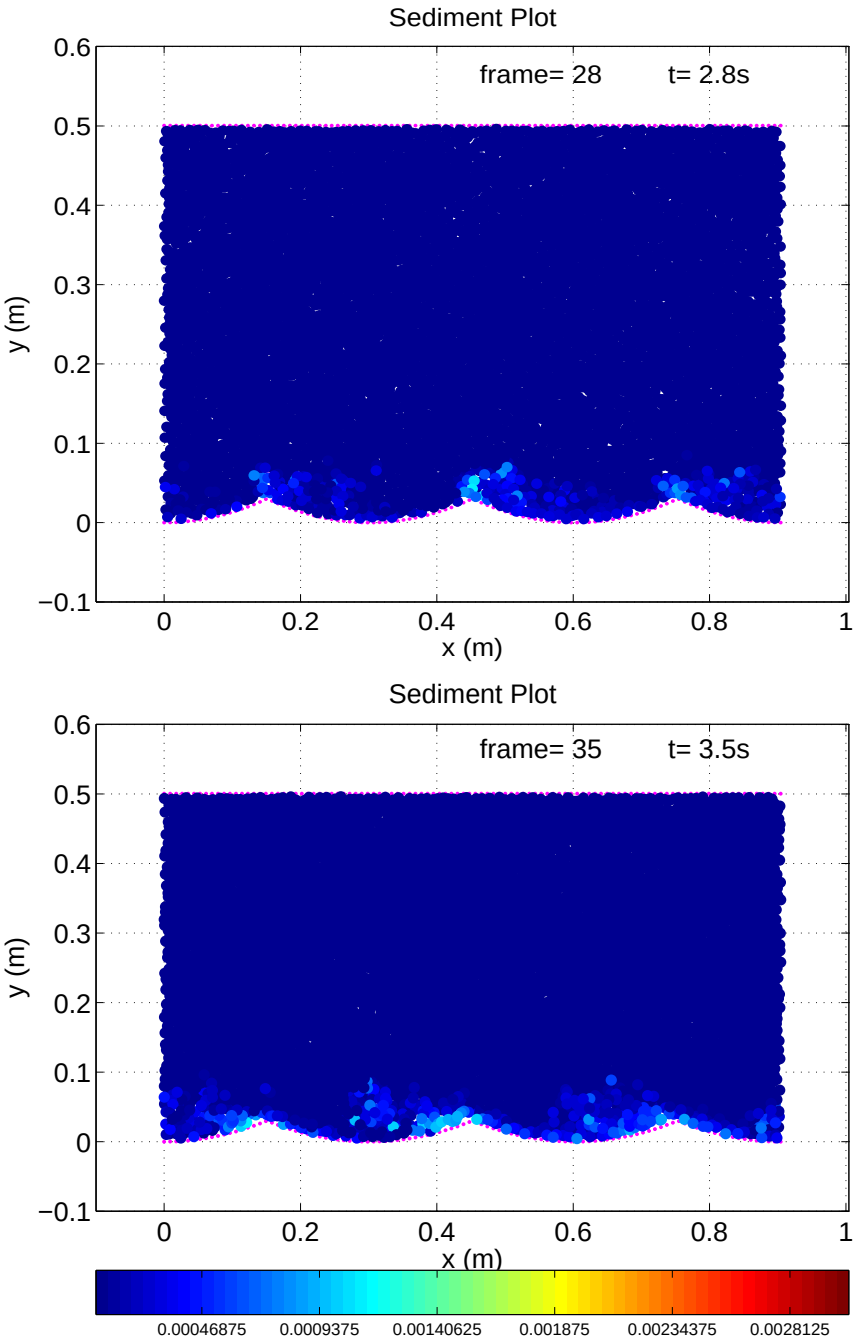

Figure 4.15: Snapshots of flow and sediment suspension over parabolic ripples at different times

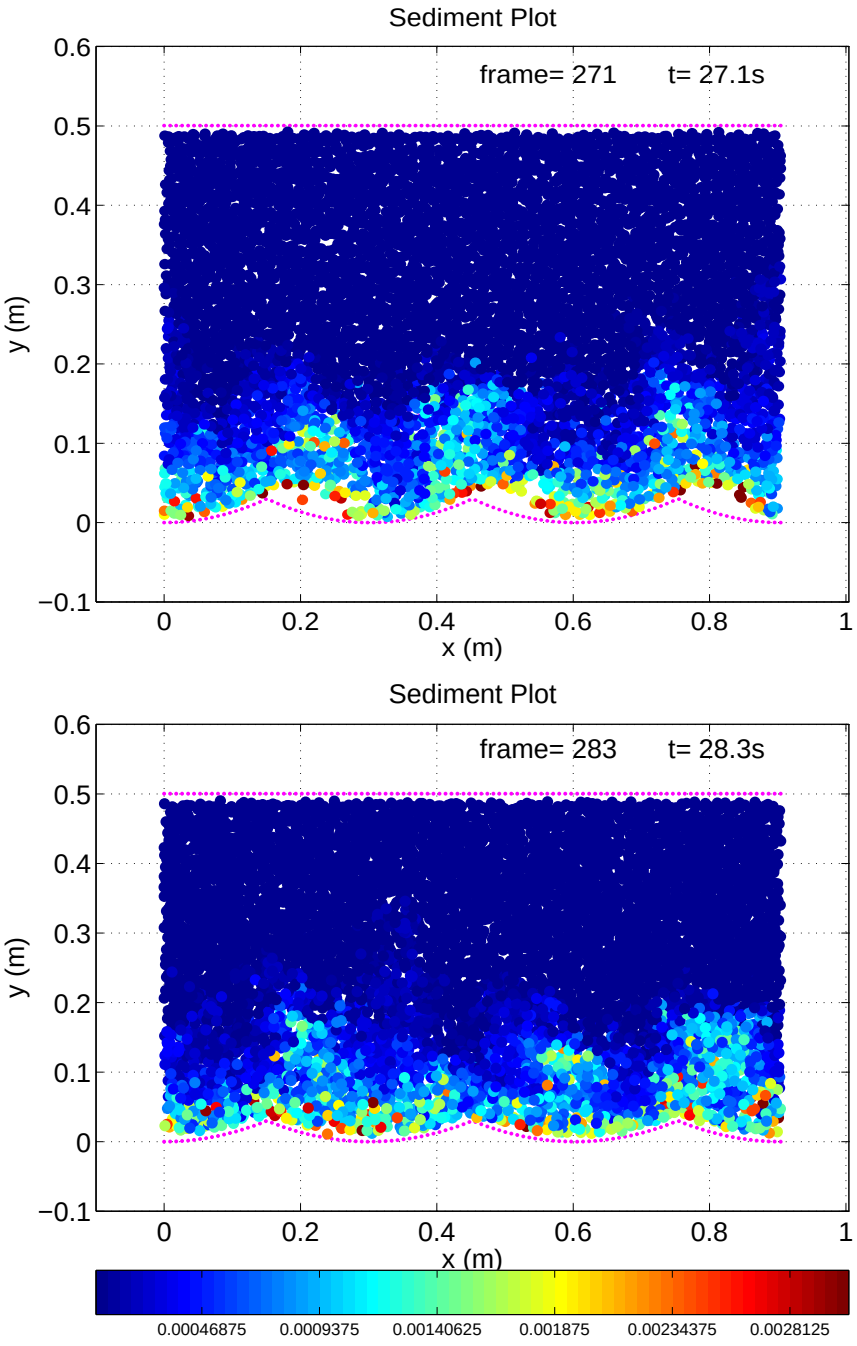

Figure 4.16: Snapshots of flow and sediment suspension over parabolic ripples (continued)

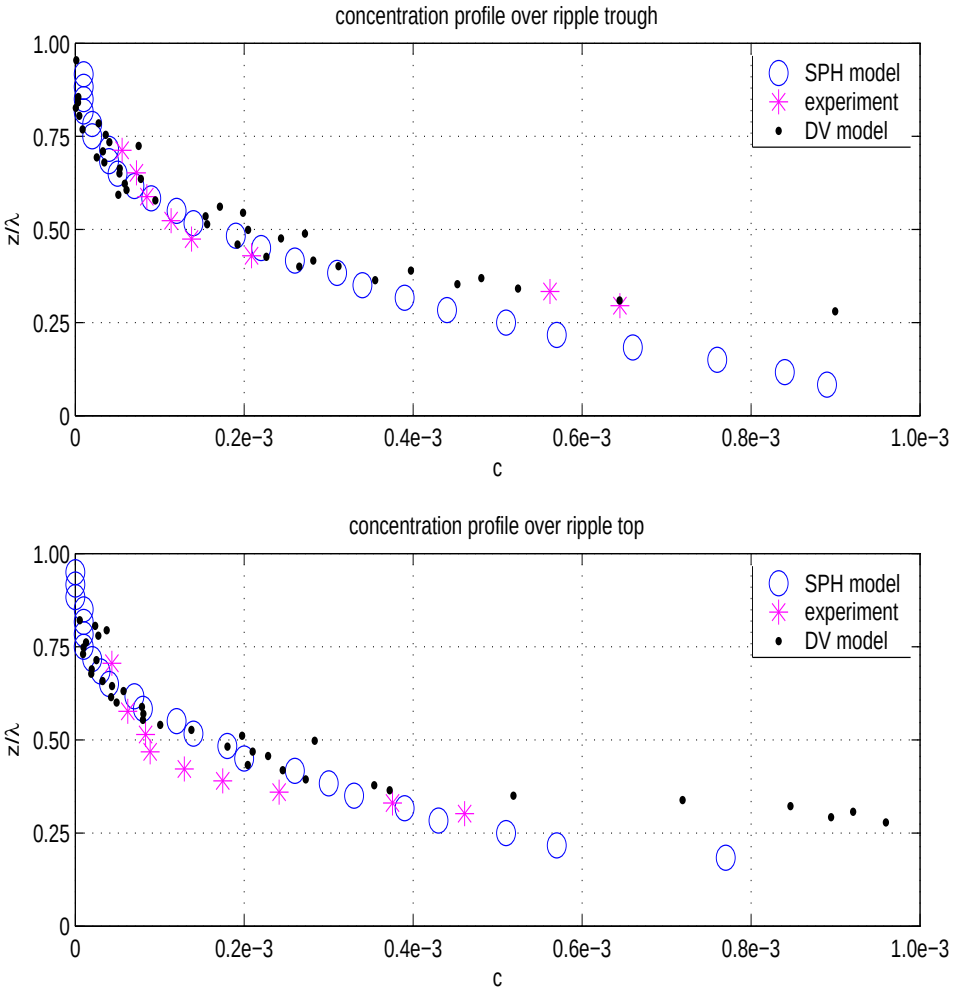

Figure 4.17: Comparison of sediment concentration profile for experiment A: SPH, experimental data and Discrete Vortex Model

size of vortex structure is bigger than experiment A, which almost covers the whole trough region. These results confirm the discoveries of Barr *et al.*[3] that the increasing of steepness of the topography enhances the existence of small-scale turbulence throughout the domain.

The period-averaged sediment concentration profile is shown in the figure 4.19. The SPH result is close to the discrete vortex model results, in that both the model results overestimate the sediment concentration. It is believed that it is due to the error caused by the representation of irregular bed forms with sinusoidal profile. The difference of sediment concentration near bed is caused by the inclusion of the boundary layer.

4.3.2 Simulation of Oscillatory Flow over Flat Bed

For weak wave conditions (equivalent to small Shields parameter or deep water), parabolic shaped ripples can be formed on the sea bed and the sediment transport process is generally dominated by the cyclic development and convection of vortices. For moderate wave conditions (equivalent to high Shields parameter or relative deep water), the sea bed becomes irregular and the ripple crest is smoother, the transport process is dominant by convection. For extreme wave condition, (equivalent to very high Shields parameter or shallow water), the sea bed becomes plane and sheet flow becomes the dominant transport process [79]. Since the SPH model simulates the ripple cases satisfactorily, the simulation of sheet flow condition over plane bed condition is conducted here.

Experiments

The experiments were conducted in LOWT in Delft Hydraulics by Ribberink and Al-Salem [79]. There are three oscillatory flow conditions used in the experiment: two regular asymmetric oscillatory flow condition and one sinusoidal conditions in the table 4.2. The size of sediments in the bed is $d_{10} = 0.15mm$, $d_{50} = 0.21mm$ and $d_{90} = 0.32mm$. In the experiment the instantaneous flow velocities are measured by the Laser-Doppler Flow Meter (LDFM), the instantaneous sediment concentrations are measured by the Optical Concentration Meter (OPCON) for suspended sediment

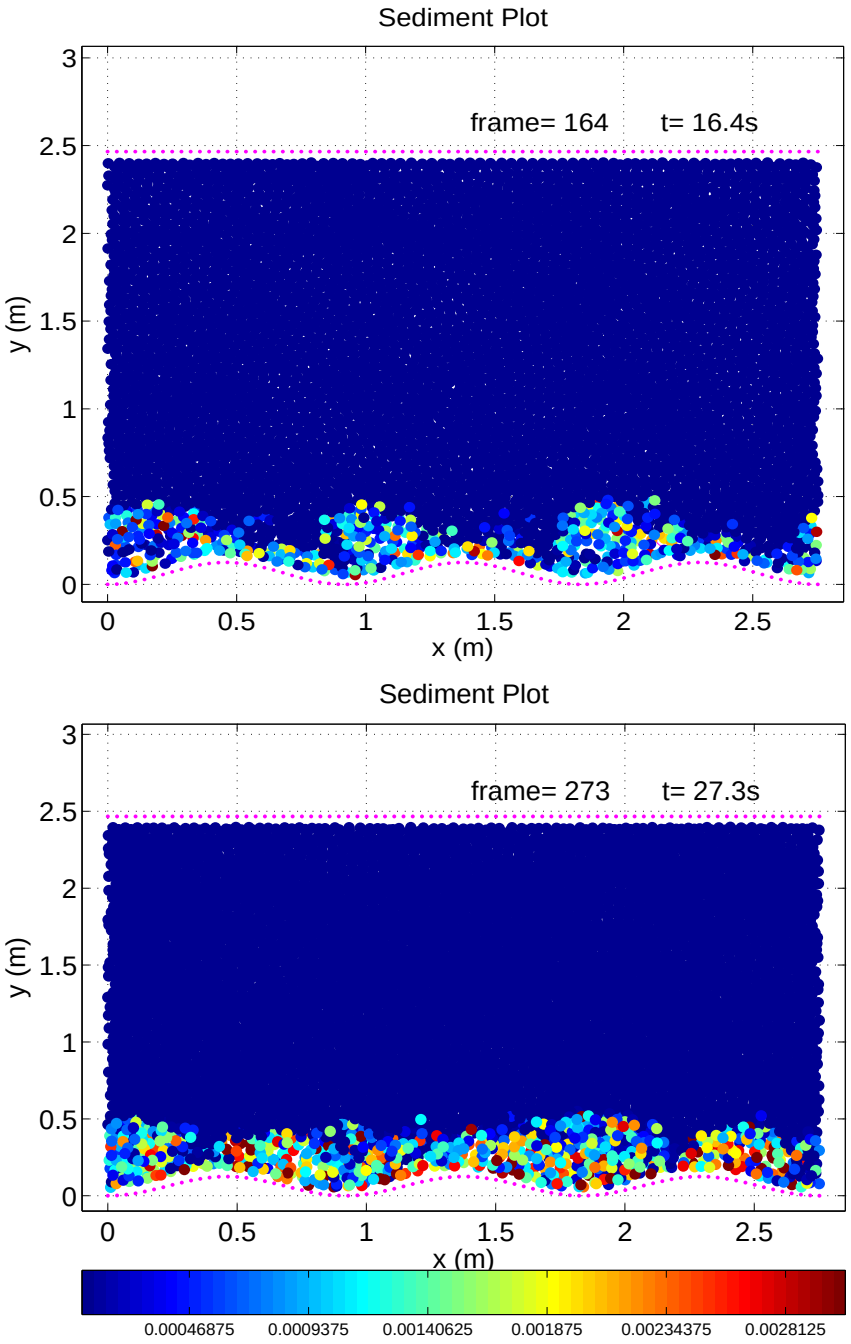

Figure 4.18: Snapshots of flow and sediment suspension over sinusoidal ripples at different times

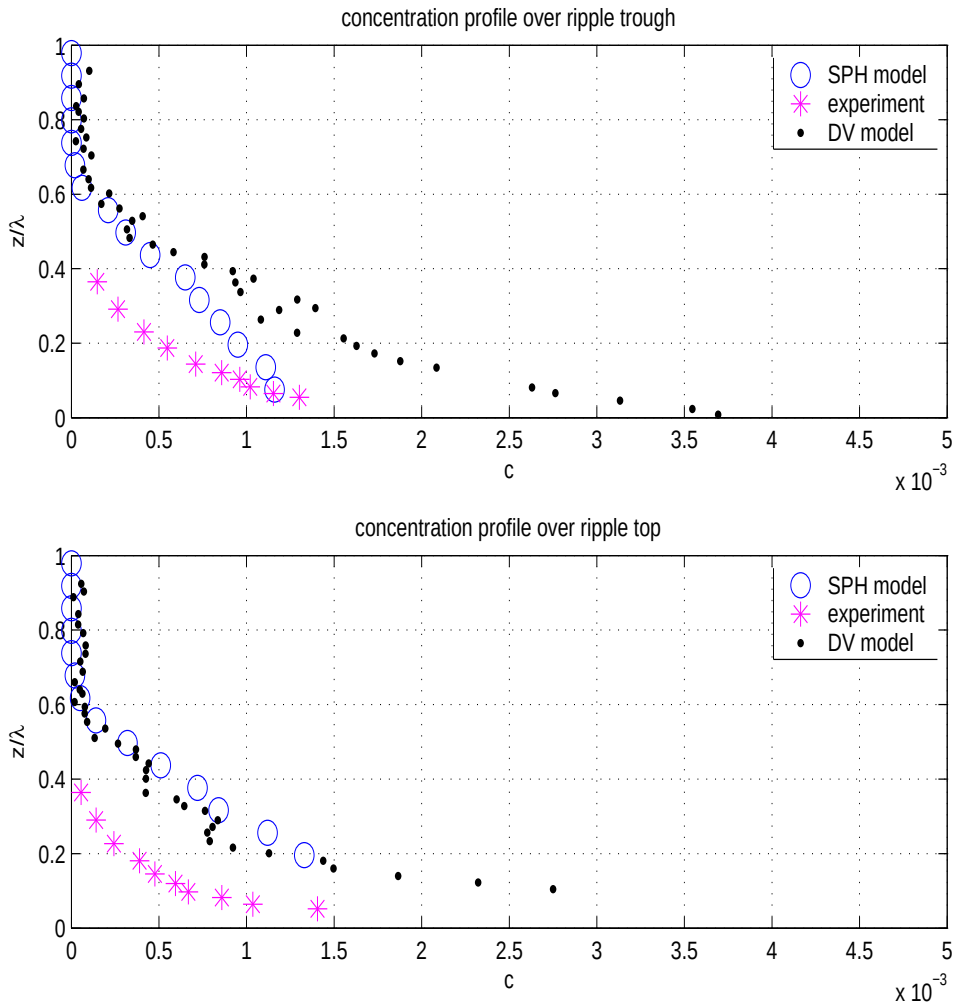

Figure 4.19: Comparison of sediment concentration profile for experiment B: SPH, experimental data and Discrete Vortex Model

and Electro-Resistance Probe (CCM) for sheet flow.

Condition	$U_{rms}(m/s)$	$T(s)$	Type of oscillatory flow	Degree of asymmetry R
1	0.60	6.5	2nd-order Stokes	0.66
2	0.60	9.1	2nd-order Stokes	0.64
3	1.20	7.2	sinusoidal	0.5

Table 4.2: Experimental conditions for oscillatory flow

$$R = \frac{U_c}{U_c + U_t}$$

where U_c and U_t is the velocity amplitude at the crest (positive direction) and at the trough (negative direction).

The measured velocity profiles for Condition 1 show that the oscillatory boundary layer is less than 10 cm, especially in the range of 2 cm $\leq$ z $\leq$ 5 cm. There is streaming measured for asymmetric conditions but not for symmetric conditions.

The measured time-averaged sediment concentration profiles above the bed show the similar results for Condition 1 and 2. The concentrations under condition 3 were about a factor 10 higher than Condition 1 and 2 due to the higher oscillatory flow velocity of a factor 2. Another important result is the large vertical concentration gradients that occur in the sheet flow layer, which is between the bed and suspension layer, of the order of millimeters. For instantaneous sediment concentration, the higher elevation, the concentration peaks reduce in magnitude and the phase lags increase. These phase lags are caused by the travel time of sediment grains for suspension and settling. The phase lags are different for different wave conditions.

In their paper, they represent a one dimensional vertical model for boundary layer flow and transport, which is based on Bakker and Fredsoe's work [2] [30]. There are several assumptions in the modeling:

1. the hydrodynamics is modeled as a uniform unsteady turbulent boundary layer;

2. there are no vertical velocities;

3. pressure gradient term is replaced by the flow acceleration term, which means that the shear stress in the free stream is neglected;

4. mixing-length theory is used as turbulence closure;

5. turbulent sediment-flux gradients are represented by turbulent diffusion;

The governing equations include equation of motion and convection-diffusion equation:

$$\begin{aligned} \frac{\partial U}{\partial t} &= \frac{\partial U_0}{\partial t} + \frac{\partial}{\partial z}(\nu_t \frac{\partial U}{\partial z}) \\ \frac{\partial C}{\partial t} &= w_s \frac{\partial C}{\partial z} + \frac{\partial}{\partial z}(\nu_t \frac{\partial C}{\partial z}) \end{aligned} \tag{4.52}$$

where $U(z,t)$ is the horizontal velocity, $U_0(z,t)$ is the free stream velocity, ν_t is the eddy viscosity, $C(z,t)$ is the sediment concentration and w_s is the sediment settling velocity. It is noted that the model used the same vertical sediment diffusion coefficient as the eddy-viscosity.

SPH simulation

The SPH simulation has 6008 particles and dimension of the computational domain is $0.50m \times 0.50m$. Smoothing length $h = 1.3\Delta x = 0.0085m$, where Δx is the particle spacing, and time step is $\Delta t = 0.00001s$.

The animation shows that there is a sediment cloud appearing in the tube. The reason for this could be the instability of the oscillatory flow. Another possibility is the Brownian motion of the SPH particles, which is irregular motion around the equilibrium position. How much error this Brownian motion can bring to the system and the features of it are interesting research topic in SPH studies. The figure 4.20 shows a snapshot of the sediment cloud for oscillatory flow over the flat bottom.

The time-averaged concentration profiles for the one dimensional vertical model, SPH model results, and experiment data are shown in the figure 4.21. Both of 1DV and SPH model can predict the bed concentration very well. The SPH model used the pick-up function boundary condition but 1DV uses the Fredsoe method [30] to calculate the bed concentration. The sheet flow layer, located between bed and suspension layer, is a high concentration gradient region. The reason is the 1DV

model is the boundary layer model but in the SPH model there is no boundary layer model included, using the slip boundary condition for hydrodynamic model. The inclusion for the boundary conditions is important for plane bed condition because the skin friction effect is dominant near bed. But for ripple bed condition the convection effect is more important than the shear stress. In the range of suspension layer SPH model has the better prediction than the 1DV model. The reason could be the assumptions of no vertical velocities, no convection term in fluid motion and one dimension simplification made in 1DV model.

4.4 Summary

- Test cases show the feasibility of solving suspended sediment transport problems with SPH, the numerical schemes are verified term by term and compared with finite difference scheme and analytical solution.
- The qualitative SPH test cases are applied with very low resolution (dx=0.12 m), but they can resolve some complicated physics.
- Solving the sediment transport equation by SPH is more computational efficient than treating the sand as real particles and able to do engineering applications
- The SPH model is validated by different oscillatory flow with weak, strong and extreme condition over ripples and plane bed. The quantitative predictions agree with experimental data very well.

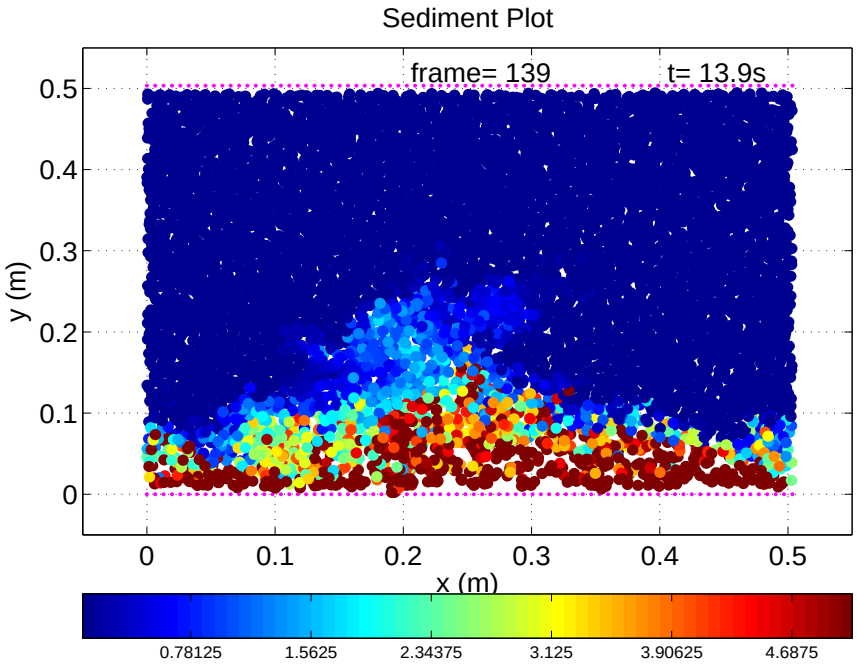

Figure 4.20: Snapshot of sediment suspension over flat bed under oscillatory flow

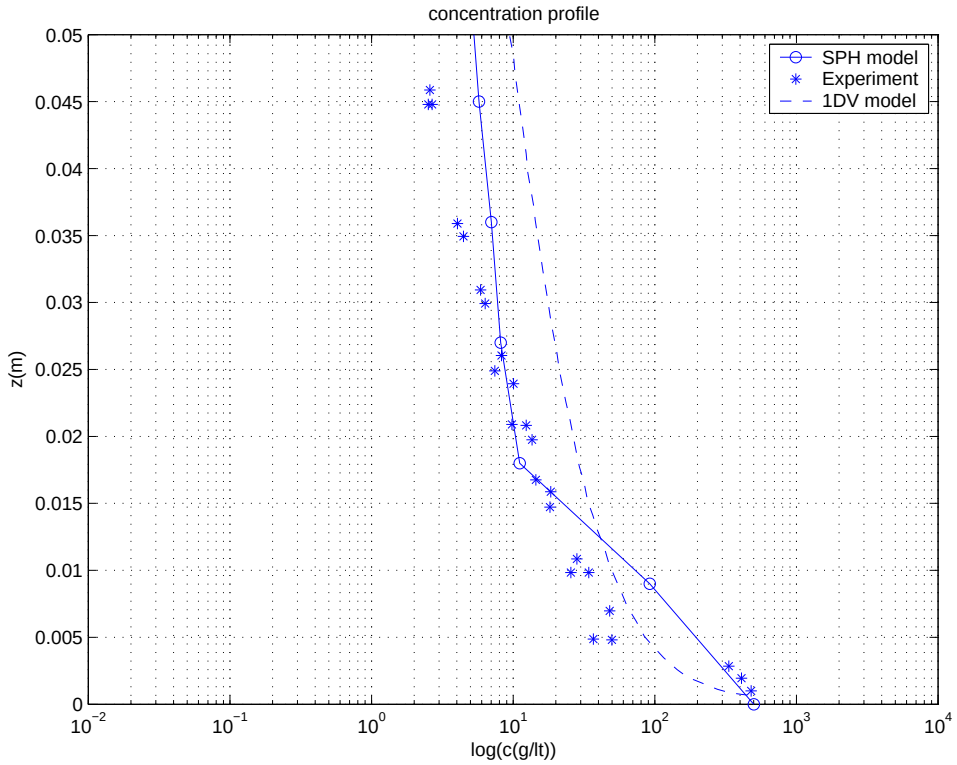

Figure 4.21: Comparison of sediment concentration profile for oscillatory flow over the flat bed: SPH, experimental data and one dimensional vertical model

Chapter 5

Coastal Sediment Transport Simulation

The Smoothed Particle Hydrodynamics model and sediment transport model can simulate the local sediment transport and breaking waves successfully for short periods of time. In order to study the complicated physics of sediment suspension and contaminant propagation in the surf zone, the SPH concentration model is applied to breaking waves and the resulting morphological change in this chapter. The numerical results show that considerable feasibility of predicting the complex physics of interaction between breaking waves, sediment and coastal topography at least in the short time. Using constant diffusion coefficients, a reasonable distribution of concentration along the beach slope can be shown. Another important discovery is the coastal circulation system generated by breaking waves is obtained by time-averaging.

5.1 Introduction

In the nearshore area, sediment transport and contaminant dispersal are very important topics in coastal engineering, which relate to beach evolution and coastal water quality. The turbulence caused by breaking waves near the bottom boundary layer is a major agent for sediment suspension. Near the shoreline the mixing by wave-induced vortices of different length scales is dominant in the transport process.

In order to predict the sediment distribution correctly, considerable turbulence information is needed during the breaking process. The general transport processes include convection and diffusion processes. The mass and momentum flux in vertical associated with the waves generates a cross-shore circulation, which moves the sediment in the onshore and offshore directions. In the surf zone, some previous works consider the convection effect is much smaller than diffusion, but some others argue that convection caused by large-scale mixing cannot be neglected. Duy and Shibayama [23] did a quantitative evaluation of these two terms and show that both processes should be considered in order to predict the sediment concentration in surf zone.

Numerical models of surf zone hydrodynamics can be divided into two categories: wave-averaged models and phase-resolving models. *Wave-averaged models* consider the effect of waves by time-averaged quantities including mean mass flux, mean momentum flux, and mean dissipation of energy, which provide the forcing for wave-averaged motion. All of these mean values are provided by averaging the short waves motion from another wave model, called wave-driver. The wave-averaged model has no details of the short wave motion. It is also called nearshore circulation model. SHORECIRC is a typical wave-averaged model for surf zone hydrodynamics model[87].

The *phase-resolving model* have very detailed information about the wave phase variation, particle motion and surface elevation by solving the shallow water equations using different CFD method, such as Boussinesq model, Large Eddy Simulation (LES), Direct Numerical Simulation (DNS), and Volume-of-Fluid (VOF). The SPH model falls in the category of phase-resolving models and we will use it to study some features of wave-averaged motion too.

There are four typical phase-resolving numerical models to simulate wave breaking: the Roller model [88], which can calculate the wave height before and after the breaking based on the hydraulic jump theory; depth-integrated models [99], which solves the shallow water equations and treat the breaking process with a dissipation term; and Reynolds Averaged N-S (RANS) model, combined with $k - \epsilon$ equation, which not only predicts the wave conditions and the turbulent kinetic energy but

also the energy dissipation. Lin and Liu [53] applied this method, using the Volume of Fluid (VOF) method to track the free surface. Christensen and Deigaard [13] used 3D Large Eddy Simulation (LES) model, combined with free surface model to study the features of the breaking waves. But the free surface was assumed uniform by 2D model. All of the traditional wave models need additional models to predict the details of free surfaces during breaking process, especially for large deformation and separation. Rogers and Dalrymple [81] developed the SPH method to simulate the weakly plunging breaker and obtained detailed results during the entire process of breaking. They show it is very straightforward to capture the complicated free surface of breaking waves due to the pure Lagrangian nature of the SPH method.

The wave characteristics in the surf zone are different from waves in deep water in phase velocity, surface shape, crest elevation and particle motion. The phase velocity of incident waves in the surf zone will change with the shoaling effect. The surface profiles change as the waves approach the shore line, which is far from sinusoidal wave. And the variation is different wave by wave. The wave profile peaks at a crest and flattened at a trough, it becomes sawtooth in shape near the breaking point. After the breaking the steepness of the wave is decreasing as it approaches to the shore. The crest elevation, which is the ratio of crest elevation above mean water level η_c over the wave height H, is large at the breaking point and decreases shorewards.

The coastal sediment transport problem usually considers the cross-shore and longshore sediment transport separately. The cross-shore sediment transport is considered to be significant for the short term variation of coastal process and longshore sediment transport is more used for the long term variation of the coastal topography change [44]. The SPH model in this research will apply for the cross-shore sediment transport for the purpose of short term predictions.

The characteristics of sediment transport in the surf zone is different from that in the offshore zone, in which the sediment transport is induced by wave action as a combination of bed load and suspended load, and the sand ripples play an important role. But in the surf zone the sediment transport mode is dominant by suspended mode, especially near the breaking point, caused by strong turbulence of breaking waves. The patterns of suspended sediment are different for the breaker

type. Horikawa *et al.* [44] concluded the four sediment transport patterns due to the wave action based on the observation of wave flume experiments, which is helpful to understand the test cases in this chapter:

1. Bed load transport is dominant and no suspension sand cloud exists. The net sediment transport is in the onshore direction.

2. Suspended sand clouds are formed, both bed load and suspended load should be considered. The net sediment transport direction is either onshore or offshore depending on the dominance of the sediment transport mode.

3. Suspended sediment transport is dominant. Suspended sand clouds are formed only on the onshore sides of ripples. The net sediment transport is in the offshore direction.

4. Suspended sediment transport is dominant. Suspended sand clouds are formed on the both sides of ripples, but the net sediment transport is in the offshore direction.

In general, the net sediment transport for solely bed load is in the onshore direction and the net transport of solely suspended load is in the offshore direction.

The most commonly used model for sediment suspension is the convection-diffusion equation. It has been applied in a grid method for a long time with satisfactory results[69][79]. The convection term in this model sometimes causes numerical difficulty due to its nonlinearity. The results in previous chapters show the capability of the SPH model to simulate the wave hydrodynamics and sediment suspension.

This chapter presents a vertical 2-D SPH model to simulate the sediment suspension under breaking waves. The breaking wave model includes wave shoaling, breaking, run-up, and run-down. The sediment suspension model shows the spatial and temporal distribution during the breaking process.

5.2 Governing Equations

The present model includes two submodules: one is the hydrodynamics model to simulate the breaking wave and the other is sediment concentration model. Both are solved by the SPH method.

5.2.1 Breaking Wave Model

The hydrodynamics model of breaking waves is simulated by the N-S equation in Lagrangian form. In order to capture turbulence during the breaking process, the sub-particle scale (SPS) method is applied which is able to simulate the turbulence at scales smaller than particle scale.

$$\frac{d\vec{v}}{dt} = -\frac{1}{\rho}\nabla P + \nu\nabla^2\vec{v} + \vec{f} + \frac{1}{\rho}\nabla\cdot\overline{\tau} \tag{5.1}$$

$$\frac{1}{\rho}\frac{d\rho}{dt} + \nabla\cdot\vec{v} = 0 \tag{5.2}$$

$$P = B[(\frac{\rho}{\rho_0})^\gamma - 1] \tag{5.3}$$

where $\vec{v}$ is particle's velocity, $\vec{f}$ is the external forces acting on particles, $\overline{\tau}$ is SPS stress tensor, γ is constant for the equation of state 5.3, we use $\gamma = 7$ here. The SPS scheme used here is followed the paper by Lo and Shao[56], using Smagorinsky eddy viscosity model.

$$\frac{\tau_{ij}}{\rho} = 2\nu_t S_{ij} - \frac{2}{3}k\delta_{ij} \tag{5.4}$$

$$\nu_t = (C_s\Delta l)^2\|\overline{S}\| \tag{5.5}$$

$$\|\overline{S}\| = (2S_{ij}S_{ij})^{1/2} \tag{5.6}$$

where S_{ij} is SPS strain tensor, k is SPS turbulence kinetic energy, ν_t is turbulence eddy viscosity, Δl is particle spacing and C_s is Smagorinsky constant.

5.2.2 Sediment Suspension Model

The Lagrangian form of convection-diffusion equation describe the general transport process.

$$\frac{dC}{dt} = w_s \frac{\partial C}{\partial z} + \nabla \cdot (\epsilon_s \nabla C) \tag{5.7}$$

where C is sediment concentration, w_s is sediment settling velocity and ϵ_s is the diffusion coefficient. The two terms in the right hand side represent the settling and diffusion process.

5.2.3 Morphological Model

$$(1-n)\frac{\partial z_b}{\partial t} = D - E \tag{5.8}$$

$$D = w_s C_{nb} \tag{5.9}$$

$$E = p \tag{5.10}$$

where D is the downward flux due to settling, E is the upward flux by pick-up effect, C_{nb} is the sediment concentration of the near-bed particle, z_b is the bed elevation, p is the pick-up rate.

The most common used morphological model updates the bathymetry based on the sediment transport rate q_s instead of local deposition and erosion rate.

$$(1-n)\frac{\partial z_b}{\partial t} = -\frac{\partial q_s}{\partial x} \tag{5.11}$$

This equation is a convection equation that numerical analysis shows that it is not trivial to select a proper numerical scheme to solve this equation. In the finite difference method, the Forward Time Central Space (FTCS) scheme requires an additional diffusive term for the numerical stability. Another option is the modified Lax-Wendroff scheme with no additional diffusion [77].

Another important aspect in the cross-shore sediment transport is the smoothing of the calculated transport, due to the discontinuity near the breaking point. The

calculated sediment transport needs to be smoothed at each time step in the morphological model before it is used to calculate the bed level change. The sediment transport rate is calculated at each grid point or particle position. They are not smooth and continuous. It will be not stable for most of numerical algorithm to use them directly due to the discontinuities. The smoothing method cab be applied two ways: by a running average or by applying a response function [47]. Hedegaard *et al.*[42] have made simulations using different combinations of these two smoothing methods and compared with the measurements.

In our study, a five-point running average is applied to smooth out the noise in the net flux of sediment and bed level change calculation.

5.3 Boundary Conditions

The boundary conditions for hydrodynamics model use the Monaghan boundary force mentioned before. Here the details of boundary conditions for sediment transport are presented.

For sediment far away from the boundary, the concentration is determined by the settling and turbulent diffusion effect as shown in the figure 4.1.2. For the sediment near the bed, the case is different because of the existence of interface between fluid and solid. The downward exchange process still can be modeled as settling term, but the upward exchange can not be modeled as turbulent diffusion term. The study shows that the sediment grains can be suspended not only by bottom shear stress but also by turbulence burst effects, which means the sediment particle can be suspended if the shear stress is smaller than the critical value. So for the near-bed particles, the setting term can be regarded as sink term (deposition, D) and pick-up term as source term (Erosion, E). The net flux (D-E) causes the bed level change, which is used in the morphological model.

There are two important concepts are used in this model: pick-up function and wave friction factor.

5.3.1 Pick-up Function

For the steady flow and assuming the equilibrium between the bed shear stress and near-bed sediment concentration, the popular boundary condition for sediment concentration is determined by the near-bed shear stress and sediment parameters. The value of C_b, the sediment concentration of the bed particles, is a critical parameter determining the vertical distribution of suspended sediment. There are several approaches to calculate the bed sediment concentration. One, proposed by Einstein[24], is that C_b is proportional to the concentration of bed load and can be predicted by the rate of bed load transport. Englund and Fredsoe [25] developed another formula derived by a different approach and obtained similar results.

For the non-uniform or steady flow, the equilibrium assumption between bed shear stress and near-bed sediment concentration does not make sense. Nielsen[69] suggested the modified Van Rijn's pick-up function as the vertical flux of sediment in unsteady flow. The following equations show his form of pick-up function and the net sediment vertical flux in convection-diffusion model.

$$p(t) = 0.00033(\frac{\theta(t) - \theta_c}{\theta_c})^{1.5} \frac{(s-1)^{0.6} g^{0.6} d^{0.8}}{\nu^{0.2}} \tag{5.12}$$

$$\theta(t) = \frac{\tau_b}{\rho(s-1)gd} = \frac{u_*^2}{(s-1)gd} \tag{5.13}$$

where $p(t)$ is pick-up function, which is the instantaneous rate at which sand is picked up from the bed. It is a non-negative function with the dimensions of sediment flux in the unit of velocity m/s, $\theta(t)$ is the instantaneous Shields parameter, θ_c is the critical Shields parameter, here $\theta_c = 0.05$ is used, $s = \rho_s/\rho$ is the relative density of sediment, ν is the kinematic viscosity coefficient, and u_* is the friction velocity.

For stationary bed conditions and assuming instantaneous local equilibrium, the vertical flux of sediment is given by the following equation:

$$p(t) = (w_s C)|_{z=z_b} \tag{5.14}$$

which gives the bed concentration $C(z_b, t)$. This assumption is reasonable because ϵ_s is proportional to eddy viscosity of turbulence and it approaches zero near the bottom while the gradient of sediment concentration is almost constant. Finally the production term near bottom goes to zero.

5.3.2 Wave Friction Factor

Jonsson relates the bottom shear stress to the maximum bottom shear stress by the wave friction factor. The calculation of bottom shear stress is given by:

$$\frac{\tau_b}{\rho} = \frac{1}{2} f_w u_b |u_b| \tag{5.15}$$

The friction factor is a function of the wave Reynolds number $u_b A_b/\nu$ and the relative roughness a_b/k_s as:

$$f_w = f_w(\frac{u_b a_b}{\nu}, \frac{a_b}{k_s}) \tag{5.16}$$

where τ_b is bed shear stress,f_w is the wave friction factor, u_b is the near-bed maximum horizontal velocity, a_b is the excursion amplitude, k_s is the Nikuradse sand roughness.

The formula of instantaneous bottom shear stress is calculated by the following formula [17][48]:

$$\begin{cases} f_w = 0.3 & \text{for } \frac{a_b}{k_s} \leq 1.57 \\ \frac{1}{4\sqrt{f_w}} + \log \frac{1}{4\sqrt{f_w}} = -0.08 + \log \frac{a_b}{k_s} & \text{for } \frac{a_b}{k_s} > 1.57 \end{cases}$$

5.3.3 Bathymetry Update

The bathymetry updating in the morphological model can be done using either an uncoupled or a coupled method. In the uncoupled method, the hydrodynamics model provides the driving force for sediment transport but there is no feedback from the computed bathymetry to the hydrodynamics model, also called this as one-way coupling. This model can only be applied for short term predictions due to accuracy because the hydrodynamics should change with significant morphological change. The beach profile should reach the equilibrium instead of continuing change.

The coupled method calculates the fluid dynamics based on the evolving, computed bathymetry so that the hydrodynamics changes in response to the bathymetry change. The altered fluid motion will affect the sediment transport calculations in the next time step. For computational efficiency, the time step of morphological model is larger than the time step of hydrodynamic model. The coupled method requires the more strict conditions for model stability than the uncoupled method. Additional diffusion term or filtering techniques are needed for the governing equation of morphology. In this SPH model, the fluid motion is completely coupled with the morphological model.

5.4 Numerical Procedure

First the computation domain is initialized, the boundary and water particles are placed in their position in lattice, assigned and carrying all the the scalar variables including position coordinates, mass, density, and hydrostatic pressure. The wave paddle motion is prescribed. At each time step, the hydrodynamics model computes the dynamic properties for each fluid particle, such as the position, velocity, pressure, and vorticity. The smoothed near-bed velocity can be used to estimate the Shields parameter and allows the determination of the bottom boundary condition for sediment concentration. The sediment distribution can be determined by solving the convection-diffusion equation. The smoothed near bed velocity is the smoothed value, similar with field value in finite element method, which is calculated by the integration of neighboring particles:

$$< u > (x,y) = \int_{\Omega} u_p(r')W(r(x,y) - r', h)dr' \simeq \sum_j u_j W(r(x,y) - r_j, h)\frac{m_j}{\rho_j} \quad (5.17)$$

where $< u > (x,y)$ is the smoothed value of velocity at the (x,y), $u_{r'}$ is the velocity of neighboring particles, W is kernel function, m and ρ are the mass and density of the particles, h is the smoothing length.

The bottom boundary condition for the fluid is imposed using discrete fixed particles that exert the boundary force on fluid particles, as proposed by Monaghan and

Table 5.1: Different wave conditions for four cases in beach evolution tests

Case No.	Case 1	Case 2	Case 3	Case 4
Wave Height (m)	0.08	0.04	0.08	0.04
Wave Period (s)	1.40	1.40	2.80	2.80

Kos [66].

The velocity and position for wave paddle particles were given by known amplitude and period of oscillating motion to generate waves. The net flux at the interface of fluid and bed is used to calculate the bed level change based on the sediment mass conservation. Wavemaker particle motion exert forces to fluid particles. The forces change the fluid particle acceleration. For details on hydrodynamics model, refer to Rogers and Dalrymple[81].

The details of numerical scheme for sediment transport were presented in the previous chapter.

5.5 Numerical Tests

Four cases are tested in a numerical wave tank with slope 1/13.5. The assumed uniform sediment size is 0.2 mm. In all cases, the wavemaker was started with the fluid at rest; we are examining the transient motion as the waves begin the process of suspending the sediment. Table 5.1 shows the wave conditions in the tested.

The numerical experiments are used to check the ability of the model in predicting erosion and accretion under different wave conditions. For each case, the snapshot of wave breaking, sediment concentration distribution, and the beach evolution are shown in figures. Time-averaged motion is obtained by averaging over the wave period. All of the animations for 4 cases can be requested from author.

5.5.1 Case 1

Figures 5.1 to 5.2 show snapshots of sediment distribution, the change of beach profile, and the wet-averaged mean current. The wet-averaging is the mean velocity

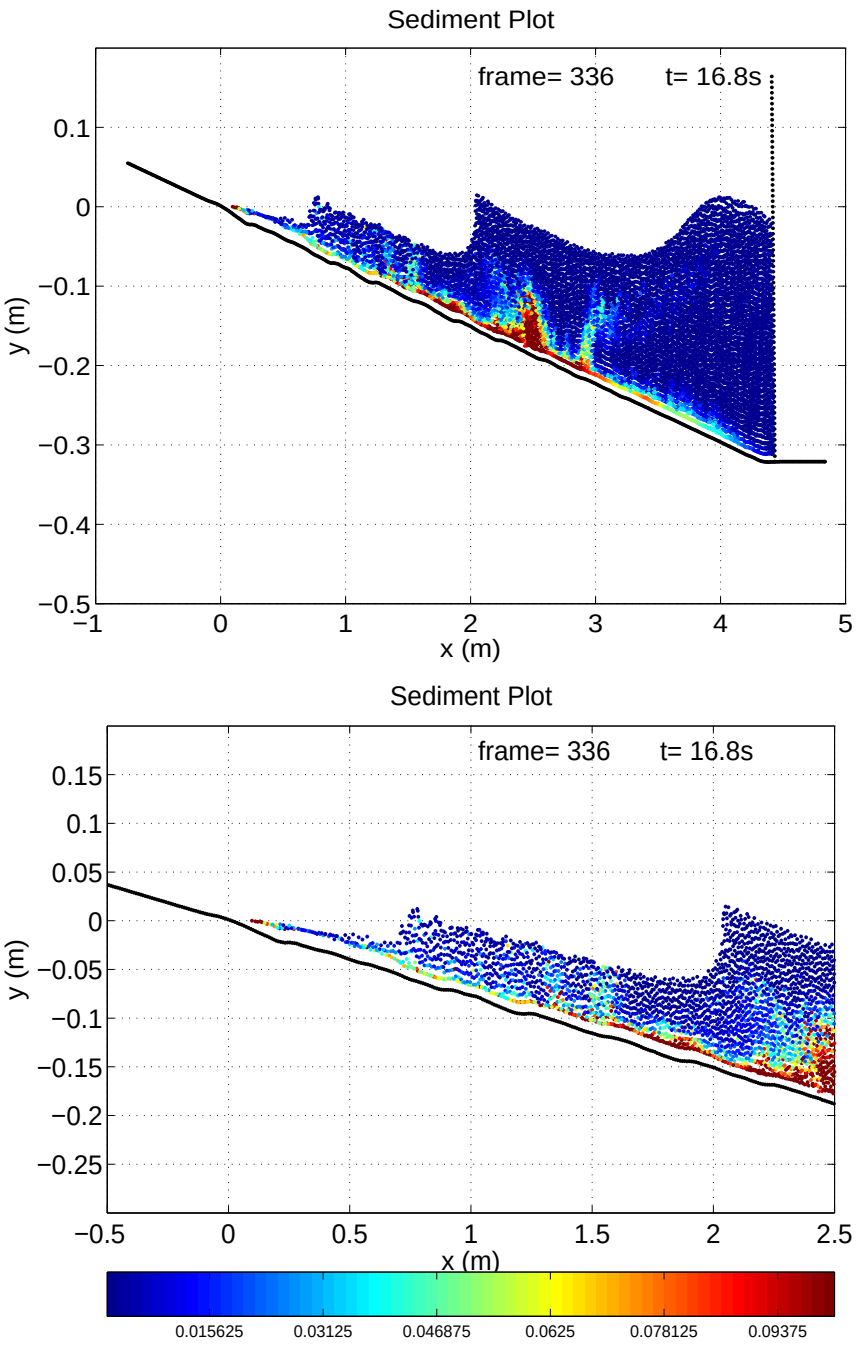

Figure 5.1: Snapshot of sediment concentration and morphological change for Case (1), 16.8 seconds after the initiation of wave motion. Here $T = 1.4s$, $H = 0.08m$, the slope is 1/13.5, with 11395 particles.

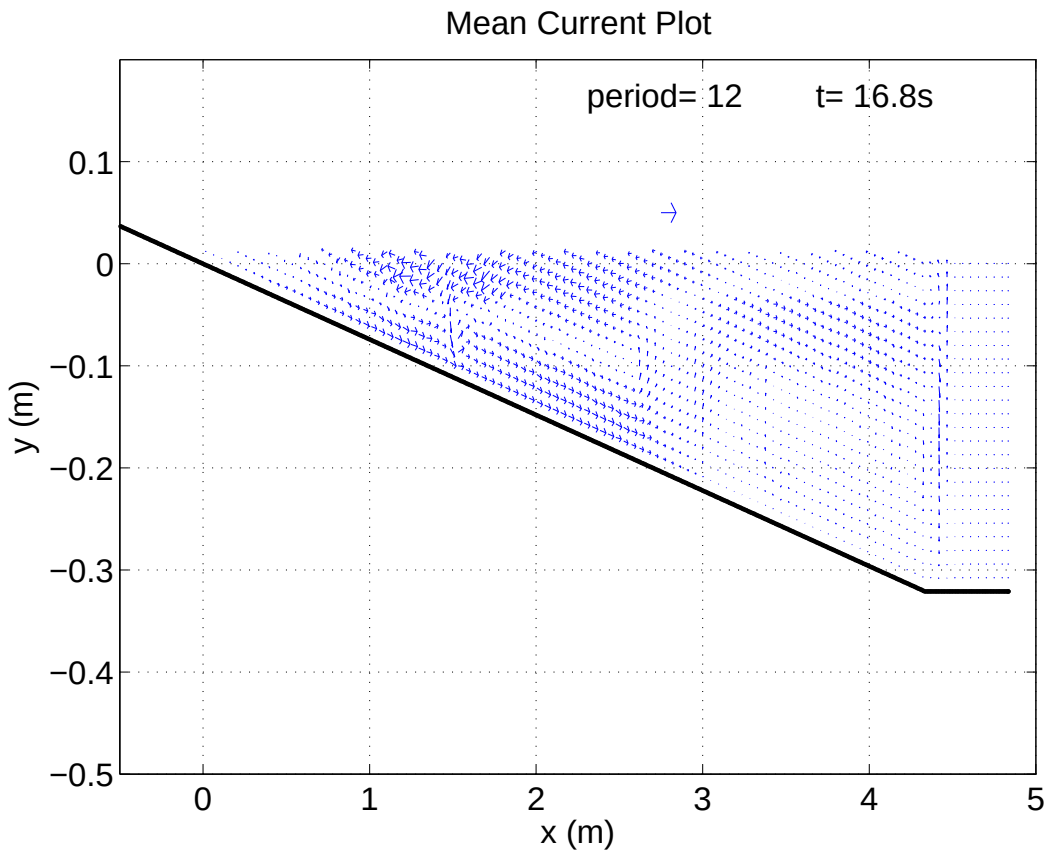

Figure 5.2: The coastal circulation of Case (1) obtained by time-averaging between 16.8s-T and 16.8s.

obtained by averaging the fluid velocity at a fixed point and dividing by the time that the measurement point is under water, rather than the wave period. For points below wave trough level, the average over wave period and the wet average are the same. From the figures, we can see that:

The first breaking point is located at $x = 0.6m$ and the backwash of water pushes the breaking point further offshore with time to the position $x = 1.5m$. The maximum run-up is reached by the first wave and the following waves' run-up is smaller than the first wave due to backwash of water. The breaker shape is a typical plunging breaker. The wave crest protrudes forward, forms the jet, and impinges on the water surface near the toe of the wave crest. During the breaking process there is an obvious forward splash and backward splash that is observed in the experiments. The turbulence and mixing near the breaking point are very strong. The waves break into small-scale turbulence and some coherent large-scale eddy structures, which can be the size of the entire water depth. After the waves transform into bore-like broken waves, they keep propagating toward the shore and run-up onto the dry beach. In the region between shoreline and breaking point, the wave height is reduced dramatically due to the loss of energy. Outside of surf zone, the near-bed velocities are increased as the waves pass by, which can be observed based on the sediment concentration. It is emphasized here that the vortices caused by breaking (breaker vortices) are very important features in the surf zone as they are involved in the exchange of momentum and turbulence with the lower part of the water column. They are the primary driving force for pick-up and suspension of sediment.

A large amount of sediment is suspended and moves seaward with offshore undertow. The maximum concentration is near the breaking point.

The wet-averaged mean currents are obtained by averaging the wave motion to eliminate the phase information. The wave motion and wave breaking are the driving force for agitation and suspension of sediment and the wave-averaged motion is the driving force for sediment transport and mass flux. The cross-shore circulation is generated after wave breaking. The cross-shore circulation system with this configuration, there are two large vortices: one is an anti-clockwise circulation, which is composed by the onshore current near the free surface and undertow near the bottom.

The strength of undertow is determined by mass flux of breakers. The other is the clockwise circulation close to wave paddle, which is believed to be an artifact of a wave tank. Finally there is upward current or plume between them that moves from paddle toward the shoreline until around the breaking point, when the wave tank reaches a quasi-stationary wave condition.

The beach is, in general, eroding status because of the strong wave and steep slope. The area that experiences the most erosion is located where the sediments are suspended by wave breaking and carried away by undertow. The undertow is weakened by the onshore currents from the outside of surf zone.

5.5.2 Case 2

For Case 2, which is the same as Case 1 but with a smaller wave height, the first wave breaking occurs around $x = 0.5$. The steady breaker line location is at $x = 0.8$, which is shallower than Case 1. The amount of suspended sediments decreases considerably and the suspended area ranges from the breaking point to $x = 1.5$, which is smaller than Case 1. The onshore free surface current and the offshore undertow are much weaker than Case 1 based on the time-averaged motion. There is no significant bed level change in the nearshore area. It is concluded that the smaller wave height results in a reduction in the amount of suspended sediment and the strength of nearshore currents.

For the cross-shore mean circulation system with this configuration, there is only a weak circulation observed in front of wavemaker. The circulations near the shore line are not obvious.

5.5.3 Case 3

For Case 3, with the same wave height as Case 1 but longer wave period, the range of suspended sediment is narrower than in Case 1 but with a similar amount of suspended sediment. The strength of undertow is slightly weaker than that of Case 1. This is caused by the milder wave steepness with longer period which generates less mass flux and momentum flux. With a longer wave period, the strong wave

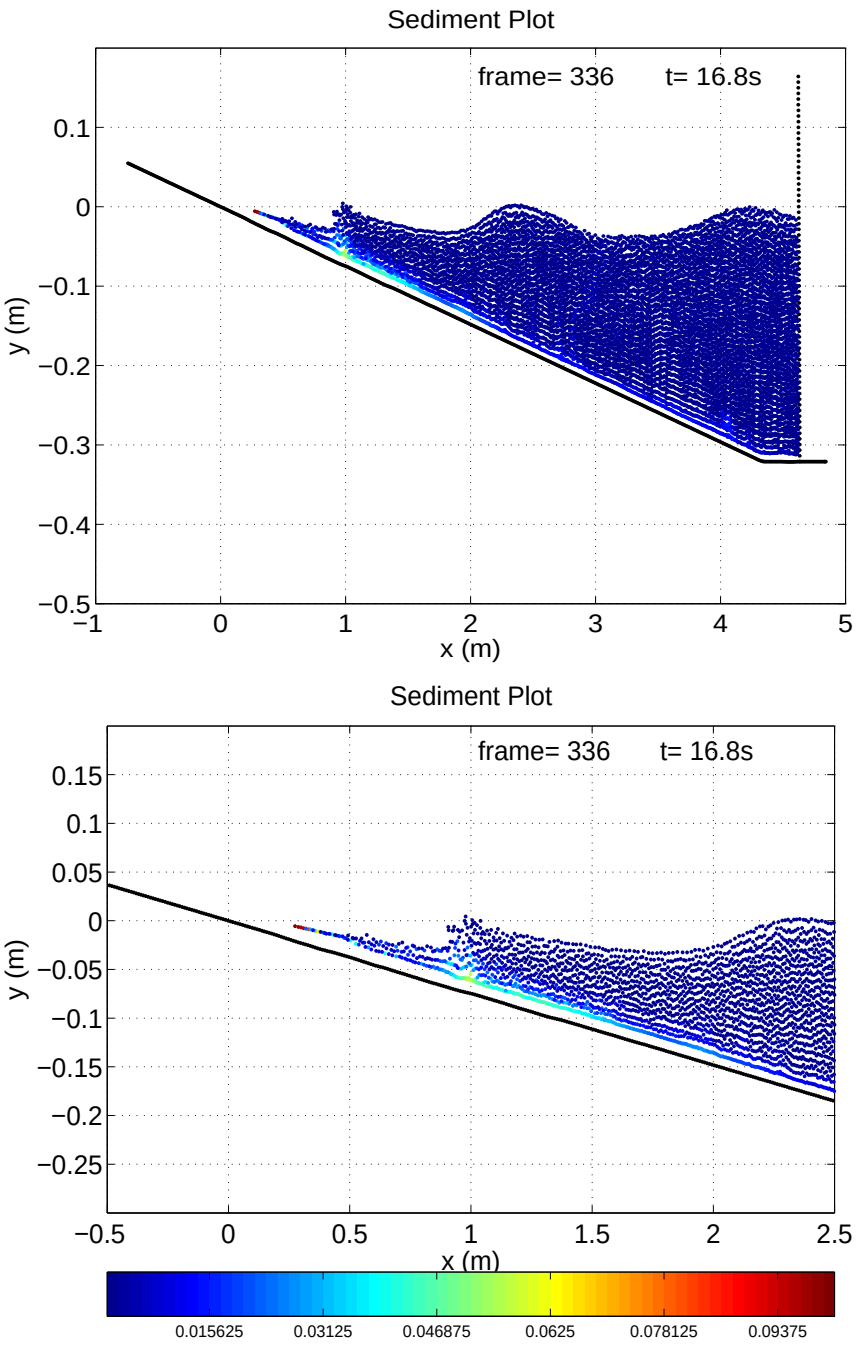

Figure 5.3: Snapshot of sediment concentration and morphological change for Case (2), 16.8 seconds after the initiation of wave motion. Here $T = 1.4s$, $H = 0.04m$, the slope is 1/13.5, with 11283 particles.

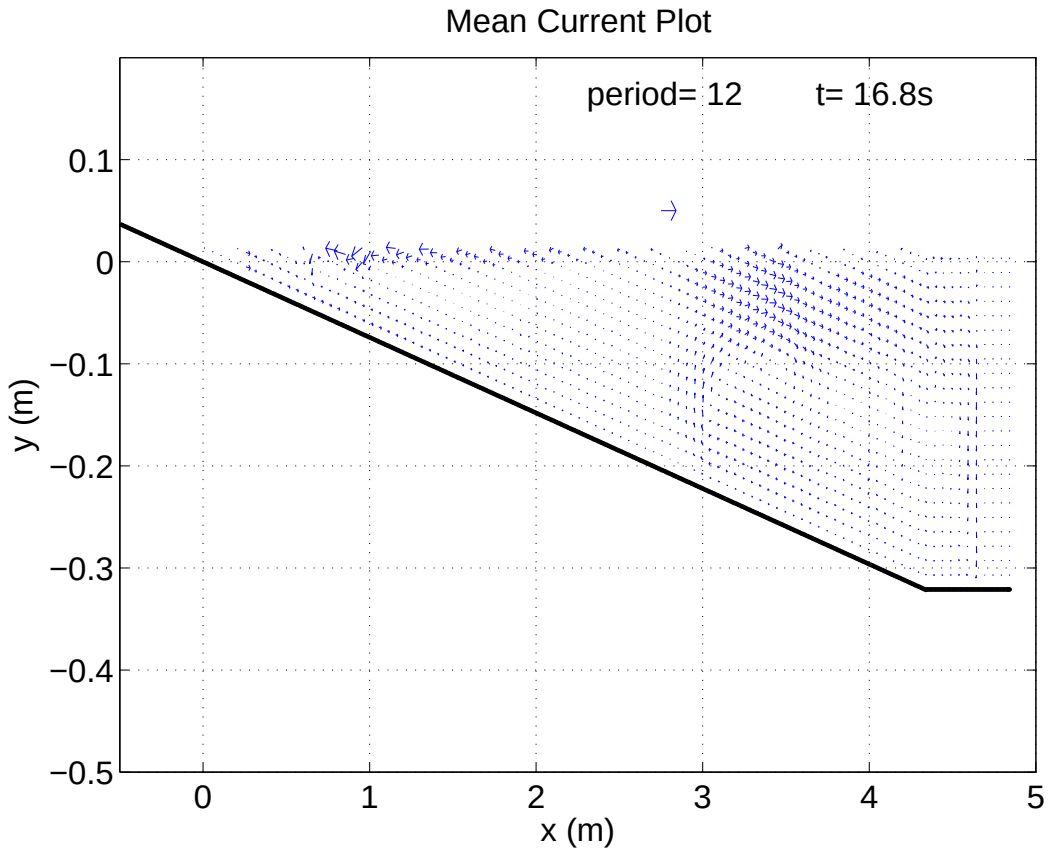

Figure 5.4: The coastal circulation of Case (2) obtained by time-averaging between 16.8s-T and 16.8s.

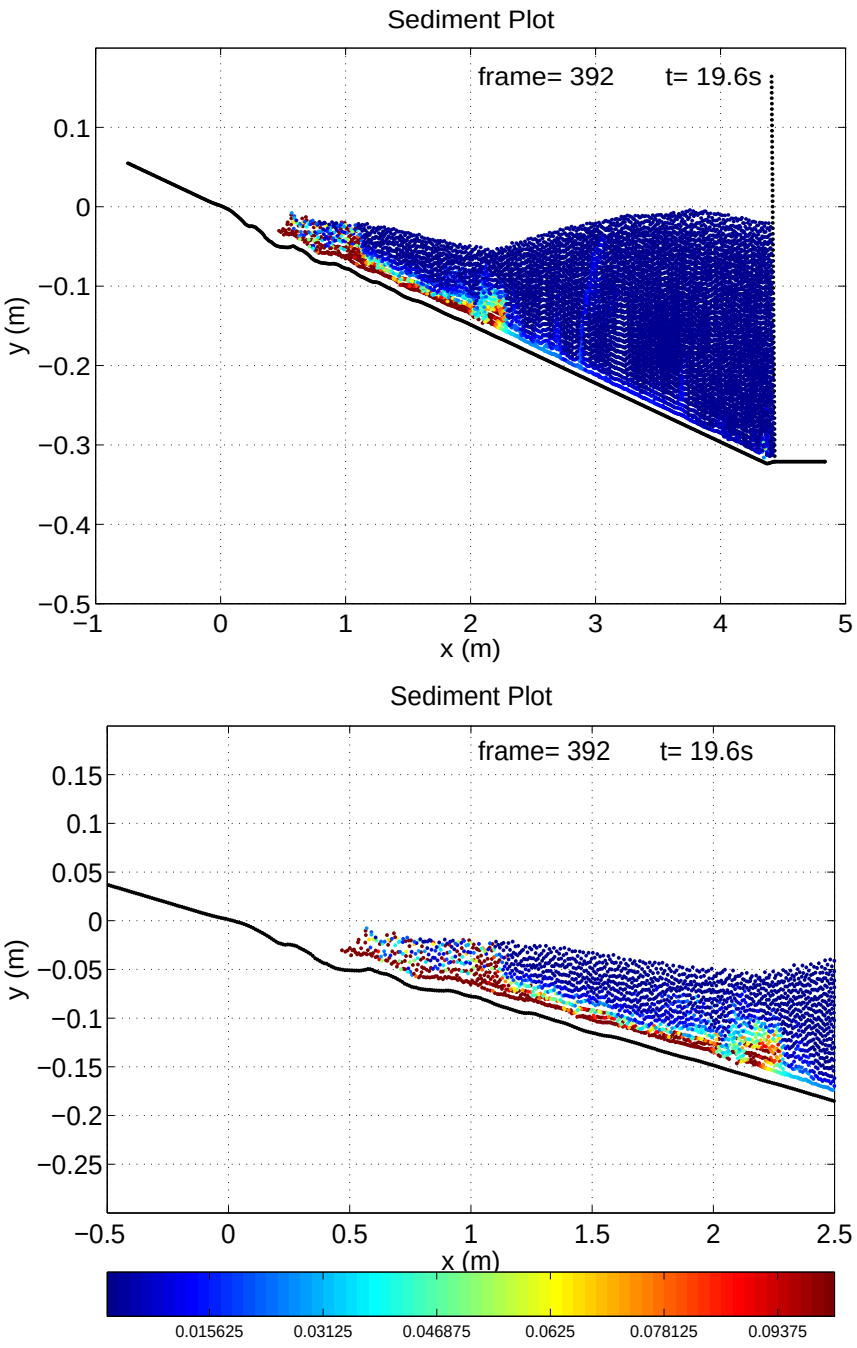

Figure 5.5: Snapshot of sediment concentration and morphological change for Case (3), 19.6 seconds after the initiation of wave motion. Here $T = 2.8s$, $H = 0.08m$, the slope is 1/13.5, with 11395 particles.

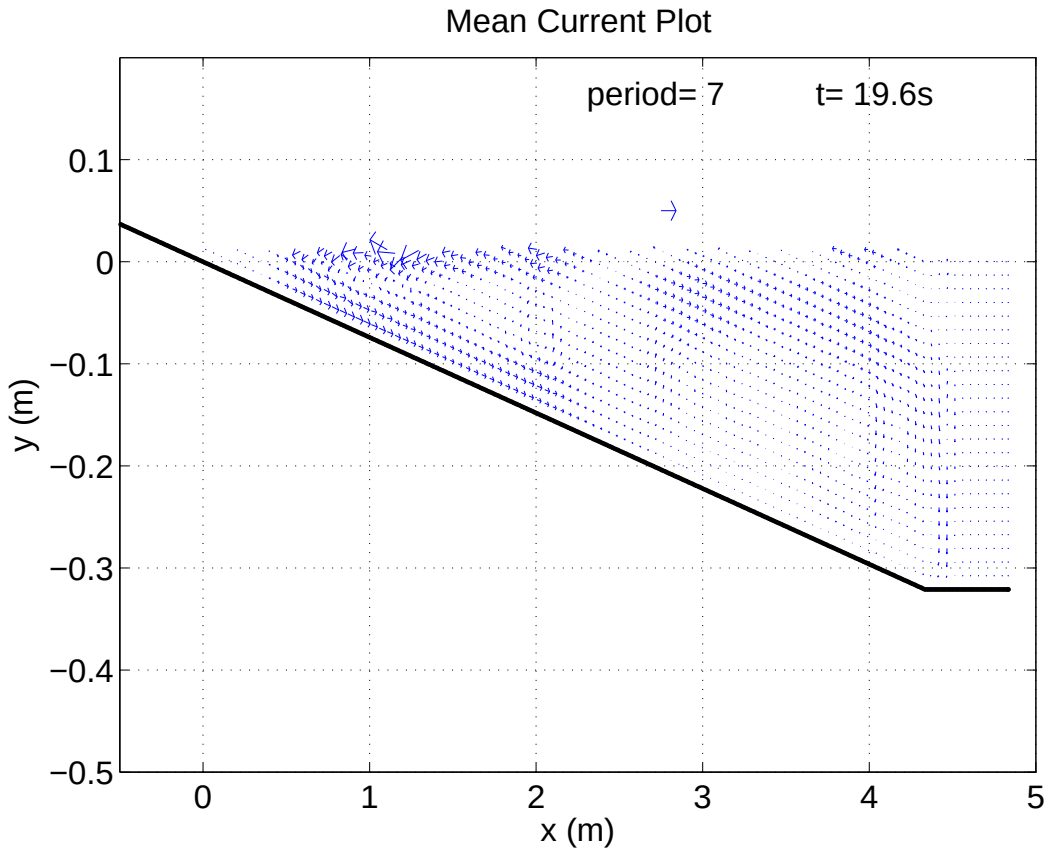

Figure 5.6: The coastal circulation of Case (3) obtained by time-averaging between 19.6s-T and 19.6s.

backwashes inhibits the wave bore propagation to shoreline and reduces the mass and momentum flux. The jet of the breaker points to the bottom and the mixing over the whole depth is much stronger than Case 1 and 2. The most significant erosion spot is around the breaking point, while the range of high concentration of suspended sand is between breaking point to $x = 2.0$, It is concluded that longer wave periods change the pattern of wave breaking with stronger vertical mixing and resulting significant erosion near the breaking point.

5.5.4 Case 4

For Case 4, with smaller wave height, the sediment motion is similar with Case 3 but is more restricted near the breaking point.

For all of the cases there is a vortex in front of the wave paddle. It is generated by the paddle motion and is close to paddle initially. It diffuses and moves shore-wards with time. The figure 5.9 shows the circulation system in the wave tank obtained by time-averaging. This phenomenon need to be verified by experiments.

5.6 Summary

1. The wave height determines the breaker line location, as expected.

2. Strong breakers can produce an undertow in the SPH model, which is the seaward-directed current flowing in the middle part of the water column under breaking waves. It is fed by the mass flux of the incoming breakers.

3. Large amounts of sediment are removed seaward by strong breakers similar to those observed in storm situations.

4. Weak breakers only suspend sediment near the shoreline inshore of the breaking point.

5. The strength of cross shore circulation is related to the size of breakers.

6. The existence of the weak upward current needs further investigated, but it is believed to be an artifact of wave tank.

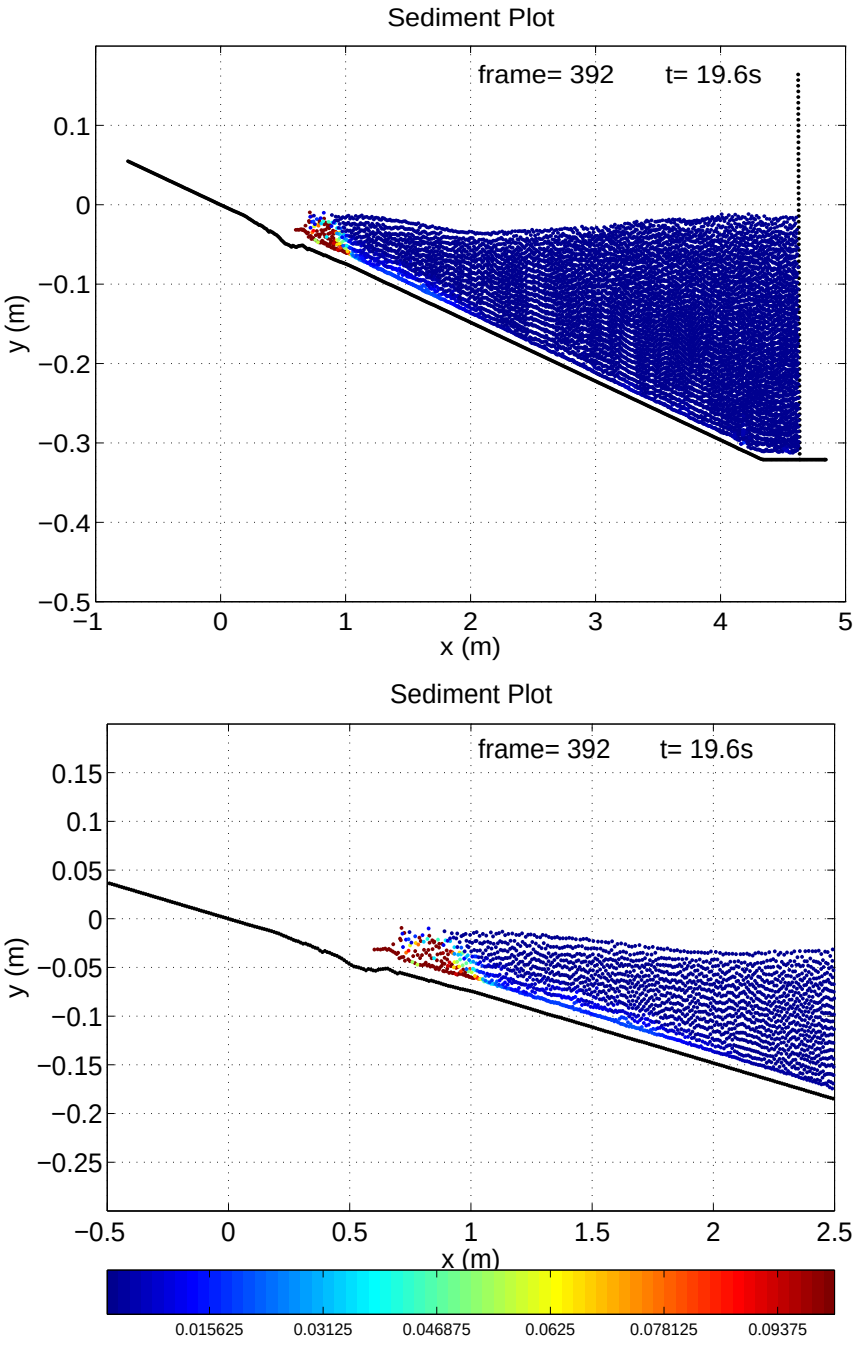

Figure 5.7: Snapshot of sediment concentration and morphological change for Case (4), 19.6 seconds after the initiation of wave motion. Here $T = 2.8s$, $H = 0.04m$, the slope is 1/13.5, with 11283 particles.

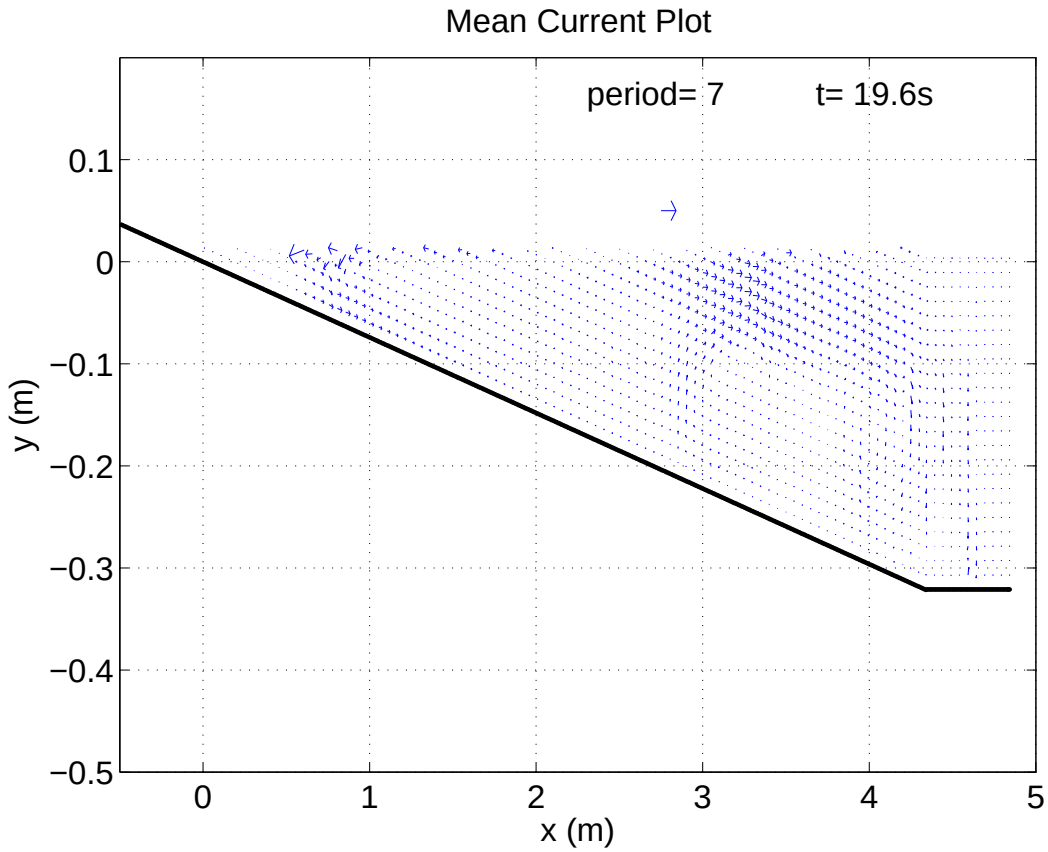

Figure 5.8: The coastal circulation of Case (4) obtained by time-averaging between 19.6s-T and 19.6s.

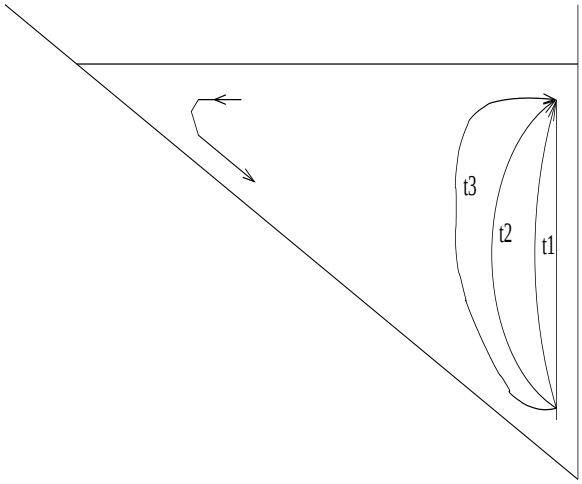

Figure 5.9: The coastal circulation system in the wave tank obtained by time-averaging

In general, the model shows the capability to capture the complicated physics for sediment suspension under breaking waves.

Higher resolution is needed for quantitative comparison with experimental or field data, and the boundary condition and other important sediment parameters, such as diffusion coefficients which need further investigation.

Chapter 6

Conclusions

Coastal sediment transport is one of the most challenging problems for coastal engineers and scientists. The planning and design of the waterfront structures, marinas, and harbors require the feasibility study, performance evaluation, optimization and prediction of impacts on the environment. Traditional design relies heavily on the engineering experience, intuition and physical model. Currently the numerical models have become popular tools for evaluating designs because they are cheap,quick and reasonably reliable. Numerical simulations require the coastal engineers and scientists to have solid mathematics and physics background to understand their theory, assumptions and limitations. This research has addressed and developed a numerical model for coastal sediment transport by Smoothed Particle Hydrodynamics Method in the surf zone, including breaking wave model, sediment transport and morphology model. It was applied for reproducing the experiments in order to validate.

The SPH model of coastal sediment transport only looks at two dimensional beach evolution for a short period of time. More work is needed to apply for practical engineering problems. Currently the model solves the problem at experimental scale. Currently this research is for the feasibility study of SPH model, not an engineering tool. But the final goal is to make it applicable for field scale.

6.1 SPH Method

Brief history and fundamentals of SPH method are reviewed in the Chapter 2. It is helpful to understand the difference between the traditional numerical methods and the meshfree method. The kernel and particle approximation are the basis of SPH method, which represents the continuous system by particles. It is shown how to approximate the first order and second order derivatives by a set of particles, instead of the vortices or nodes of mesh. Most of SPH algorithms are proposed by Monaghan *et al.*[62]. Some other SPH numerical techniques are also mentioned: artificial viscosity is designed for numerical stability and has no relation to real viscosity; XSPH is another numerical technique for stability, which is a equivalent to numerical filter to smooth the computation, to make the particles moving with neighboring particles as continuum material.

The SPH hydrodynamic model is used to a numerical wave tank and simulate the non-breaking and breaking waves. There are several assumptions and limitations in the model:

- compressible fluid approximation; the incompressible water is approximated by a slightly compressible fluid. So the pressure is calculated by the equation of state based on the slight density fluctuations. This approximation requires the low Mach number flow.

- boundary force; the particle boundary condition is more natural than Monaghan boundary force condition. The former has the penetration problem, which particles could pass through boundary particles and make the model unstable. The Monaghan boundary force is an artificial force that needs correction and adjustments to the magnitude factor for different cases.

The sub-particle scheme is used in the model in order to capture the features of a small-scale turbulence that is smaller than particle size. It is a turbulence model similar to sub-grid scheme in traditional numerical methods.

The boundary condition is improved by changing the force amplitude factor, which gives correct run-up and run-down process.

The comparison of SPH results and experiment data shows the SPH hydrodynamics model can simulate the non-breaking and breaking waves very well in wave shoaling, breaking, run-up and run-down process. In general, the SPH hydrodynamics model is an effective computational algorithm for complicated fluid mechanics problem. It is robust to deal with fluid splitting and merging problems. Even low resolution in the model can capture the complicated physics.

The possible sources of errors for SPH hydrodynamics model include artificial dissipation introduced by the XSPH correction, the artificial boundary forces which cause the gap between water particle and boundary, and acoustic wave from the small compressibility.

6.2 Coastal Sediment Transport Simulation

Chapter 4 and 5 proposed a sediment transport and morphological model to simulate the sediment suspension, deposition and resulting bed level change. The sediment suspension model is modeled by the convection-diffusion equation. The first reason for using concentration model instead of SPH two phase flow is that the concentration is widely used model in coastal engineering, but the SPH two phase flow is in stage of developing. The former is more reliable than the latter currently. The second reason is the scale of the problem. The concentration model can solve the problems from experiment scale up to engineering scale but the latter can only deal with experiment scale.

The new algorithms are proposed in order to solve the convection-diffusion equation. The standard SPH scheme for settling term has numerical dispersion problem because the standard SPH scheme is equivalent the central difference scheme in finite difference method, which has serious numerical dispersion and dissipation effects. The first order upwind SPH scheme is a dissipative, but conservative scheme which introduce the artificial diffusion effect. The second order SPH upwind scheme is proposed by the modified equation approach. The comparison for SPH schemes and finite difference schemes show the almost same accuracy. The SPH algorithm for diffusion term, which is the second derivative representation, is adopted from the scheme de-

veloped by Brookshaw, which is very similar with the artificial viscosity expression. The second derivative is not expressed by the second derivative of kernel function because it is not accurate when the particles are disordered. The SPH algorithm for diffusion term is compared with the finite difference scheme and has almost same accuracy. The comparisons show that both of SPH algorithms are of the same order of accuracy as the finite difference schemes.

After the test on these schemes, they are applied into a two dimensional problem with a block of high concentration in order to check the schemes and the mass exchange between fluid and bottom. This test confirms the net flux, calculated by deposition D and the erosion E, and the resulting bed level change are mass conserved.

In order to validate the sediment transport model, the SPH model system reproduced the experiments of sediment suspension on the ripples and plane bed in the oscillatory flow. All of these experiments were conducted in Large-scale Oscillatory Water Tunnel, Delft. The wave motion is simulated by the sinusoidal motion of two pistons at ends of a horizontal pipe. There are three wave conditions and their corresponding bed configuration: Case 1: weak wave condition over its parabola ripples; Case 2: strong wave condition over sinus ripples and Case 3: the extreme wave condition on plane bed. The SPH model results are compared with the experiment data and the other existing numerical models. For case 1, both SPH model results and the Discrete Vortex model results agree with the experiment data satisfactorily. The ratio of ripple length and ripple height is smallest and the convection effect is the most important in three cases. For the case 2, the SPH results is close to Discrete Vortex model, but both of them are over predicted. One reason is the use of sinusoidal ripple profiles for irregular bed forms. For case 3, under the extreme wave condition, the ripples are washed out. The boundary layer effect is more important than the convection effect. The comparison shows that the SPH results are a better fit with experiment data in the suspension layer than the One Dimensional Vertical model (1DV)[79]. But 1DV results are better for the sheet layer. In general, the SPH simulations produced results that are consistent with observations of sediment transport in the laboratory and have almost same accuracy as the other models in

finite difference method. These tests has demonstrated the ability of SPH sediment transport model to simulate the time evolution of sediment transport over the ripples and plane bed, and this offers the hope and basis for application in coastal sediment transport study.

Shore protection design requires the evaluation of beach process under the wave and wave-induced current action. The SPH hydrodynamics, sediment transport, and morphological models are applied for the coastal sediment transport and resulting beach evolution in the surf zone. The reliability of SPH hydrodynamic model has been verified in Chapter 3, in which the SPH results agree with experiment data. The SPH hydrodynamic model results provide the driving force and information for sediment transport model, including near-bed velocity, undertow, run-up or run-down, turbulence, mixing and energy dissipation caused by wave breaking. The bed level change is calculated based on the deposition and erosion rate on every bed particles' positions. There are four wave conditions varying wave heights and wave periods are tested. For each case the instantaneous distribution of sediment concentration, instantaneous erosion and deposition of bed, and the wave-averaged currents are shown. The qualitatively analysis confirms the capability of the SPH model to simulate the beach evolution for both erosion and accretion conditions. The SPH results are reasonable.

6.3 Recommendations for Future Work

6.3.1 SPH Hydrodynamic Model

The SPH hydrodynamics model is used for breaking wave model, which is very powerful, potential method. But there are a lot of numerical techniques, algorithms and strategies which need further studies for wave breaking simulation.

A better boundary condition is needed. Currently there are two popular boundary conditions: particle boundary condition and Monaghan boundary force condition. Particle boundary condition is natural and robust and Monaghan boundary force condition is an artificial force. Both of them are not good for high speed impact

problems. The former has a penetration problem and the latter could generate the unphysical, huge boundary force due to the high speed impact. Monaghan boundary condition needs to be corrected near the free surface for beach slope in order to make the wet-dry interface smoothly connected. Another important topic related to the boundary conditions is the boundary layer model. It is a challenge for SPH method to simulate the boundary layer flow due to the separation of particle in the high shear layer. Currently there are only some literatures for very small Reynolds number flow. All of the SPH sediment transport model results show that the inclusion of boundary layer flow is very important for the concentration calculation near the bed. The gap between bed and water particles is due to the boundary condition problem, in which the boundary force is artificial force. When the bed is eroded, it becomes worse.

The turbulence model of sub-particle scheme is used in the SPH hydrodynamics model. The sub-grid scheme has been studied in the finite difference method. But how this scheme affect and be sensitive to the energy dissipation and other features for breaking wave simulation need further studies. Further Smagorinsky model is the simplest. The more complicated dynamics models are needed in the future.

This study consider the effect of sub-particle scheme for sediment concentration, which has an additional SPS flux term for convection-diffusion equation. But in the sediment transport simulation, the results show the diffusion effect is overestimated and the SPS scheme for sediments make the results worse. So the SPS flux term is not included in the sediment simulation. Its effect needs further study.

6.3.2 SPH Sediment Transport Model

The concentration equation is widely used for modeling sediment transport but the validity needs further studied, especially for high concentration problem. Under the high concentration condition, the particle-fluid, particle-particle interaction and the settling velocity of sediment become important. In this study, these effects are neglected due to the lack of universal model.

The vortex distribution and propagation are very important for the sediment suspension for the case of oscillatory flow over sand ripples. The features of vortices

and the suspension height of sediment are closely related to the shape of ripple and the ratio between ripple length and ripple height. The mechanism of sediment suspension from the the bottom not only includes the bottom shear stress but also the turbulence burst caused by the vortices break and touch the bottom. So the more details of vortex studies are necessary for understanding the sediment suspension process over the sand ripples.

The bed level change is calculated based on the deposition and erosion rate at different position. Another method is based on the sediment transport rate, which is more common method for morphological model. The reliability of these two methods need to be verified. Coastal sediment transport applications are qualitatively tested in this study and it needs to be validated by the experiment and field data.

There is important assumption in these model. The critical Shields parameter is chosen as a constant of 0.05 which is from the experiments on flat bed. The effect of slope of bed is not considered. For a steep beach slope, this effect on the critical Shields parameter is important. It will affect both of the distribution of sediment suspension and the bed level change.

Appendix A

Parallel Computing for Particle Method

The computation of SPH model is so expensive that it need parallel computing. The Message-Passing Interface (MPI) method is used in the SPH model. This chapter will discuss the global structure of parallel computing used in the SPH model and explain some details of the use of the MPI functions in the model. The efficiency of parallel computing will be compared.

A.1 Global Structure of Parallel Computing

A.1.1 Introduction

Raw computational power is always a driving force for the development of computers. Many problems in science and engineering require greater computational power than we currently have. To obtain the more power from the current well understood technologies is the objective of *parallel computing* which is a computer or collection of computers that work together [71]. With this idea, a grand challenge problem can be divided into small tasks (subproblems) and assigned to separate processors, which complete the task independently. In theory, unlimited computational power can be obtained by this idea. How the multiprocessors work together, sharing memory and

interconnections is solved by *parallel programming*.

There are many different architectures for parallel computers. The typical parallel computers is Multiple-Instruction Multiple-Data system (MIMD). MIMD systems correspond to two kinds of parallel computers: shared-memory machines and distributed-memory machines.

In the shared-memory machine, all the processors share the same memory module. The programming for this kind of machine is simple but the machine is expensive due to the specially designed hardware and the maximum number of processors is limited due to the bandwidth between CPU and memory. The common programming language is OpenMP (Open Multi-Processing), which is nothing but a set of compiler directives.

For the distributed-memory machine, each processor has its own private memory and it could be a cluster of computers by network. It is cheap for hardware but needs the software to coordinate the communications and tasks. The common programming language is MPI which is the most commonly used method for distributed-memory machine.

A.1.2 Planning for SPH model

The method of parallel computing in this SPH model used here is MPI for cluster of distributed-memory machines. MPI is not a new programming language but a library of definitions and functions that can be used in C or Fortran programs. The goal of the parallelization for the SPH model here is to make it portable, easy to use and easy to be understood. So only a few of fundamental MPI functions are used in the SPH code to obtain the speedup.

The parallel computing for particle method is more complicated than the traditional grid method because the size of communication is different in every time step. The global structure of parallelization is that:

1. All the processors execute the same program;

2. The whole computational domain is decomposed into sub-domains and assigned

to each processor;

3. Sub-domains are connected by overlapping region which need communications by message passing functions;

4. Buffering and non-blocking communication are used in the computing.

In a serial code program, the whole domain is divided into many cells, in which the particles are located, so that it is not necessary to search in whole domain for neighboring particles. The particles are moving around in the domain, entering and exiting the cells, but the position of cells is fixed.

In parallel code, the domain is decomposed into vertical blocks with overlapping edges at two ends. Every processor deal with its own block. The shape and area of the blocks depend on the load balancing, that means the width of block is determined in the way that every block has similar number of particles. This parallelization is suitable for any shape of domain in which the number of particles in sub-domain keeps roughly equal to each other or the difference could be negligible compared to the number of local particles.

Global variables and local variables are two important concepts in parallel computing for efficiency use of memory. The global variables whose contents are significant to all processors are broadcast to or read by all processors at initial time. The local variables is limited to individual processor and it can be reached by point-to-point communication.

A.2 Understanding the Functions Used in the Model

The MPI functions used in the SPH code are listed in the table A.1. They are explained for the use in the SPH model, but not intent to explain the details of the function itself. For the details of MPI function please refer to the reference books [86] [40].

A.2.1 Domain Decomposition

Table A.1: List of MPI functions used in the SPH model

MPI function name	Subroutine
mpi_init(ierr)	main
mpi_comm_size	main
mpi_comm_rank	main
mpi_wtime	main
mpi_finalize	main
mpi_cart_create	main
mpi_cart_coords	main
mpi_cart_shift	main
mpi_recv	main
mpi_send	main
mpi_sendrecv	updatebuffer
mpi_barrier	global

```
include 'mpif.h'
...
call mpi_init(ierr)
call mpi_comm_size(MPI_COMM_WORLD,npes, ierr)
call mpi_comm_rank(MPI_COMM_WORLD,irank,ierr)
...
call mpi_finalize(ierr)
end
```

All functions here are needed in every MPI program. The preprocessor directive $include' mpi f.h'$ contains definitions and declarations necessary for compiling an MPI program. $mpi\_init(ierr)$ and $mpi\_finalize(ierr)$ are the first and last executable MPI function in the main program, indicating the beginning and endind calls to the MPI functions.

```
call MPI_CART_CREATE(MPI_COMM_WORLD, 1, npes,
     &         periods, reorder, comm_1d, ierr)
call MPI_COMM_RANK(comm_1d,myrank,ierr)
call MPI_CART_COORDS(comm_1d, myrank, 1, coord, ierr)
call MPI_CART_SHIFT(comm_1d, 0, 1, ibelow, iabove, ierr)
```

These functions are used to creat a new communicator for Cartesian topology and cache the relation of processor rank and Cartesian coordinate. Usually the SPH

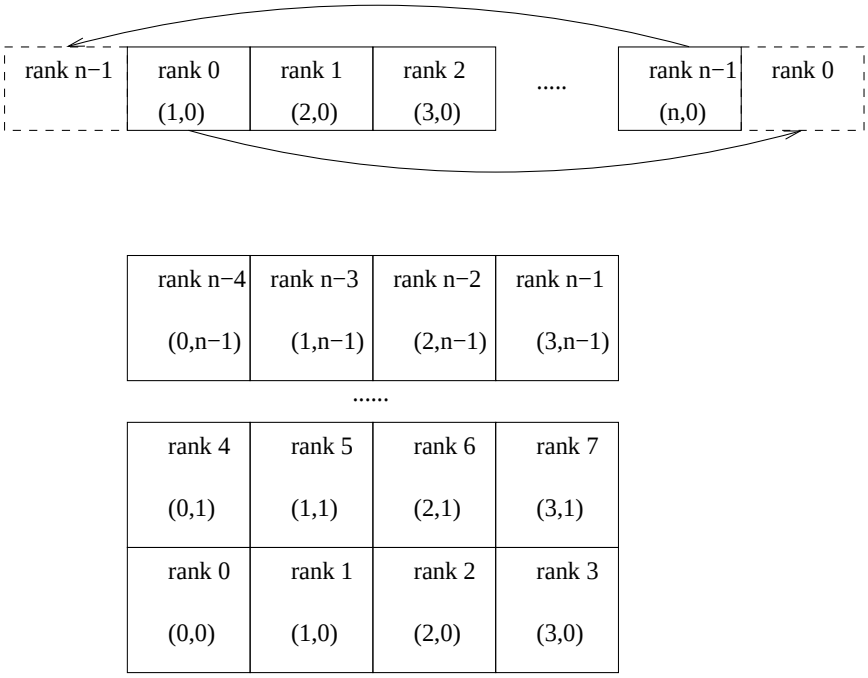

Figure A.1: An example of one and two dimensional Cartesian topology: numbers without bracket are rank of processor; numbers with bracket are coordinates.

computational domain is divided into blocks for one dimensional problem and grid squares for two or three dimensional problem. *mpi_cart_create* creates the new communicators for $n = 1, 2, 3$ dimensional coordinate system and defines the boundary condition such as with or without periodic condition. *mpi_comm_rank* assigns the processors, identified by rank, to the new communicator and *mpi_cart_coords* gives the coordinates to each processor. mpi_cart_shift is used to find the neighboring blocks or grid squares. The figure A.1 shows the example of Cartesian topology for one and two dimensional coordinate system.

```
call mpi_barrier(MPI_COMM_WORLD,ierr)
```

This is a very common MPI function to make all processors stop here for debugging and timing purposes.

A.2.2 Load Balancing

```
      idomain_s(1)=1
      idomain_e(1)=1
      do i=1,npes
         isum_nc=0
         do icell=1,ncx*ncy
            isum_nc=isum_nc+nc(icell,2)
            if(i*(np-nbp1)/(1.0*npes).le.isum_nc) then
               idomain_e(i)=ncy*int(icell/ncy)
               idomain_s(i+1)=idomain_e(i)+1
               go to 1000
            endif
         enddo
1000     continue
         if(i.eq.npes)idomain_e(i)=ncx*ncy

         if(irank.eq.i-1) then
            startcell=idomain_s(i)
            endcell=idomain_e(i)
         endif
      enddo
```

The domain of SPH model is decomposed into the vertical blocks which have many cells. How many cells in each block depends on how many particles in these cells. In order to make sure the computation load of each processor is balanced, each processor should have roughly equal number of particles. To simplify the buffered communication and reduce the amount of messages between processors, each sub-domain here has a rectangular shape. The figure A.2 shows an example of how to divide the computation domain into blocks in vertical. First count the number of particles in every cell and the sum of numbers of particles from cell 1 to 14 is equal to $np/npes$, where np is the total number of particles, $npes$ is the total number of processors. But the whole column, in which the cell 14 is located, is assigned to rank 0 to make the shape of sub-domain to be rectangular. So the start cell and end cell of first sub-domain are cell 1 and cell 16. Repeat this process for other processors. The width of sub-domain is different because some of the cells are empty.

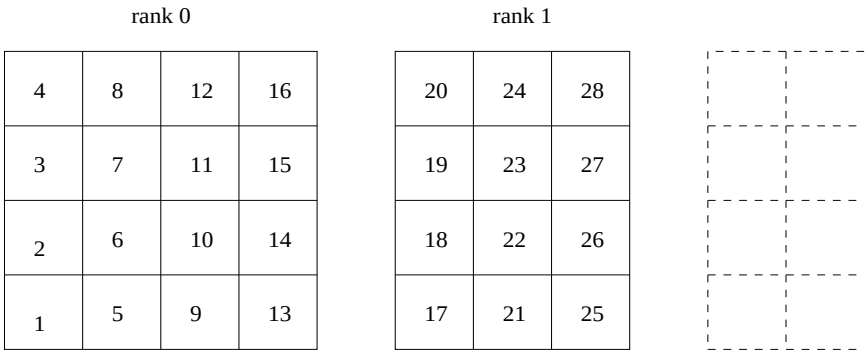

Figure A.2: An example of domain decomposition by column-major cells in vertical

A.2.3 Buffered Communication

The columns at the two ends of sub-domain is called 'edge column' or 'edge cells'. After the domain is decomposed, a problem arises. The calculation for particles in the edge cells require the data from a different processor. The array to hold these data is called 'buffer variables'. The elements(or particles) in these arrays are called 'ghost points' (or 'ghost particles') A.3.

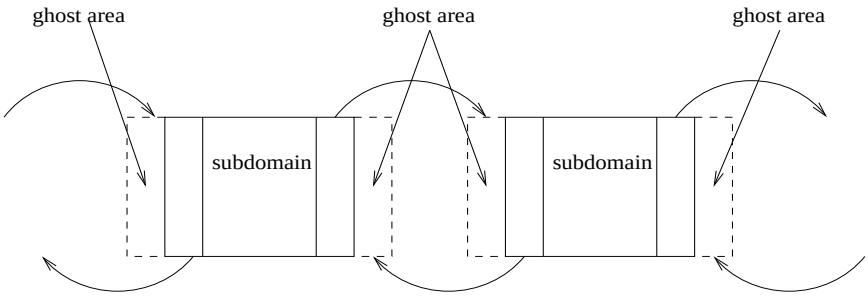

Figure A.3: Two steps to transfer the data of ghost particles

```
call MPI_Sendrecv(outtot,1,MPI_INTEGER,iabove,1,
     &     intot,1,MPI_INTEGER,ibelow,1,comm_1d,
     &     status,ierr)
        call mpi_barrier(mpi_comm_world, ierr)

call MPI_Sendrecv(out_buff, outtot, MPI_REAL, iabove, 2,
```

```
&    in_buff, intot, MPI_REAL, ibelow, 2, comm_1d,
&   status,ierr)
   call mpi_barrier(mpi_comm_world, ierr)
```

The buffer variables are used for ghost particles because it is not efficient to call the communication function for every individual message. The elements of the ghost particles are packed in an array to send and recieve, then it is unpacked to restore them to particles.

A.2.4 I/O in Parallel System

Every processor of most cluster machines has its own write and read capability. The global variables are read from external files or broadcast to processors. Every processor outputs the results for its sub-domain and saves in the different data files which contain the time step and processor information. It is not necessary and effecient to synchronize all the data into one big file.

A.3 Parallel Algorithm Performance Analysis

The difference between the serial and parallel program performance estimation is the runtime, which depends on the number of particles in the SPH model and the number of CPUs used for computation. The most commonly used measures are speedup and efficiency. The speedup is the ratio of the runtime of a serial program to that of parallel program. expressed as:

$$S(n,p) = \frac{T_\sigma(n)}{T_\pi(n,p)} \tag{A.1}$$

where $S(n,p)$ is the speedup, $T_\sigma(n)$ is the runtime of a serial program, $T_\pi(n,p)$ is the runtime of parallel program, n is the number of particles, p is the number of CPUs used for parallel program.

An alternative to speedup for performance estimation is efficiency, which is a measure of process utilization in parallel program, relative to the serial program. It is defined as:

$$E(n,p) = \frac{S(n,p)}{p} = \frac{T_\sigma(n)}{pT_\pi(n,p)} \tag{A.2}$$

The figure A.4 shows the performance of the parallel algorithm for the SPH model. The computation time is proportional to the number of particles and the runtime reduces with the number of CPUs used. The speedup has an upperbound for a certain number of particles due to the cost of communication and overhead, which is the Amdahl's Law in the parallel computing[71]. The parallel algorithm for SPH model in this study performs well, with speedup 6.3 for 8 CPUs. The speedup of the standard parallel program for trapezoidal rule, used in Pacheco's textbook[71] is around 7 for 8 CPUs.

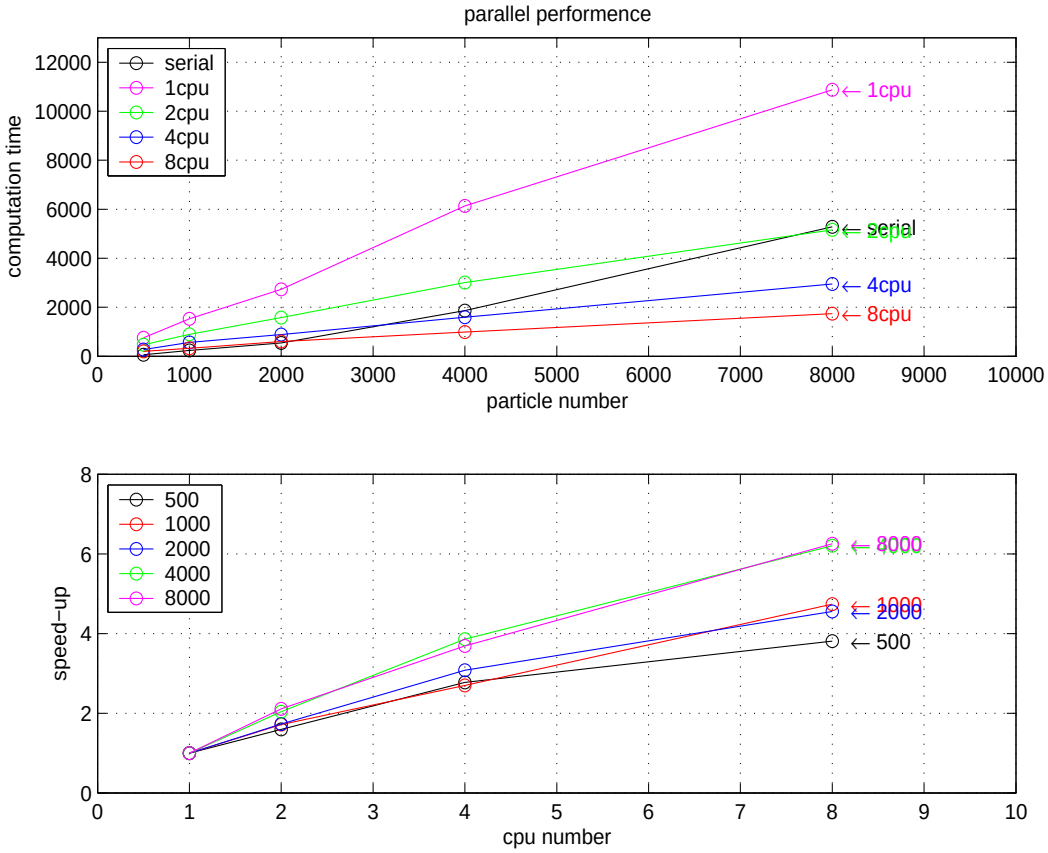

Figure A.4: The performance of the SPH parallel program: above, runtime; below, speedup

Bibliography

[1] J.A. Bailard and D.L. Inman. An Energetics bedload model for a Plane Sloping Beach:local transport. *Journal of Geophysical Research*, 86, 1981.

[2] W.T. Bakker. Sand concentration in oscillatory flow. In *Proceedings 14th International Conference on Coastal Engineering, Copenhogen*, pages 1129–1148, 1972.

[3] B.C. Barr, D.N. Slinn, T. Pierro, and K.B. Winters. Numerical simulation of turbulent, oscillatory flow over sand ripples. *Journal of Geophysical Research*, 109, 2004.

[4] G.K. Batchelor. *Introduction to Fluid Dynamics*. Cambridge Press, 1974.

[5] J. A. Battjes. Surf-zone dynamics. *Annual Review of Fluid Mechanics*, 20:257–293, 1988. PT: J.

[6] W. Benz and E. Asphaug. Simulations of Brittle Solids Using Smoothed Particle Hydrodynamics. *Comutational Physics Cmmunication*, 87:253–265, 1995.

[7] P. Blondeaux and G. Vittori. Vorticity dynamics in an oscillatory flow over a rippled bed. *Journal of Fluid Mechanics*, 226:257–289, 1991.

[8] J. Bonet and S. Kulasegaram. Correction and Stabilization of SPH Methods with Applications in Metal Forming Simulations. *International Journal for Numerical Method in Engineering*, 47:1189–1214, 2000.

[9] L. Brookshaw. Solving the Heat Diffusion Equation in SPH. *Mem. S.A. lt*, XX:1189–1214, 1993.

[10] I. Celik and W. Rodi. Modeling suspended sediment transport in onoequilibrium situation. *Journal of Hydraulic Engineering*, 114:1157–1191, 1988.

[11] K-A Chang and Philip L-F. Liu. Velocity, Acceleration and Vorticity under Breaking Waves. *Physics of Fluids*, 10:327–329, 1998.

[12] J.K Chen, J.E. Beraun, and C.J. Jih. Completeness Of Corrective Smoothed Particle Method For Linear Elastodynamics. *Computational Mechanics*, 24:279–287, 1999.

[13] E.D. Christensen and R. Deigaard. Large eddy simulation of breaking waves. *Coastal Engineering*, 42:53–86, 2001.

[14] J.P. Christiansen. Numerical Simulation of Hydrodynamics by the Method of Point Vortices. *Journal of Computational Physics*, 13:363–379, 1973.

[15] P. W. Cleary and J. J. Monaghan. Conduction Modelling Using Smoothed Particle Hydrodynamics. *Journal of Computational Physics*, 148:227–264, 1999.

[16] A. Colagrossi and M. Landrini. Numerical Simulation of Interfacial Flows by Smoothed Particle Hydrodynamics. *Journal of Computational Physics*, 191:448–475, 2003.

[17] D.T. Cox, N. Kobayashi, and A. Okayasu. Bttom Shear Stress in the Surf Zone. *Journal of Geophysical Research*, 101:14337–14348, 1996.

[18] W.R. Dally and R.G. Dean. Suspended Sediment Transport and Beach Profile Evolution. *Journal of Waterway, Port, Coastal, Ocean Engineering*, 110:15–33, 1984.

[19] R.A. Dalrymple and O. Knio. SPH modeling of Water Waves. *Proceeding of Coastal Dynamics*, 10:227–264, 2001.

[20] R.A. Dalrymple and B.D. Rogers. Numerical modeling of water waves with the SPH method. *Coastal Engineering*, 53:141–147, 2006.

[21] R.G. Dean and R. A. Dalrymple. *Water Wave Mechanics for Engineers and Scientists*. World Scitific, 1992.

[22] T. G. Drake and J. Calantoni. Discrete Particle Model for Sheet Flow Sediment Transport in the Nearshore. *Journal of Geophysical Research*, 106(9):19859–19868, 2001C.

[23] N. T. Duy and T. Shibayama. A Convection-Diffusion Model for Suspended Sediment in the Surf Zone. *Journal of Geophysical Research*, 102(10):23169–23186, 1997c.

[24] H.A. Eistein. The Bedload Function for Sediment Transport in Open Channel Flow. *United States Dept. of Agricultrue, Technical Bulletin, NO.1026*, 14, 1950.

[25] F. Engelund and J. Fredsoe. A sediment transport model for straight alluvial channel. *Notdic Hydrology*, 7:293–306, 1976.

[26] F. Engelund and J. Fredsoe. Sediment ripples and dunes. *Annual Review of Fluid Mechanics*, 14:13–37, 1982.

[27] J. H. Ferziger. *Computational Methods for Fluid Dynamics*. Springer, 2002.

[28] B.L. Finlayson, C.J. Gippel, T.A. McMahon, and N.D. Nancy D. Gordon. *Stream Hydrology: an introduction to ecologist*. John Wiley and Sons, 2004.

[29] C.A.J. Fletcher. *Computational Techniques for Fluid Dynamics*. Springer, 1991.

[30] J. Fredsoe, O.H. Andersen, and S. Silberg. Distribution of suspended sediment in large waves. *Journal of Waterway, Port, Coastal, Ocean Engineering*, 111, 1985.

[31] D. Fulk and D. W. Quinn. An Analysis of 1-D Smoothed Particle Hydrodynamics Kernels. *Journal of Computational Physics*, 126:165–180, 1996.

[32] R.A. Gingold and J.J. Monaghan. Smoothed particle hydrodynamics: theory and application to non-spherical stars. *Mon. Not. R. astr. Soc.*, 181:375–389, 1977.

[33] M. Gomez-Gesteira, D. Cerquiero, A. Crespo, and R.A. Dalrymple. Green Water Overtopping Analyzed with an SPH Model. *Ocean Engineering*, 32:223–238, 2005.

[34] M. Gomez-Gesteira and R.A. Dalrymple. Using 3D SPH Method for Wave Impact on a Tall Structure. *Journal of Waterway, Port, Coastal, Ocean Engineering*, 130:63–69, 2004.

[35] D. Goring and F. Raichlen. The Generation of Long Waves in the Laboratory. *Coastal Engineering*, 5:763–783, 1980.

[36] H. Gotoh and J. Fredsoe. Lagrangian two-phase flow model of the settling behavior of fine sediment dumped into water. *Coastal Engineering Journal*, pages 3906–3919, 2000.

[37] H. Gotoh and T. Sakai. Lagrangian Simulation of Breaking Waves Using Particle Method. *Coastal Engineering Journal*, 41(3):303–326, 1999.

[38] H. Gotoh, T. Shibihara, and T Sakai. Sub-particle-scale Model for the MPS Method- lagrangian flow model for hydraulic engineering. *Computaional Fluid Dynamics Journal*, pages 339–347, 2001.

[39] M. D. Greenberg. *Advanced engineering mathematics*. Prentice Hall, 1998.

[40] W. Gropp, Ewing Lusk, and A. Skjellum. *Using MPI-Portable parallel programming with the message-passing interface*. MIT Press, 1994.

[41] E. A. Hansen and R. Fredsoe, J.and Deigaard. Distribution of suspended sediment over wave-generated ripples. *Journal of Waterway Port Coastal and Ocean Engineering-Asce*, 120(1):37–55, Jan-Feb 1994.

[42] I.B. Hedegard, R. Deigaard, and J Fredsoe. Onshore-Offshore Sediment Transport and Morphological Modeling of Coastal Profile. In *Coastal Sediment*, pages 643–657, 1991.

[43] F. Hoefel and S. Elgar. Wave-induced sediment transport and sandbar migration. *Science*, 299(5614):1885–1887, MAR 21 2003.

[44] K. Horikawa. Coastal sediment processes. *Annual Review of Fluid Mechanics*, 13:9–32, 1981.

[45] K. Horikawa, T. Sunamura, and T. Shibayama. Labotory Study on the Two-dimensional Beach Profile Change. In *Proceedings 24th Coastal Engineering Conference in Japan*, pages 170–174, 1977.

[46] K. Horikawa, A. Watanabe, and S. Katori. A Labotory Study on Suspended Sediment due to Wave Action. In *Proceedings 18th ICCE*, pages 1335–1352, 1982.

[47] Fredsoe J. and R. Deigaard. *Mechanics of coastal sediment transport.* World Scientific, 1992.

[48] T.V. Karambas and C. Koutitas. Surf and Swash Zone Morphology Evolution Induced by Nonlinear Waves. *Journal of Waterway, Port, Coastal, Ocean Engineering*, 128:102–113, 2002.

[49] S. Koshizuka, A. Nobe, and Y. Oka. Numerical Analysis of Breaking Waves Using the Moving Particle Semi-Implicit Method. *International Journal for Numerical Method in Fluid*, 26:751–769, 1998.

[50] D.L. Kriebel and R.G. Dean. Beach and Dune Response to Severe Storms. In *Proceedings 19th International Conference on Coastal Engineering*, pages 1584–1599, 1984.

[51] M. Larson, N.C. Kraus, and T. Sunamura. Beach Profile Change. In *Proceedings 21st International Conference on Coastal Engineering*, pages 1295–1309, 1988.

[52] L.D. Libersky and et al. High Strain Lagrangian Hydrodynamics. *Journal of Computational Physics*, 109:67–75, 1993.

[53] P. Z. Lin and P. L. F. Liu. A numerical study of breaking waves in the surf zone. *Journal of Fluid Mechanics*, 359:239–264, MAR 25 1998.

[54] G.R. Liu. *Mesh Free Methods - Moving beyond the finite element method*. CRC Press, 2002.

[55] G.R. Liu and M.B. Liu. *Smoothed Particle Hydrodynamics - a meshfree particle method*. World Scitific, 2003.

[56] E. Y. M. Lo and S. D. Shao. Simulation of near-shore solitary wave mechanics by an incompressible sph method. *Applied Ocean Research*, 24(5):275–286, OCT 2002.

[57] M. S. Longuet-Higgins. Oscillating flow over steep sand ripples. *Journal of Fluid Mechanics*, 107:1–35, 1981.

[58] P. Lubin, S. Vincent, S. Abadie, and J. Caltagironw. Three-dimensional large eddy simulation of air entrainment under plunging breaking waves. *Coastal Engineering*, 53:631–655, 2006.

[59] L.B. Lucy. A Numerical Approach to Testing the Fission Hypothesis. *Astronomy Journal*, 82(12):1013–1924, December 1977.

[60] P.A. Madsen and H.A. Schaffer. Surf zone dynamics simulated by a boussinesq type model. *Coastal Engineering*, 32:255–287, 1997.

[61] J.J. Monaghan. Shock Simulation by the Particle Method SPH. *Journal of Computational Physics*, 52:374–389, 1983.

[62] J.J. Monaghan. Smoothed Particle Hydrodynamics. *Annual Review of Astronomy and Astrophysics*, 30:543–74, 1992.

[63] J.J. Monaghan. Simulating Free Surface Flows with SPH. *Journal of Computational Physics*, 110:399–406, 1994.

[64] J.J. Monaghan. SPH Simulation of Multi-phase Flow. *Computer Physics Communication*, 87:225–235, 1995.

[65] J.J. Monaghan. Smoothed particle hydrodynamics. *Reports on Progress in Physics*, 68(8):1703–1759, AUG 2005.

[66] J.J. Monaghan and A. Kos. Solitary Waves on A Cretan Beach. *Journal of Waterway, Port, Coastal, Ocean Engineering*, 125(3):145–154, 1999.

[67] J.P. Morris and J.J. Monaghan. A Switch to Reduce SPH Viscosity. *Journal of Computational Physics*, 136:41–50, 1997.

[68] K. Nadaoka, M. Hino, and Y. Koyano. Structure of the turbulent-flow field under breaking waves in the surf zone. *Journal of Fluid Mechanics*, 204:359–387, JUL 1989. PT: J.

[69] P. Nielsen. *Coastal Bottom Boundary Layers and Sediment Transport*. World Scientific, 1992.

[70] H. Nishimura and T Sunamura. Numerical Simulation of Beach Profile Changes. In *Proceedings 20th International Conference on Coastal Engineering*, pages 1444–1455, 1986.

[71] P.S. Pacheco. *Parallel programming with MPI*. Morgan Kaufmann Publishers, 1997.

[72] A. Panizzo. *Physical and Numerical Modeling of Subaerial Landslide Generated Waves*. Ph.D. dissertation, Universita Degli Studi di L'Aquila, Italy, 2004.

[73] D. H. Peregrine. Breaking waves on beaches. *Annual Review of Fluid Mechanics*, 15:149–178, 1983.

[74] A. G. Petschek and L. D. Libersky. Cylindrical Smoothed Particle Hydrodynamics. *Journal of Computational Physics*, 109:76–80, 1993.

[75] S. Plimpton. Fast Parallel Algorithms for Short-Range Molecular Dynamics. *Journal of Computational Physics*, 117:1–19, 1995.

[76] S. B. Pope. *Turbulent Flows*. The Cambridge Press, 2000.

[77] K.A. Rakha, R. Deigaard, and I. Broker. A Phase-Resolving Cross Shore Sediment Transport Model for Beach Profile Evolution. *Coastal Engineering*, 31:231–261, 1997.

[78] J.S. Ribberink and A. Al-Salem. Bedforms, near-bed sediment concentrations and sediment transport in simulated regular wave conditions. Technical Report Report H840, Delft Hydraulics, Delft, The Netherlands, 1989.

[79] J.S. Ribberink and A.A. Al-Salem. Sheet Flow and Suspension of Sand in Osillatory Boundary Layers. *Coastal Engineering*, 25:205–225, 1995.

[80] W. Rodi. Turbulence models and their application in hydraulics. *IAHR*, 1980.

[81] B.D. Rogers and R.A. Dalrymple. Three Dimensional Modeling of Wave Breaking. In *Proceedings 25th International Conference on Coastal Engineering*, 2004.

[82] H.A. Schaffer, P.A. Madsen, and R. Deigaard. A Boussinesq Model for Waves Breaking in Shallow Water. *Coastal Engineering*, 20:185–202, 1993.

[83] T. Schlicke. *Breaking Waves and the Dispersion of Surface Films*. Ph.D. dissertation, University of Edinburgh, 2001.

[84] J. S. Schoonees and A. K. Theron. Evaluation of 10 cross-shore sediment transport morphological models. *Coastal Engineering*, 25(1-2):1–41, MAY 1995.

[85] T. Shibayama and K. Horikawa. Sediment Transport and Beach Transformation Due to Waves. In *Proceedings 18th International Conference on Coastal Engineering*, pages 1439–1458, 1982.

[86] M. Snir, S.W. Otto, S. Huss-Lederman, D.W. Walker, and J. Dongarra. *MPI-The complete reference*. MIT Press, 1996.

[87] I. A. Svendsen. *Nearshore Hydrodynamics*. Lecture Notes, 2002.

[88] I.A. Svendsen, P.A. Madsen, and J.B. Hansen. Wave characteristics in the surf zone. In *Proceedings 16th International Conference on Coastal Engineering, Hamburg*, pages 529–539, 1978.

[89] D.H. Swart. Predictive Equations Regardung Coastal Transports. In *Proceedings 15th International Conference on Coastal Engineering*, pages 1113–1132, 1976.

[90] C. E. Synolakis. The Run-up of Solitary Waves. *Journal of Fluid Mechanics*, 185:523–545, 1987.

[91] C.E. Synolakis. *The run-up of long waves*. Ph.D. dissertation, California Institute of Technology, 1986.

[92] H. Takeda, S.M. Miyama, and M. Sekiya. Numerical Simulation of Viscous by Smoothed Particle Hydrodynamics. *Progress of Theoretical Physics*, 92(5):939–960, 1994.

[93] F.C.K. Ting and J.T. Kirby. Observation of undertow and turbulence in a laboratory surf zone. *Coastal Engineering*, 24(1-2):51–80, NOV 1994. PT: J.

[94] F.C.K. Ting and J.T. Kirby. Dynamics of surf-zone turbulence in a strong plunging breaker. *Coastal Engineering*, 24(3-4):177–204, MAR 1995. PT: J.

[95] L. Verlet. Computer Experiments on Classical Fluids. *Physical Review*, 159:98, 1967.

[96] P. Wang, B. A. Ebersole, and E. R. Smith. Beach-profile evolution under spilling and plunging breakers. *Journal of Waterway Port Coastal and Ocean Engineering-Asce*, 129(1):41–46, JAN-FEB 2003.

[97] A. Watanabe, T. Shimizu, and K. Kondo. Field application of a numerical model of beach topography change. In *Coastal Sediment*, pages 1814–1828, 1991.

[98] Y. Watanabe, H. Saeki, and R.J. Hosking. Three-dimensional Vortex Structures under Breaking Waves . *Journal of Fluid Mechanics*, 545:291–328, 2005.

[99] G. Wei, J.T. Kirby, S.T. Grilli, and R. Subramanya. A Fully Nonlinear Boussinesq Model for Surface Waves. *Journal of Fluid Mechanics*, 294:71–92, 1995.

[100] J.A. Zelt. The Run-up of Nonbreaking and Breaking Solitary Waves. *Coastal Engineering*, 15:205–246, 1991.

[101] S. Zou. SPH model and coastal applications. Master's thesis, University of Delaware, 2002.

[102] S. Zou and R.A. Dalrymple. Sediment Suspension Modeling by Smoothed Particle Hydrodynamics. In *Proceedings 25th International Conference on Coastal Engineering*, 2004.

[103] S. Zou and R.A. Dalrymple. Sediment Suspension Under the Breaking Waves. In *Waves Conference*, 2005.

[104] S. Zou and R.A. Dalrymple. Sediment Suspension Over Ripples under Oscillatory Flow. In *Proceedings 26th International Conference on Coastal Engineering*, 2006.

Vita

Shan Zou was born on July 9, 1971 in Jiangsu Province, China. His undergraduate studies were at Ocean University of Qingdao, where he received a B.S. in Physical Oceanography. In 2000, he received an M.S.E. in Coastal and Ocean Engineering from Nanjing Hydraulic Research Institute for research on the tidal hydraulics and sediment transport. In 2003, he received a second M.C.E. in Civil and Environmental Engineering from University of Delaware for the research of SPH and coastal applications. In 2003, he enrolled the Ph.D.program in the Department of Civil Engineering at The Johns Hopkins University.

The author has worked as a research engineer for Nanjing Hydraulic Research Institute. The author has a fondness and passion for coastal engineering, especially for sediment transport and morphological dynamics. He has worked as a consultant to many projects of coastal structures, harbors, bridges and tunnels throughout China.